AFWAL-TR-81-4144

EFFECT OF DEFECTS IN ALUMINUM P/M

J. S. Santner
Materials Research Laboratory, Inc.
One Science Road
Glenwood, Illinois 60425

DECEMBER 1981

TECHNICAL REPORT
Final Report for Period August 1980 – September 1981

MATERIALS LABORATORY
AIR FORCE WRIGHT AERONAUTICAL LABORATORIES
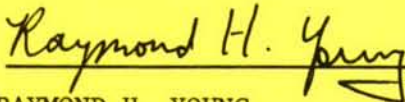AIR FORCE SYSTEMS COMMAND
WRIGHT-PATTERSON AIR FORCE BASE, OHIO 45433

RAYMOND H. YOUNG
Structural Metals Branch
Metals & Ceramics Division

FOR THE COMMANDER:

GAIL E. EICHELMAN
Chief, Structural Metals Branch
Metals & Ceramics Division

REPORT DOCUMENTATION PAGE		READ INSTRUCTIONS BEFORE COMPLETING FORM
1. REPORT NUMBER AFWAL-TR-81-4144	2. GOVT ACCESSION NO.	3. RECIPIENT'S CATALOG NUMBER
4. TITLE (and Subtitle) EFFECT OF DEFECTS IN ALUMINUM P/M		5. TYPE OF REPORT & PERIOD COVERED Final Technical Report August 1980 - Sept. 1981
		6. PERFORMING ORG. REPORT NUMBER 791
7. AUTHOR(s) J. S. Santner		8. CONTRACT OR GRANT NUMBER(s) F33615-80-C-5089
9. PERFORMING ORGANIZATION NAME AND ADDRESS Materials Research Laboratory, Inc. One Science Road Glenwood, Illinois 60425		10. PROGRAM ELEMENT, PROJECT, TASK AREA & WORK UNIT NUMBERS 62102F, 2418, 01, 19
11. CONTROLLING OFFICE NAME AND ADDRESS Materials Laboratory, (AFWAL/MLLS) Air Force Wright Aeronautical Laboratories Wright-Patterson AFB, OH 45433		12. REPORT DATE December, 1981
		13. NUMBER OF PAGES 97
14. MONITORING AGENCY NAME & ADDRESS(if different from Controlling Office)		15. SECURITY CLASS. (of this report) Unclassified
		15a. DECLASSIFICATION/DOWNGRADING SCHEDULE

16. DISTRIBUTION STATEMENT (of this Report)

Approved for public release; distribution unlimited.

17. DISTRIBUTION STATEMENT (of the abstract entered in Block 20, if different from Report)

18. SUPPLEMENTARY NOTES

Presented, in part, at the 1982 AIME Annual Meeting at Dallas, Texas on 14-18 February.

19. KEY WORDS (Continue on reverse side if necessary and identify by block number)

Aluminum, powder metallurgy, high strength, 7000 series, notched fatigue, fatigue, extrusion, forging, X 7091 aluminum, aluminum alloy CT 91.

20. ABSTRACT (Continue on reverse side if necessary and identify by block number)

No previous work on the first generation P/M aluminum alloys studied whether foreign contaminants were limiting the potential of these materials. The present program conducted fatigue tests on a forging, an extrusion, and an as-compacted billet of the CT 91 (formerly MA 87) composition. Specimens taken from both the L and L-T orientations were tested with fatigue lives between 10^3 and 10^6 cycles. Specimens

DD $_{1 \text{ JAN } 73}^{\text{FORM}}$ 1473   EDITION OF 1 NOV 65 IS OBSOLETE

20. Abstract (continued)

with abnormally short or unusually long fatigue lives were fractograph-ically examined and compared with typical failures. No obvious dif-ferences were noted among the three types of failures, although several types of defects were characterized at the initiation sites. These include (1) alumina inclusions ($\sim$ 60 percent occurrence), (2) transition metal inclusions ($\sim$ 30 percent occurrence), and (3) microstructural boundaries ($\sim$ 10 percent occurrence).

The fatigue strength at 10^7 cycles was also measured for specimens with a theoretical stress concentration factor, K_t, of three and ten. The milder notched specimens, $K_t = 3$, had a 70 percent greater fatigue strength than that measured for high strength ingot alloys. The $K_t = 10$ fatigue strength is the same as that measured for 7000 series ingot alloys.

Table of Contents

Table of Contents, Continued

List of Tables

List of Illustrations

List of Illustrations, Continued

List of Illustrations, Continued

FOREWORD

The fabricated products used in this study were produced and supplied by Alcoa to the Air Force in 1977 for testing. During the period following the manufacture of the aforementioned products, modifications were made in the atomization equipment and procedures. In particular, alterations in collection, metal transfer and filtration methods have been made which are believed by Alcoa to significantly improve metal quality. Thus, the properties of the 1977 products, reported in this study, do not fully represent the properties of the materials currently being produced by Alcoa.

This investigation was conducted by the Materials Research Laboratory, Inc., Glenwood, Illinois. Dr. E. J. Ripling was project manager and Dr. J. S. Santner was the project engineer. Dr. Gregory Campbell, of Purdue University, served as a statistical consultant.

Capt. Stephen H. Doerr and Lt. Raymond H. Young were project coordinators for the Air Force Wright Aeronautical Laboratories, Inc., Wright-Patterson AFB, Ohio.

1.0 INTRODUCTION

Processing metals via P/M techniques provide several inherent advantages over I/M techniques: (1) more homogeneous microstructures due to a small, more uniform size of precipitates, (2) supersaturated compositions for radically new alloy compositions, and (3) a low-cost approach for producing complex shapes and forging preforms. To date, two P/M aluminum alloys, X7091 (formerly MA87 and CT91, more recently) and X7090 (formerly MA67, and CT90, more recently) have been developed as potential candidates for a wide variety of aerospace applications. At equivalent levels of stress-corrosion cracking resistance, X7091 exhibits equivalent fracture toughness with higher strength and exfoliation resistance than the most advanced I/M alloys, 7050 and 7475[1, 2]. The P/M alloy X7090 has superior combinations of strength and corrosion resistance compared to conventional 7000 series aluminum alloys.

While rapid solidification holds much promise for property improvements for all structural metals, the prior experience with P/M titanium alloys[3, 4] and P/M superalloys[5, 6, 7] has shown that foreign contaminants can be introduced during the processing of these materials. A small volume fraction of contaminants can decrease the tensile (8, 9) as well as fatigue properties[4, 5] of P/M alloys.

Foreign contamination comes from either the powder production process or subsequent handling before the material is densified. As P/M billet production is scaled up from laboratory bench sizes to pilot plant production, the possibility of contamination by inexperienced operators increases. To date, there has been no reported incident of property degradation in the new P/M aluminum alloys X7090 and X7091. The fact that forgings, extrusions, and plates of these alloys have been successfully produced from a 3200 pound (1500 kg) billet in a commercial plant[10] makes this point noteworthy. However, previous work did not directly investigate whether foreign contaminants and/or processing anomalies were potentially limiting the P/M aluminum properties. The present program was undertaken to answer this question.

A second objective of the present program was to investigate the effect of notch acuity on the fatigue behavior of CT91. Its $K_t =$ 3 fatigue strength at 10^7 cycles was measured twice that of 7075 or 7050, both I/M alloys[10]. However, fatigue tests with more severe notches found the fatigue strength to be the same as that in I/M alloys[12]. Since I/M aluminum alloys have nearly the same notched fatigue strength irrespective of the notch acuity, the issue is raised whether the P/M aluminum alloys have improved notched fatigue behavior over I/M aluminum alloys.

2.0 SCOPE OF PRODUCT EVALUATION

Air atomized powder of the CT91 composition (6.5 Zn-2.5 Mg- 1.5 Cu-0.4 Co) was chosen for evaluation as this material was considered to be of greatest commercial interest. The consolidated material was produced under a previous Air Force contract[11]. Subsequently, Alcoa has made changes in their powder producing facility to improve the product quality[13]. Hence, the alloy will not be identified by its most recent Aluminum Association experimental designation (X7091), but by its precursor designation (CT91).

Two worked product forms, a forging and an extrusion, were evaluated in the longitudinal and long-transverse direction. Both products were stress relieved to minimize residual quenching stresses. Ancillary tests were conducted on an as-compacted billet to provide a reference fracture surface against which the worked material can be compared.

3.0 APPROACH

3.1 Sensitivity of Notch Acuity

This portion of the test program is to determine the notched high cycle fatigue behavior of P/M forging and extrusions for two orientations. The objective is to establish whether P/M aluminum alloys, unlike I/M aluminum alloys, have a fatigue strength (at 10^7 cycles) which is sensitive to the notch acuity. Therefore, the notched fatigue

strength must be measured for at least two notch geometries. Eight combinations of product form, orientation, and notch acuity are considered as outlined in the first three rows of Table 1. For a full factorial experiment with these conditions twelve specimens were available for testing. The two point method has been developed and found more efficient than other techniques to measure the fatigue strength[14]. It also offers the advantage that the median fatigue limit and its two standard deviations confidence interval can be estimated from tabulated quantities[16] if too few specimens have been tested. However, the two point strategy requires an accurate estimate of the approximate fatigue strength. Therefore, preliminary tests of two specimens for each combination of product form and orientation are conducted to establish whether the fatigue strength is nearer the I/M value or the factor of two higher values reported earlier for the P/M alloy. Ultimately, ten specimens are tested using the two point strategy.

3.2   Sensitivity of CT91 to Foreign Contaminants and Processing Anomalies

To test the sensitivity of CT91 to foreign contaminants and processing anomalies, there are two requirements: (1) a wide range of fatigue lives should be tested, and (2) outliers due to test scatter must be distinguished from those caused by material defects. It is desirable to test a wide range of fatigue lives since one defect type may initiate cracks at long fatigue lives, while a different material defect may control the behavior at short fatigue lives. Since the S-N curve is sigmoidal in shape with asymptotic behavior for both short and long fatigue lives, the inherent test scatter is greatest in the regions of most interest. The scatter at the upper asymptote, the ultimate tensile strength for a one-half cycle test, can be reduced by conducting strain-controlled tests rather than load control tests. The inherent scatter cannot be reduced by this technique near the lower asymptote, the fatigue limit. Therefore, sufficient replication is necessary to

establish the variance for these testing conditions so outliers due to material defects can be identified.

3.2.1 Phase 1: Preliminary Testing

The testing program is divided into three phases, as shown in Fig. 1. The preliminary testing program verifies the adequacy of the specimen design, establishes the general shape of both the load life (S-N) and strain-life (ε-N) curves, and measures the tensile and cyclic properties. Fracture surfaces from broken tensile bars and microstructures provide comparison during subsequent fractographic analysis of sectioned fatigue specimens in Phase 2.

The adequacy of specimen design is a concern as previous smooth fatigue tests[10] on CT91 forgings had 29 percent of the specimens fail in the shoulder, while seven percent of the extrusions had similar problems. The general shape of the fatigue-life curves established test conditions for obtaining selected mean fatigue lives of interest during the second phase.

3.2.2 Phase 2: Detailed Testing and Fractography

Multiple tests are conducted for three target fatigue lives. Two load levels are chosen to bracket fatigue lives of approximately 10^5 cycles, as this is the fatigue life of most interest for aerospace structural applications of aluminum alloys. Fatigue lives of approximately 10^3 cycles are near the transition fatigue life where the total specimen deformation is equally divided between elastic and plastic strain. These tests are conducted under strain control for the reasons discussed in Section 3.2. Load and strain levels are analyzed separately for each test condition (product form and orientation). A statistical confidence interval of ±1.5 standard deviation establishes which specimens are outliers in a statistical sense. This means if the outliers are normally distributed, an average of thirteen percent of the specimens are defined as outliers. On average, one outlier is produced for each combination of test variables if ten specimens are tested under identical conditions.

Since ten is a relatively small sample size, and the distribution may not be symmetric, a sterile analysis of fatigue life data does not provide sufficient information for the detection of outliers. Therefore, all the fractured specimens are given a preliminary optical fractography (up to 40X) examination to provide complementary information and help identify outliers without relying solely on a statistical analysis from fatigue life data. The optical fractography identifies the number of initiation sites, their location (e.g., surface vs. internal), and the orientation of the fracture plane with respect to the tensile axis.

The outliers are characterized in a SEM equipped with an EDX spectrometer. Where appropriate, the samples are sectioned, polished, and etched perpendicular to the fracture surface to further characterize the relationship between the initiation site and the microstructure. The scope of the detailed test program is given in Table 2.

3.2.3 Phase 3: Verification Testing and Fractography

The purpose of the verification test phase is to provide feedback within the test program. As mentioned in Section 3.2.2, only one outlier can be identified if ten replicate specimens are run under identical conditions. The outlier could have an abnormally short (-1.5 standard deviation) or an abnormally long (+1.5 standard deviation) life. In order to assess whether the presence of foreign contaminants and/or processing anomalies cause premature failure or prevent radically improved performance, outliers from both extremes need to be analyzed. The program is designed to allow expansion of the test conditions (e.g., product form, orientation, load) once the analysis of the second phase is complete.

4.0 EXPERIMENTAL

4.1 Specimen Preparation

As mentioned in the scope of product evaluation, three product forms are evaluated: a two-inch (50 mm) thick triple axis forging; three 7/16 inch (11 mm) thick extrusions with a 20:1 reduction ratio; and a 3/4 inch (20 mm) thick cross-section from a 6½ inch (165 mm)

diameter as-compacted billet. An equal proportion of test coupons are cut from the three extrusions. The two worked product forms (the forging and the extrusions) have their deformation concentrated in different regions. In an extrusion, the mid-width material is subjected to elongation, while the edges are heavily sheared. In a forging, the friction at a billet/platen interface limits the metal flow to create an upper and lower "dead zone". Beyond this region, the metal flows laterally from the center of the work piece to the edges. This metal flow produces the barrel shape which is characteristic of an open die forging. Previous fatigue test results on a single axis forging of CT91[17] show the location within the product form affected the fatigue life. Consequently, within each product form an equal population of test coupons are taken from the different regions illustrated in Fig. 2 where it is reasonable to expect different concentrations of local strain. By drawing equal populations of specimens from these different regions within the product forms, any effect of local strain on the fatigue life is normalized. Furthermore, the effect of local strain is evaluated in addition to the primary objective evaluating the sensitivity of CT91 to foreign contaminants and processing anomalies.

4.2   Notched Fatigue

The two theoretical stress concentration factors chosen for this study are a K_t of 3 and a K_t of 10. The former is chosen because a fastener hole increases the local stress by a factor of three, and is, therefore, of practical significance. A radius of 0.001 inch (25 μm) is the smallest radius which can be reproducibly machined into a specimen. Therefore, the largest K_t which can be machined is limited by this fact. Figure 3 gives the geometry of the specimens.

The notch for the K_t = 3 specimens is polished, in turn, with a 600 grit slurry of SiC and 6 μm diamond paste. A jig saw is used to hold a nylon thread while the specimen is turned in a lathe. The thread is held at an oblique angle with respect to the tensile axis to produce a smooth continuous radius at the notch root. This is verified

-6-

by checking the notch geometry in an optical comparator after polishing. The notch for the K_t = 10 specimens is tested in the as-machined condition, as there is no means to polish an 0.001 inch (25 μm) radius notch without changing its radius.

All the notched fatigue tests are conducted on an electro-hydraulic closed-loop test machine. Prior to testing, the alignment of the test machine is verified with a strain gaged specimen. The percent bending stress is consistently less than three percent in the apparatus shown in Fig. 4. This figure also shows the plastic bag used to contain a gaseous nitrogen atmosphere. This precaution is taken to assure that the relative humidity of the test environment would remain constant during the course of the testing program. The specimens are kept in a dessicator before and after the testing.

A dummy specimen is used to adjust the feedback electronics to obtain the highest possible frequency to expedite the testing. A frequency of 72 Hz produced stable readings of the maximum and minimum loads, which are measured with a commercial peak reader (MTS 430 Digital Indicator). The tests are run with an R-ratio (minimum load/maximum load) of 0.1 so the results could be compared with previous work[10, 12].

4.3   Smooth Fatigue

The preliminary smooth fatigue specimens are machined with an 0.253 inch (6.4 mm) diameter, as shown in Fig. 5. The specimens are mechanically polished with a 600 grit SiC slurry impregnating a felt wheel on a high speed grinding tool to remove any circumferential machining marks. The specimens are subsequently electropolished in a 0°C (32°F) solution of 500 ml HNO_3, 500 ml CH_3OH, and 20 ml HCl at four volts.

This specimen design proved to be inadequate, as thread failures occurred on the early tests. Interestingly, a stress concentration factor of three is calculated from the root of a single thread. The threaded cross-sectional area is three times larger than the gage cross-sectional area. For this reason the gage diameter is reduced 25 percent to make

-7-

the threaded cross-sectional area five and one half times larger than the gage area. Unfortunately, even this new specimen design did not always eliminate the problem, as illustrated in Fig. 6.

The load control tests are conducted at a frequency of 30 Hz on a Sonntag test machine. As done in the notched fatigue test program, the specimens are enclosed in a test chamber continuously flooded with room temperature gaseous nitrogen to maintain a constant relative humidity during the test program. This precaution is not used during the strain controlled tests, as these fatigue lives are so short as to make them insensitive to changes in the relative humidity. The tests are conducted at an R-ratio of 0.1 so the results could be compared with existing data for I/M alloys.

The strain controlled tests are conducted on a closed-loop electro-hydraulic system with a commercial extensometer (MTS Model 632.26B-20) using axial strain control. The extensometer is calibrated to resolve 0.05 percent strain in the range of 0 to 3 percent. The frequency is changed to maintain a constant strain rate of 5×10^{-3}/sec. Tests are conducted at a positive S-ratio (minimum strain/maximum strain) of 0.1 to be in parallel with the positive R-ratio in the load control tests.

5.0   PRELIMINARY EVALUATION OF THE THREE PRODUCT FORMS

The metallurgical structure within the extrusion provides stronger evidence for a variation of local deformation within the product form than reflected in the microstructure of the forging. Figure 7 shows the principal planes of the extrusion at the edge and middle locations. The L and T planes contain patches of the unrecrystallized subgrain boundaries at the edge location, while the less heavily worked region at the middle location is completely recrystallized by comparison. Figure 8 shows the microstructure at the four locations defined in Section 4.1. On average, its grain size is larger than that of the extrusion. In addition, areas of recrystallized and unrecrystallized grains are found at all four locations.

The tensile properties for the as-compacted billet, forging and extrusion are tabulated in Table 2 (Si units) and Table 4 (English units). It is interesting to note that the extrusion, which has a finer grain size than the forging, has approximately a seven percent higher tensile strength than the forging. The unworked product form (billet) has the lowest strength, as expected. These results are illustrated in Fig. 9 along with the results of the cyclic stress-strain curves. While it is beyond the scope of the present work to understand the mechanism of cyclic hardening/softening behavior in these P/M alloys, the cyclic behavior is the opposite from that reported for high strength I/M alloys; namely, the cyclic stress-strain curves lie below the monotonic stress-strain curves. This causes the cyclic work hardening rate to be higher than the monotonic work hardening rate.

Preliminary strain-control tests at an 0.1 S-ratio (minimum strain/maximum strain) suggest for fatigue lives greater than 10^3 cycles the extrusions outperform the forgings. The opposite is true when the fatigue lives are less than 10^3 cycles. This observation is consistent with the fact that the extrusion has a modestly higher strength and lower ductility than the forging. The improved ductility of the forging gives it an advantage for fatigue lives less than 10^3 cycles, while the improved strength of the extrusion improves the fatigue life greater than 10^3 cycles.

6.0   EFFECT OF NOTCH ACUITY: RESULTS AND DISCUSSION

The results of the replicate tests using the two point method are given in Tables 5 and 6 for the $K_t = 3$ and $K_t = 10$ specimens, respectively. After 10^7 cycles, the tests are terminated and considered run-outs. For convenience, the data are ordered to check for obvious trends in the specimen location code. None are detected. Table 7 gives the 10^7 notched fatigue strength of the specimens when analyzed by the methods outlined by Little and Jebe[15]. Neither product form nor orientation significantly changes the fatigue strength at 10^7 cycles. However, the $K_t = 3$ fatigue strength is 70 percent greater than that measured for high strength I/M alloys. This value is somewhat lower than that

reported by Cebulak[10]. The reason for this difference is believed to be the different techniques used to calculate the fatigue strength. The $K_t = 10$ fatigue strength is the same as that reported for more severe notches[12].

It is speculated that the $K_t = 3$ notch is sufficiently mild for a significant portion of the specimen life to be spent initiating a crack. On the other hand, nearly the entire specimen life is spent in crack propagation with the sharp $K_t = 10$ notch. Recent work[11] has demonstrated that the fatigue crack growth rates are approximately the same in both commercial high strength I/M alloys and the first generation P/M alloys. Therefore, both these alloy systems will give the same fatigue strength for sharply notched specimens. The fatigue crack initiation process in mild notches has been studied by Kung and Fine[18]. They found that the probability of crack initiation at constituent particles drops very rapidly below 7 μm. Since P/M alloys generally do not have constituent particles above this size range, this mechanism of crack initiation is greatly reduced: therefore, the improved fatigue crack initiation resistance of P/M alloys is reflected in the fatigue strength of specimens with mild notches.

7.0   SENSITIVITY OF Al P/M TO FOREIGN CONTAMINANTS
      AND PROCESSING ANOMALIES:
      RESULTS AND DISCUSSION

7.1   Data Analysis of Multiple Strain Control and
      Load Control Tests

As discussed in Section 3.2.2, the data for each load and strain level is first analyzed separately for both product forms (forging and extrusion) and orientations (L and L-T). Since fatigue life data are normally plotted on a logarithmic scale, the log-normal distribution, rather than the normal distribution, is used in the data analysis. Specimens with fatigue lives more than (or less than) ±1.5 standard deviation from the mean are defined as statistical outliers. This criteria

limits the program scope to approximately 13 percent of the samples for detailed SEM/EDX fractography. Table 8 gives the means and the standard deviations for the three testing conditions for both product forms and orientations. It should be noted that the standard deviation below the mean is smaller than the standard deviation above the mean. This is a consequence of using the log-normal distribution to predict the number of cycles to failure for a given set of test conditions. Figures 11-16 illustrate the relation between the individual test results and the linear least squares regression line for the log-normal distribution. The cumulative log-normal distribution is linear when plotted on normal probability vs. logarithmic scales. The log-normal distribution adequately describes the data for fatigue lives shorter than 10^5 cycles (the strain-controlled and high load tests). For fatigue lives longer than 10^5 cycles, the low load fatigue tests fit the log-normal distribution less perfectly; the data appear to be truncated at the left, which is shown by the horizontal slope for the first few data points. This type of behavior is expected when a guaranteed minimum life exists, i.e., a fatigue limit is being approached. A three parameter Weibull distribution is used to describe this type of situation. However, with at most ten data points available, there is an insufficient amount of data to confidently specify the three parameters of the Weibull distribution.

Figures 11-16 are replotted in Figs. 17-19 to illustrate the effect of product form and orientation. The fatigue lives for the extrusion specimens consistently show a larger dispersion (smaller slope) than the forging specimens. While the extrusions have a higher strength than the forgings, this advantage is partially offset by increased scatter in the fatigue data. Thus, a guaranteed minimum fatigue life for these two product forms may be identical, but for different reasons.

The preliminary strain control results in Fig. 10 suggest that the higher strength extrusion has an advantage only for fatigue lives greater than 10^4 cycles. The data for the load controlled tests in Figs. 18 and 19 show this is generally the case. Interestingly, for

fatigue lives near 10^3 cycles shown in Fig. 17, the forging specimens have over a 20 percent longer fatigue life than extrusion specimens. There is a modest effect of product form, but this effect is a function of the fatigue life. This same kind of behavior is noted with the effect of orientation. For fatigue lives greater than 10^4 cycles (see Figs. 18 and 19), the L orientation is stronger than the L-T orientation. For fatigue lives near 10^3 cycles, the opposite is true (see Fig. 17). These observations on the effect of product form and orientation, however, must be tempered with the realization that as trends are tested with a non-parametric procedure called the Kruskal-Wallis Test, differences are detected if a large α (ten percent) is used as a criterion.

As discussed in Section 4.1, a record of the specimen locations within the two product forms is made to test whether this parameter has any systematic effect on the measured fatigue lives. Table 9 gives the mean, standard deviation, and the number of observations comparing the effect of the edge and the middle locations on the fatigue life for the three different tests. In light of the large values of the standard deviations, no trends are identified. A similar situation occurs when the effect of the surface and the center locations (defined in Fig. 2) of the forging are tested. These results are consistent with the observations of Walker[19] who noted a variation in metallurgical structure exists as a consequence of non-uniform metal flow. This creates subtle differences in the tensile properties within P/M extrusions, but this variation is insignificant when comparisons are made between P/M and I/M products.

In order to place the present program results into perspective, the load control data for the CT91 extrusions given in Figs. 13 and 14 are shown on a conventional S-N plot, Fig. 20. The scatter bands for P/M CT91 and I/M 7050 extrusions from previous work are drawn in for comparison. Clearly, the data at 60 ksi are taken near the knee of the CT91 S-N curve. Below this point the scatter in fatigue life increases dramatically. A comparison of the scatter bands for the P/M CT91 extrusions suggests that the earlier work[21] drew a narrower scatter band

than is given by the present work. The average fatigue life for the earlier work is smaller than is predicted by the current results. Since the scatter bands for the CT91 and 7050 extrusions from previous work are not based on any statistical analysis, but drawing boundaries around data for tests run at many different loads, it is unreasonable to say the scatter for the P/M CT91 is twice that observed for I/M products. The fact that the scatter band defined for the I/M 7050[20] and the P/M CT91[21] is comparable may suggest that they may represent ±3/4 standard deviations or over 50 percent of the observed data.

7.2 Fractography

7.2.1 Optical Fractography

All the fatigue samples fractured during the detailed smooth fatigue test program (Table 2) are examined at low magnifications using a binocular microscope. Characterizing the general morphology of the failure provides complementary information to the statistical analysis to aid the identification of abnormal failures (i.e., either short or long fatigue lives). Tables 10-12 give the results of the optical fractography, identify which samples are calculated to be statistical outliers (greater than ±1.5 standard deviation from the mean), and indicate which samples are further characterized by SEM-EDX. Samples which are not statistical outliers, but show an unusual failure morphology are frequently chosen for analysis in addition to samples which show abnormal statistical behavior. It should be noted that 15 of the 113 specimens tested, or 11.5 percent, are identified as statistical outliers. This percentage is slightly less than the number of anticipated outliers in designing the test program when a standard deviation of 1.5 is used. Of the 15 statistical outliers, only 20 percent have abnormally short lives. The overwhelming majority of the statistical outliers have fatigue lives longer than the average behavior. This observation is even more significant when it is recalled that the log-normal distribution, which is skewed to the right on a linear scale, is used to identify outliers. This analysis

-13-

provides additional supporting evidence to argue that foreign contaminants and/or processing anomalies are not limiting the P/M aluminum fatigue properties tested in this program.

One interesting trend revealed by the optical fractography is the change in the failure morphology as the fatigue lives increase from approximately 10^3 cycles (the strain control tests) to near 10^5 cycles (the load control tests). Table 13 summarizes the results from Tables 10-12 for the three types of tests. The load control tests typically have a single initiation site with the loading axis perpendicular to the macroscopic fracture plane. The strain control tests are more likely to produce multiple initiation sites with the macroscopic fracture plane at an oblique angle to the loading axis. No correlation was observed between the appearance of multiple initiation or slant fracture and abnormal fatigue lives.

7.2.2 Detailed SEM-EDX Fractography

Tables 14-16 summarize the characteristics of the initiation sites observed for specimens with either short or long fatigue lives. Statistical outliers and samples with unusual fracture morphologies are included in these tables. Without including the latter samples, there would be no examples of short-lived specimens for the strain-controlled tests (Table 14) or the lower load control tests (Table 16).

The shortest lived specimens have the largest inclusions. For example, a 300 μm diameter zinc rich area is identified as the initiation site for the strain-controlled tests (specimen number FLC 39). For the short-lived load controlled tests, initiation sites are typically 70 μm in size. In one case a 300 μm diameter defect is observed (Table 16). The long-lived load control specimens typically have defects between 10 and 30 μm in size. There is an apparent exception to this behavior in sample FTC19, which is classified as a long-lived specimen (see Table 12-d). Its fatigue life is approximately one tenth of the average within its group (Table 16). Thus, the presence of a 50 μm diameter

internal defect, which is nearly twice the size typically found for long-lived load control specimens can be explained as a misclassification. Utilization of all the test data to identify statistical outliers has avoided misclassifying test results. A similar situation of misclassifying long-lived specimens appears in Table 14 with specimen EL 110, which has a 100 μm iron rich ribbon identified as the initiation site. This defect size is greater than the typical values of 10-30 μm defects reported for the strain-controlled tests.

Figure 21 is an overview of a strain controlled specimen which is a statistical outlier. The multiple initiation sites of this sample provide a survey of the various types of defects observed, in addition to an example of secondary cracking noted in Tables 10-12. Figure 11a-e illustrates the types of defects located at the five initiation sites. An irregularly shaped inclusion is found at initiation site A, Fig. 22a. Its spectrum is composed primarily of aluminum with trace amounts of silicon, sulfur, chlorine, potassium, calcium, and iron. It appears to be charging in the beam, suggesting it is non-conductive. Initiation site B has two particles seen at 200X in Fig. 22-b. One is shown in the boxed area at a higher magnification, while the other is within the shadow of the peak near the top of the photograph. The second is visible, because it is charging in the beam. Both show spectrums composed almost entirely of aluminum similar to that found at initiation site A. One of the largest initiation sites is located at C, which has a number of 10 μm diameter inclusions present at the initiation site, Fig. 22-c. These particles are dispersed over a 50 μm square area and appear to be charging in the beam. Their composition is similar to the previous two initiation sites. The line scan shows that these particles contain a measurable amount of silicon. Figure 22-d shows that the second large initiation site, D, has three 0.5 μm diameter particles spaced equidistant along a 50 μm line defined by the intersection between the fracture plane and the polished surface. The spectrum of the particles shows the presence of aluminum, with trace amounts of magnesium,

silicon and phosphorus. The last initiation site contains a massive inclusion approximately 150 µm in diameter, Fig. 22-e, and the spectrum shows only the presence of aluminum. The 500X image shows three small fingers extending out from the inclusion in the lower right hand portion of the photograph. This suggests the inclusion may have been connected to something larger.

Figure 21 illustrates the types of defects most frequently found at the fatigue initiation sites: aluminum rich inclusions with trace amounts of silicon, sulfur and calcium. These inclusions are believed to be oxides, as they appear to be charging when they are imaged with secondary electrons (SE). To further support this contention, these defects are observed with the image formed by the back-scattered electrons (BSE). Figure 23 shows an example from an extrusion and a forging specimen which compares the two different types of images. The BSE images of the defects are a darker grey than the base metal, the opposite contrast of the SE image. Since the BSE signal increases with average specimen atomic number[22], it is concluded that the defects have a smaller effective atomic number than the surrounding base metal. The defects contain elements lighter than those which can be detected by the energy dispersive X-ray spectrometer (EDX), namely, sodium. Within this group of elements, oxygen is the logical candidate, suggesting the inclusions are alumina with trace amounts of silicon, sulfur and calcium.

In addition to the aluminum rich oxide inclusions, two other types of defects are identified at the fatigue crack initiation sites. They are transition metal inclusions (e.g., Fe, Zn) and enriched areas of either silicon or grain boundary alumina which form microstructural boundaries. These other types of initiation sites are typically found in approximately one-third of the initiation sites, as can be seen by inspection of Tables 14-16 (nine out of 28 initiation sites).

Figures 24 and 25 give examples of transition metal inclusions
found at the initiation sites.   Figure 24 shows a line profile of the
zinc X-ray signal as the electron beam is traced across the initiation
site of a forging tested at a maximum stress of 66 ksi (455 MPa).
Figure 25 is an example of a ferrous rich inclusion found at the initia-
tion site of an extrusion tested at a maximum stress of 60 ksi (415 MPa).
The zinc rich inclusion is approximately 70 μm in diameter and is asso-
ciated with a specimen with an abnormally short fatigue life.   The fer-
rous rich inclusion is approximately 15 μm in diameter.   This size is
typically found in other examples of transition metal inclusions.   Since
premature failures are associated with five to ten times larger defects,
this class of inclusion does not adversely affect the fatigue life.

Two examples of areas which form microstructural boundaries
are given in Figs. 26 and 27.   Figure 26-a gives an overview of a forg-
ing which had an internal defect initiate the fatigue crack.   Figures 26-b
and 26-c show the initiation area when the sample is rotated 180° from
the position shown in Fig. 26-a.   Secondary cracking parallel to the
tensile axis is visible in all three views.   In fact, the upper and lower
plateaus seen in Fig. 26-a are connected by a vertical cliff.   At the
base of the cliff is a 50 μm square area with the internal defect.   While
there are rub marks visible at the top of the 2000X image, the lower half
clearly shows a structure which can be described as dendritic in appear-
ance.   Figure 27 shows an example of Si segregation found at the fatigue
initiation site.   The 100X image at the center gives an overview of the
initiation site, while the higher magnification views in the boxed areas
show a distinct change in topography between the surface and the interior
area of the initiation site.   The EDX spectrum shows the exclusive presence
of silicon at the initiation site.

The nature of the fatigue crack initiation sites was further char-
acterized by a precision section technique originally developed on

titanium alloys[3]. One particularly large defect at the initiation site of a short lived extrusion specimen is illustrated in Fig. 28-a. The EDX spectrum of the defect area (Fig. 28-b) compared to the surrounding material shows the presence of aluminum and the absence of zinc, copper and magnesium, which are the primary alloying elements of CT91. Once the defect area is sectioned, Fig. 28-c, it becomes clear that the defect is not an alumina rich grain boundary area, but 3 μm thick splinter.

A particularly unusual fatigue failure in a short lived forging specimen is shown in Fig. 29. The fracture has an internal initiation site with a large F shaped area darker in appearance than the surrounding area, Fig. 29-a. The sample is sectioned as illustrated in Fig. 29-b. A higher magnification view in Fig. 29-c shows no evidence of rub marks in the dark areas. However, there is evidence of porosity in the metallurgically polished section below the dark area. Figure 29-d shows another example of the porosity found in the polished section. The porosity is aligned with the elongated grain structure and coincident with the grain boundaries. This is the only occurrence of porosity documented in a mechanically worked product form. Another example of porosity is found in a low cycle fatigue specimen of the as-compacted billet, Fig. 30. The EDX spectrum in Fig. 30-c shows no measurable difference in the composition between the internal defect and the adjacent background area. It should be noted that the fatigue crack did not initiate at the pore of this specimen or any specimen which was given a detailed fractographic examination. However, secondary cracking parallel to the stress axis is frequently noted (Tables 9-12). The presence of porosity in the alumina rich grain boundaries would assist this mode of fracture. Moreover, this mode of cracking is not limited to powder products. Secondary cracking parallel to the stress axis of fatigue specimens has previously been reported for a high strength conventional ingot alloy[23].

In summary, there are three types of defects observed at the fatigue crack initiation sites found in fatigue samples of CT 91 forgings and extrusions:

1.   Alumina inclusions ($\sim$ 60 percent occurrence).

2.   Transition metal inclusions ($\sim$ 30 percent occurrence).

3.   Microstructural boundaries ($\sim$ 10 percent occurrence).

7.3   Verification Testing

The results from Section 7.2 suggest that the short lived specimens are associated with abnormally large defects present at the initiation site.   Tables 14-16 show some exceptions to this behavior for both long-lived and short-lived test specimens.   In addition, the short-lived specimens fatigued at the lowest load, 60 ksi (425 MPa), appear to have a horizontal slope when plotted on normal probability paper, Figs. 13-16. This could mean that the distribution is more asymmetric than the log-normal distribution.   However, the volume of data is insufficient to judge whether this is the case[24], Section 7.1.   Based on the effect of defects in P/M titanium alloys, as illustrated in Fig. 31[25], this question has important implications.   If one is testing material with defects near the fatigue limit, then a highly skewed distribution is anticipated judging by a horizontal line at the fatigue limit.   On the other hand, the distribution will be less skewed in sound material where the S/N curve never becomes horizontal.   The verification test program is designed to answer these questions by increasing the test population at 60 ksi (415 MPa).

Only the extrusion is used in this portion of the program.   Although the forging is stress relieved by compressive deformation, through-the-thickness slices produce an 0.13 inch (3.4 mm) deflection in the 0.5 inch (12.7 mm) high beam, Fig. 32. A simple strength of materials calculation of the residual stresses estimate them to be approximately half of the tensile yield strength, 38 ksi (260 MPa).   Stress relieving extrusions

-19-

by uniformly stretching them into the plastic region is more effective than compressing a forging where the deformation may be non-uniform in an open die.

Twenty additional tests at 60 ksi (415 MPa) maximum cyclic stress increase the test population from ten to thirty. This number of specimens defines four outliers by the ±1.5 standard deviation criteria. There should be two short-lived and two long-lived outliers with this strategy, if the correct distribution is identified.

Tables 27 and 28 give the number of cycles-to-failure, N_f, the specimen number. This data is fitted to the Weibull cumulative probability function, as it is more general than the log-normal distribution[26]. The Weibull expression is linearized so that an iterative linear least squares technique would vary the location parameter, γ, and minimize the standard deviation. The slope and the intercept of the linearized expression gives the shape parameter and scale parameter, respectively. The threshold parameter is varied from zero, the smallest number of cycles to failure. The minimum standard deviation is found to be at 37 and 28 kilocycles for the longitudinal and long-transverse specimen, respectively. Figures 33 and 34 are plots of the data and the best fit line for both cases. The Weibull fit to the longitudinal data (standard deviation = 0.336) is not as good as that for the long-transverse data (standard deviation = 0.207). However, the shape parameter is less than one for both cases. This means that the failure rate is continuously decreasing, as shown in Fig. 35. While P/M aluminum alloy CT91 has a higher fatigue strength than conventional I/M alloys, the potential for further improving the fatigue crack initiation behavior is suggested by the asymmetric shape of the distribution function. It is argued that ideally homogeneous material will have a threshold value of guaranteed fatigue life. Beyond the threshold life there would be a small chance for failure, which would peak to a maximum at the mean life. Figure 35 shows that the probability density function is peaked at or near the

the threshold value.   If a specimen does not fail shortly after the threshold value is reached, then the odds are in favor of it surviving a large number of cycles to failure.

Investigating the short lived specimens suggests while a large ($\sim$ 50-100 µm diameter) inclusion can cause premature fatigue crack initiation, the presence of several smaller inclusions can act in tandem and behave as a single large inclusion[27].   One example is given in Fig. 22-d.   Another example of this phenomenon is shown in Fig. 36 of a short-lived L-T extrusion specimen.   Thus, the clustering of small inclusions explains the early fatigue crack initiation in several cases.

8.0   CONCLUSIONS

Based on the results of the notched fatigue tests, it is concluded that neither product form nor orientation significantly changes the fatigue strength at 10^7 cycles.   For severe notches there is no advantage to using P/M alloy CT91 over conventional high strength I/M alloys. For notches which simulate fastener holes, the P/M alloy CT91 has a 70 percent higher fatigue strength at 10^7 cycles than conventional aerospace aluminum.

Smooth fatigue tests of P/M alloy CT91 show it to be superior to I/M alloy 7050 (Fig. 20).   Fractographic analysis shows the short-lived specimens to have either larger inclusions at the crack initiation site or several smaller sized inclusions acting in tandem.   The short-lived specimens typically have defects on the order of 100 µm in size; the long-lived specimens typically have inclusions on the order of 10-20 µm.   Three types of defects are noted.   Approximately 60 percent of the time they are aluminum rich oxides as verified by EDX and back-scattered SEM images.   Transition metal inclusions of Ti, Fe, and Zn are observed roughly 30 percent of the time.   The third, and least frequently observed (10 percent) defect is a microstructural boundary. The ancillary testing of the extrusion product form shows the distribution

of the failures to be highly skewed with a large probability of failure to occur immediately after the threshold life is reached. This is interpreted to mean a potential exists to further improve the smooth fatigue behavior of P/M alloy CT91.

References

(1) J. P. Lyle and W. S. Cebulak, "Powder Metallurgy Approach for Control of Microstructure and Properties," presented at TMS-AIME Spring Meeting, Philadelphia, PA, June, 1973.

(2) W. L. Otto, Jr., Metallurgical Factors Controlling Structure in High Strength Aluminum P/M Products, Report No. AFML-TR-76-60, Air Force Materials Laboratory, Wright-Patterson AFB, OH, May 1976.

(3) W. Kerr, D. Eylon, and J. A. Hall, "On the Correlation of Specific Fracture Surface and Metallographic Features by Precision Sectioning in Titanium Alloys," Met. Trans., Vol. 7A, September 1976, 1477-1480.

(4) D. Eylon and N. Birla, "Fatigue Origins in Beta III Powder Compact," Met. Trans., Vol. 8A, February 1977, p. 367-369.

(5) D. Eylon and J. M. Hyzak, "An Investigation of Fatigue Origins in Superalloy Powder Compacts," Met. Trans., Vol. 9A, January 1978, p. 127-129.

(6) J. E. Smugerasky and R. M. German, "Microstructure and Properties of Hot Isostatically Pressed A-286," Met. Trans, Vol. 9A, February 1978, p. 253-259.

(7) S. Bashir, R. Taupin, and S. D. Antolovich, "Low Cycle Fatigue of As-HIP and HIP + Forged René 95," Met. Trans., Vol. 10A, October 1979, p. 1481-1490.

(8) Comparison of Processing Properties and Product Properties of Beta III Titanium Alloy Powder Metal (PM) and Ingot Metal (IM), Report No. AFML-TR-76-89, Air Force Materials Laboratory, Wright-Patterson AFB, OH, June 1976.

(9) D. Webster, R. L. Greene, and R. W. Lawley, "Factors Controlling the Strength and Ductility of High Purity Beryllium Block," Met. Trans., 5, January 1974, p. 91-96.

(10) W. S. Cebulak, Program to Develop High Strength Aluminum Powder Metallurgy Products, Phase IV Scale-Up to 3200 lb. Billet, Final Report, Contract DAAA25-72-C-0593, April 1977.

(11)   R. E. Sanders, Jr., W. L. Otto, Jr., and R. J. Bucci, Fatigue Resistant Aluminum P/M Alloy Development, Final Report, Contract F33615-77-C-5174, September 1979.

(12)   Statement of Work, Solicitation No. F33615-80R-5039.

(13)   M. E. Dalfonso, Alco Technical Center, private communication, 8 September 1981.

(14)   Charles S. Yen, "Fatigue Statistical Analysis," Metal Fatigue: Theory and Design, ed. by Angel F. Madayag, New York, John Wiley & Sons, Inc., p. 140-169 (1968).

(15)   R. E. Little and E. H. Jebe, Manual on Statistical Planning and Analysis for Fatigue Experiments, ASTM Special Technical Publication 588, American Society for Testing and Materials (1979).

(16)   R. E. Little, "Estimating the Median Fatigue Limit for Very Small Up-and-Down Quantal Response Tests and for S-N Data with Runouts," Probabilistic Aspects of Fatigue, ASTM STP 511, American Society for Testing and Materials, 1971, p. 29-42.

(17)   Harry William Antes, Role of Deformation Processing on the Fatigue Behavior of a High Strength Powder Metallurgy Aluminum Alloy, Ph.D thesis, Drexel University, June 1979.

(18)   C. Y. Kung and M. E. Fine, "Fatigue Crack Initiation and Micro Crack Growth in 2024-T4 and 2124-T4 Aluminum Alloys," Met. Trans., to be published.

(19)   John Andrew Walker, The Microstructure and Properties of Extruded P/M CT91-T7X151, M.S. Thesis, Georgia Institute of Technology, December 1980.

(20)   J. T. Staley, et al., Aluminum Alloy 7050 Extrusions, Final Report, Contract F33615-73-C-5015, March 1977.

(21)   S. J. Donachie, High Strength P/M Aluminum Mill Products, Interim Report for Jan. 1, 1980-June 30, 1980, Air Force Contract F36615-79-C-5160.

(22)   J. W. Colby, "Backscattered and Secondary Electron Emission as Ancillary Techniques in Electron Probe Analysis," Adv. Electron Phys. Suppl. 6., ed. A. J. Tousimis and L. Martin, Academic Press, New York, 1969, p. 177-196.

(23)   J. S. Santner and D. Eylon, "Fatigue Behavior and Failure Mechanisms of Modified 7075 Aluminum Alloys," Met. Trans., 10A, July 1979, p. 841-848.

(24)   C. Daniel and F. S. Wood, Fitting Equations to Data, Wiley-Interscience, New York, 1961.

(25)   D. Eylon, Y. Mahajan, N. R. Ontko, and F. H. Froes, "Fatigue Crack initiation of Titanium Alloy Powder Compacts, Powder Metallurgy of Titanium Alloys, ed. F. H. Froes and J. E. Smugerasky, Conference Proceedings at the 109th AIME Annual Meeting, Las Vegas, NV, Feb. 26-28, 1980, p. 93-102.

(26)   W. Weibull, "A Statistical Distribution Function of Wide Applicability," J. Appl. Mechanics, 1951.

(27)   H. T. Corten, "Micromechanics and Fracture Behavior of Composites," Modern Composite Materials, ed. L. J. Broutman and R. H. Krock, Addison Wesley Pub. Co., Inc., 1967, p. 27-105.

Table 1

NOTCHED AXIAL FATIGUE TESTING PROGRAM

K_t	$K_t = 3$				$K_t = 10$				Total
Product Form	P/M Forging		P/M Extrusion		P/M Forging		P/M Extrusion		
Orientation	L	LT	L	LT	L	LT	L	LT	
Preliminary Testing	2	2	2	2	2	2	2	2	16
Detailed Testing	10	10	10	10	10	10	10	10	80
Total	12	12	12	12	12	12	12	12	96

Table 2

DETAILED AXIAL SMOOTH FATIGUE TESTING PROGRAM

Product Form	Forging		Extrusion		Billet	Total
	L	L-T	L	L-T	L*	
S_1 ($N_f = 2 \times 10^5$)	10	10	10	10	2	42
S_2 ($N_f = 5 \times 10^4$)	10	10	10	10	2	42
ε ($N_f = 10^3$)	7	7	7	7	1	29
	27	27	27	27	5	113

* This orientation is only applicable if the billet
  is subsequently formed into a single upset
  plus draw forging.

Table 3

Tensile Properties of P/M CT91 Alloy Forging, Extrusion, and Billet
(SI Units)

Product Form	Longitudinal Properties				Long Transverse Properties			
	Tensile Strength (MPa)	Yield Strength (MPa)	EL (%) (0.5" G.L.)	RA (%)	Tensile Strength (MPa)	Yield Strength (MPa)	EL (%) (0.5" G.L.)	RA (%)
Extrusion								
EL1-13	623.3	575.9	15	25.3				
ET1-13					616.3	575.2	16	25.1
EL2-12	624.0	577.2	14	20.2				
ET2-12					620.5	577.2	16	28.3
EL3-P1	626.6	580.0	17	29.2				
ET3-P1					605.2	570.3	17	26.3
EL3-P2	635.2	590.5	14	22.8				
ET3-P2					615.6	569.6	16	25.2
Average	627.5	580.7	15	24.4	614.4	573.1	16.3	26.2
Forging								
FTS6					575.9	520.0	15	25.0
FTS8					577.9	524.9	18	35.1
FLS30	594.0	542.3	18	28.9				
FLS32	591.2	538.2	19	34.6				
FTC38					569.6	503.3	16	27.5
FTC40					567.5	506.7	17	30.8
FLC8	576.5	520.7	25	36.7				
Average	587.0	534.0	20.7	33.4	572.7	513.7	16.5	29.6
Billet								
B7	522.1	557.9	15	23.7				
B12	544.4	483.0	17	28.5				
Average	533.3	470.5	16	26.1				

Table 4

Tensile Properties of P/M CT91 Alloy Forging, Extrusion, and Billet (English Units)

Product Form	Longitudinal Properties				Long Transverse Properties			
	Tensile Strength (ksi)	Yield Strength (ksi)	EL (%) (0.5" G.L.)	RA (%)	Tensile Strength (ksi)	Yield Strength (ksi)	EL (%) (0.5" G.L.)	RA (%)
Extrusion								
EL1-13	89.3	82.5	15	25.3				
ET1-12					88.3	82.4	16	25.1
EL2-12	89.4	82.7	14	20.2				
ET2-12					88.9	82.7	16	28.3
EL3-P1	89.7	83.1	17	29.2				
ET3-P1					86.7	81.7	17	26.3
EL3-P2	91.0	84.6	14	22.8				
ET3-P2					88.2	81.6	16	25.2
Average	89.9	83.2	15	24.4	88.0	82.1	16.3	26.2
Forging								
FTS6					82.5	74.5	15	25.0
FTS8					82.8	75.2	18	35.1
FLS30	85.1	77.7	18	28.9				
FLS32	84.7	77.1	19	34.6				
FTC38					81.6	72.1	16	27.5
FTC40					81.3	72.6	17	30.8
FLC8	82.6	74.6	25	36.7				
Average	84.1	76.5	20.7	33.4	82.05	73.6	16.5	29.6
Billet								
B7	74.8	65.6	15	23.7				
B12	78.0	69.2	17	28.5				
Average	76.4	67.4	16	26.1				

Table 5

$K_t = 3$ Test Results

Extrusion

	L			L-T	
S_{max} ksi (MPa)	Spec. No.	N_f	S_{max} ksi (MPa)	Spec. No.	N_f
19 (130)	EL 204	134	19 (130)	ET 301	89
	EL 203	154		ET 101	90
	EL 301	188		ET 103	114
	EL 101	211		ET 204	177
	EL 201	270		ET 202	994
17 (117)	EL 102	190	17 (117)	ET 303	130
	EL 104	323		ET 102	297
	EL 304	10,000*		ET 304	10,375*
	EL 303	10,775*		ET 201	10,740*
	EL 202	11,750*		ET 203	14,400*

Forging

	L			L-T	
S_{max} ksi (MPa)	Spec. No.	N_f	S_{max} ksi (MPa)	Spec. No.	N_f
19 (130)	FLS 16	137	18 (124)	FTC 11	165
	FLC 16	243		FTC 20	170
	FLC 1	268		FTS 7	250
	FLS 1	449		FTS 30	493
	FLS 13	527		FTS 11	10,923*
17 (117)	FLC 7	574	15 (103)	FTS 26	10,264*
	FLS 24	1,184		FTC 26	10,529*
	FLS 7	1,324		FTC 15	10,715*
	FLC 13	5,671		FTS 15	11,580*
	FLC 20	21,845*		FTC 30	15,717*

* Test terminated.

30

Table 6

$K_t = 10$ Test Results

	Extrusion						Forging					
	L			L-T			L			L-T		
S_{max} ksi (MPa)	Spec. No.	N_f	S_{max} ksi (MPa)	Spec. No.	N_f	S_{max} ksi (MPa)	Spec. No.	N_f	S_{max} ksi (MPa)	Spec. No.	N_f
12 (96)	EL 107	74	12 (96)	ET 108	127	12 (96)	FLS 3	129	12 (96)	FTS 28	204
	EL 105	108		ET 307	171		FLS 9	181		FTC 5	206
	EL 108	168		ET 107	222		FLC 18	227		FTC 18	217
	EL 205	595		ET 305	612		FLS 18	12,038*		FTS 9	391
	EL 208	10,680*		ET 106	1,830		FLC 22	12,585*		FTS 32	334
10 (69)	EL 207	10,075*	10 (69)	ET 206	268	10 (69)	FLS 22	958	10 (69)	FTS 18	289
	EL 307	10,775*		ET 306	746		FLC 9	10,750*		FTC 32	399
	EL 206	10,875*		ET 205	10,685*		FLS 14	12,358*		FTC 9	5,578
	EL 305	11,230*		ET 207	16,686*		FLC 15	18,500*		FTC 28	10,750*
	EL 306	14,775*		ET 308	17,065*		FLC 3	18,589*		FTS 13	18,850*

* Test terminated.

31

Table 7

Notched Fatigue Strength at 10^7 Cycles
(Average of ten tests for each conditions)

Product Form	Orientation	$K_t = 3$	$K_t = 10$
Extrusion	L	17.1 ± 0.5	11.6 ± 0.4
	L-T	17.1 ± 0.5	10.1 ± 0.5
Forging	L	17.1 ± 0.5	11.4 ± 1.7
	L-T	17.2 ± 0.7	9.8 ± 0.6
Average		17.1	10.7

Table 8

Summary of Detailed Test Results Using Log-Normal Distribution
to Estimate Mean and Standard Deviation

| | Extrusion | | | | Forging | | | |
| | L | | L-T | | L | | L-T | |
	Mean	Std. Dev.	Mean	Std. Dev.	Mean	Std. Dev.	Mean	Std. Dev.
Strain Control Tests ε_{max} = 1.65%, S = 0.1	903	-204 +263	971	-255 +346	1,153	-167 +196	1,294	-262 +328
High Load Tests S_{max} = 67 ksi, R = 0.1	64,715	-35,227 +77,310	46,899	-24,002 +49,163	47,418	-22,738 +43,686	45,060	-19,552 +34,539
Low Load Tests S_{max} = 60 ksi, R = 0.1	206,232	-151,579 +571,981	119,821	-81,919 +258,976	245,427	-154,687 +418,386	79,519	-40,385 +82,061

Table 9

EFFECT OF LOCATION WITHIN PRODUCT FORM ON FATIGUE LIFE

Product Form	Orienta- tion	Loca- tion	1.65% Strain Control (Cycles)			67 ksi (462 MPa) Load Control (Kilocycles)			60 ksi (413 MPa) Load Control (Kilocycles)		
			Mean Life	Std Dev	OB	Mean Life	Std Dev	OB	Mean Life	Std Dev	OB
Extrusion	L	Middle	1124	168	2	108	64	6	93	41	4
		Edge	850	216	5	46	22	4	1005	1383	4*
	L-T	Middle	775	144	3	60	40	7	401	533	4
		Edge	1190	320	4	57	55	3	435	522	6
Forgings	L	Middle	1067	39	4	49	28	6	351	290	4
		Edge	1300	283	3	69	50	4	460	686	5**
	L-T	Middle	1574	501	2	49	25	6	182	29	3
		Edge	1224	222	5	57	40	4	64	42	7

*   Two run-outs at 5 million cycles.

** One run-out at 5 million cycles.

Table 10a

EXTRUSION (L) STRAIN CONTROLLED FATIGUE

Cycles to Failure	Percent Maximum Strain	Specimen Number**	Failure Location 1-knife 2-shoulder 3-gage	Type of Initiation 1-single 2-multiple 3-	Initiation Site 1-surface 2-subsurf. 3-interior	Macro Fracture Plane 4 = 45° 9 = 90°	Remarks
630	1.65	EL 116	1	1	1	4	
705	1.65	EL 316	1	1	1	4	
779	1.65	EL 114	1	0	0	4	Smeared fract. surf.
976	1.65	EL 312	3	0	0	4	Smeared fract. surf.
1005	1.65	EL 115	3	1	1	4	
1159	1.65	EL 110*	3	1	3	4	
1243	1.65	EL 119	3	1	1	4	

* SEM-EDX Characterization

≠ Statistical outlier (<615 or >1325)

**Specimen nearest statistical mean is underlined.

Table 10b

EXTRUSION (L–T) STRAIN CONTROLLED FATIGUE

Cycles to Failure	Percent Maximum Strain	Specimen Number**	Failure Location 1-knife 2-shoulder 3-gage	Type of Initiation 1-single 2-multiple 3-	Initiation Site 1-surface 2-subsurf. 3-interior	Macro Fracture Plane 4 = 45° 9 = 90°	Remarks
633	1.65	ET 115	3	1	1	4	
770	1.65	ET 319	3	1	1	4	
910	1.65	ET 314	3	1	1	4	
921	1.65	ET 119	3	1	1	9	
1040	1.65	ET 110	3	1	3	4	Smeared fract. surf. Secondary cr.
1166	1.65	ET 118*	1, 3	2	1, 1	9	Secondary cr.
1643≠	1.65	ET 214*	3	1	3	4	Smeared fract. surf. Secondary cr.

* SEM–EDX Characterization

≠ Statistical outlier (<614 or >1543)

**Specimen nearest statistical mean is underlined.

Table 10c

FORGING (L) STRAIN CONTROLLED FATIGUE

Cycles to Failure	Percent Maximum Strain	Specimen Number**	Failure Location 1-knife 2-shoulder 3-gage	Type of Initiation 1-single 2-multiple 3-	Initiation Site 1-surface 2-subsurf. 3-interior	Macro Fracture Plane 0 = 0° 4 = 45° 9 = 90°	Remarks
1033	1.65	FLS 25	2	1	1	9	Secondary cr.
1053	1.65	FLC 39*	3	1	3	0	Black debris on fract. surface.
1058	1.65	FLS 17	2	1	1	9	
1101	1.65	FLC 50	2	1	1	4	Secondary cracks parallel to T.A.
1122	1.65	FLS 35	2	5	1	4	
1175	1.65	FLS 48	2	5	1	4	
1624 ≠	1.65	FLS 12*	1	5	1	0	Secondary cracks.

* SEM-EDX Characterization

≠ Statistical outlier (<911 or >1459).

** Specimen nearest statistical mean is underlined.

Table 10d

FORGING (L-T) STRAIN CONTROLLED FATIGUE

Cycles to Failure	Percent Maximum Strain	Specimen Number**	Failure Location 1-knife 2-shoulder 3-gage	Type of Initiation 1-single 2-multiple	Initiation Site 1-surface 2-subsurf. 3-interior	Macro Fracture Plane 0 = 0° 4 = 45° 9 = 90°	Remarks
1003	1.65	FTC 2*	3	4	1	0	Secondary cr. parallel T.A.
1100	1.65	FTS 16	3	9	1	0	Secondary cr. parallel T.A.
1131	1.65	FTS 40	2	0	0	9	Smeared fract. surf.
1219	1.65	FTC 21	3	3	1	0	Secondary cr. parallel T.A.
1328	1.65	FTS 14	3	0	0	4	Smeared fract. surf.
1560	1.65	FTC 36	1	2	1	0	Secondary cr. in shoulder
1928#	1.65	FTS 39*	3	1	3	0	2 0° planes connected by vertical cliff.

*SEM-EDX Characterization

Statistical outlier (<922 or >1817)

** Specimen nearest statistical mean is underlined.

-38-

Table 10e

BILLET STRAIN CONTROLLED FATIGUE

Cycles to Failure	Percent Maximum Strain	Specimen Number**	Failure Location 1-knife 2-shoulder 3-gage	Type of Initiation 1-single 2-multiple	Initiation Site 1-surface 2-subsurf. 3-interior	Macro Fracture Plane 0 = 0° 4 = 45° 9 = 90°	Remarks
638	1.65	B 4	1	1	1	0	--
1003	1.65	<u>B 3</u>	2	1	2	0	
1137	1.65	B 11*	3	<u>2</u>	<u>1,3</u>	4	

* SEM-EDX Characterization

≠ Statistical outlier (<570 or >1419).

**Specimen nearest statistical mean is underlined.

Table 11a

Smooth Axial Fatigue, R = 0.1, Extrusion Specimens (L)

Cycles to Failure (kilocycles)	Maximum Stress (ksi)	Specimen Number**	Failure Location 1=Grip 2=Shoulder 3=Gage	Type of Initiation 1=Single 2)=Multiple 3)	Initiation Site 1=Surface 2=Subsurface 3=Interior	Initiation Angle 2=±20° 4=±45° 9=±90°	Remarks
18‡	67.2	EL218*	3	1	1	9	--
22	67.0	EL109	2	1	1	9	Secondary Cr II T.A.
45	66.4	EL314	3	1	2	9	Secondary Cr II T.A.
48	67.6	EL118	3	1	2	9	Secondary Cr II T.A.
64	66.7	EL309*	3	1	1	9	Secondary Cr II T.A.
72	67.0	EL320	2	1	1	9	--
85	67.6	EL215*	2	2	2	9	Secondary Cr II T.A.
131	65.2	EL111	3	1	2	2	Secondary Cr II T.A.
146	66.9	EL209	2	1	1	9	Secondary Cr II T.A.
202	67.2	EL117	3	1	1	9	Secondary Cr II T.A.

* SEM-EDX Characterization.

‡ Statistical outlier (<20 or >210).

**Specimen nearest statistical mean is underlined.

Table 11b

Smooth Axial Fatigue, R = 0.1, Extrusion Specimens (T-L)

Cycles to Failure (kilocycles)	Maximum Stress (ksi)	Specimen Number **	Failure Location 1=Grip 2=Shoulder 3=Gage	Type of Initiation 1=Single 2)=Multiple 3)=	Initiation Site 1=Surface 2=Subsurface 3=Interior	Initiation Angle 2=±20° 4=±45± 9=±90°	Remarks
17	67.1	ET218*	3	1	2	9	--
25	67.5	ET117	3	1	1	9	Secondary Cr II T.A.
25	67.8	ET317	3	1	1	9	--
31	67.5	ET209	2	1	1	9	Secondary Cr II T.A.
34	67.2	ET120	2	1	1	9	--
45	67.8	ET313*	3	1	1	9	Secondary Cr II T.A.
75	67.5	ET113	3	1	1	9	--
87	67.6	ET109	3	1	1	9	Secondary Cr II T.A.
119	67.7	ET116	3	1	1	9	--
131	67.8	ET215*	3	1	1	9	--

* SEM-EDX Characterization.

≠ Statistical outlier (<16 or >138).

** Specimen nearest statistical mean is underlined.

41

Table 11c

Smooth Axial Fatigue, R = 0.1, Forging Specimens (L)

Cycles to Failure (kilocycles)	Maximum Stress (ksi)	Specimen Number**	Failure Location 1=Grip 2=Shoulder 3=Gage	Type of Initiation 1=Single 2)=Multiple 3)	Initiation Site 1=Surface 2=Subsurface 3=Interior	Initiation Angle 2=±20° 4=±45° 9=±90°	Remarks
14 ≠	66.0	FLC35 *	3	1	1	9	Secondary Cr ‖ T.A.
27	66.7	FLC32	3	1	1	9	Secondary Cr ‖ T.A.
30	66.2	FLS5	3	1	1	9	Secondary Cr ‖ T.A.
42	67.6	FLC41	2	1	1	9	--
44	66.2	FLC36*	3	2	1, 3	9	--
54	67.3	FLC21	3	1	2	9	Secondary Cr ‖ T.A.
60	66.7	FLC17	3	1	1	9	Fractured along T.A.
64	67.4	FLC30	3	1	1	9	Secondary Cr ‖ T.A.
94	67.4	FLC29	3	1	1	9	Secondary Cr ‖ T.A.
140 ≠	66.9	FLC44 *	3	1	1	9	Secondary Cr ‖ T.A.

* SEM-EDX characterization

≠ Statistical outlier (<18 or >126).

** Specimen nearest statistical mean is underlined.

Table 11d

Smooth Axial Fatigue, R = 0.1, Forging Specimens (T-L)

Cycles to Failure (kilocycles)	Maximum Stress (ksi)	Specimen Number**	Failure Location 1=Grip 2=Shoulder 3=Gage	Type of Initiation 1=Single 2)=Multiple 3)	Initiation Site 1=Surface 2=Subsurface 3=Interior	Initiation Angle 2=±20° 4=±45° 9=±90°	Remarks
19≠	67.5	FTC23*	3	1	1	9	--
25	66.3	FTC54	2	1	1	9	--
27	67.7	FTS37	2	1	1	9	Secondary Cr II T.A.
33	66.4	FTC12	3	1	1	9	--
49	66.9	_FTC17*_	3	1	1	9	--
49	67.5	FTC1	2	1	1	9	--
57	66.6	FTC56	3	1	1	9	--
59	66.6	FTC31	3	1	1	9	Secondary Cr II T.A.
89	66.9	FTS17	3	1	1	9	--
114≠	66.7	FTS44*	3	1	1	9	--

* SEM-EDX characterization.

≠ Statistical outlier (<19 or >106).

** Specimen nearest statistical mean is underlined.

43

Table 12a

Smooth Axial Fatigue, R = 0.1, Extrusion Specimens (L)

Cycles to Failure (kilocycles)	Maximum Stress (ksi)	Specimen Number**	Failure Location 1=Grip 2=Shoulder 3=Gage	Type of Initiation 1=Single 2)=Multiple 3)	Initiation Site 1=Surface 2=Subsurface 3=Interior	Initiation Angle ±45°=4 ±90°=9 ±20°=2	Remarks
59	59.3	EL315*	3	1	1	9	
65	59.4	EL311	3	1	1	9	
101	59.7	EL319	3	1	1	9	
103	59.5	EL210	3	1	1	9	
148	59.6	EL213	3	1	1	9	
425	59.5	EL112	2	1	1	9	
426	59.7	EL116*	3	1	1	9	2 secondary cracks || to surface of forging
3,067 ≠	59.8	EL310*	2	1	3	2	Obvious bull's eye
5,130	59.6	EL318≠≠	Run out	--	--	--	--
5,981 ≠	59.9	EL212*	3	1	2	9	--

* SEM-EDX characterization.

≠ Statistical outlier (<28 or >1,512).

** Specimen nearest statistical mean is underlined.

≠≠ Run out not included in averaging.

Table 12b

Smooth Axial Fatigue, R = 0.1, Extrusion Specimens (T-L)

Cycles to Failure (kilocycles)	Maximum Stress (ksi)	Specimen Number **	Failure Location 1=Grip 2=Shoulder 3=Gage	Type of Initiation 1=Single 2)=Multiple 3)	Initiation Site 1=Surface 2=Subsurface 3=Interior	Initiation Angle 4=±45° 9=±90°	Remarks
30	60.0	ET211*	3	1	1	9	Secondary Cr II T.A.
33	60.1	ET316	3	1	1	9	--
59	59.3	ET318	2	1	1	9	Secondary Cr II T.A.
74	60.6	ET213	3	1	1	9	--
160	60.5	ET114*	3	1	1	9	Secondary Cr II T.A.
257	59.6	ET220	3	1	1	9	Secondary Cr II T.A.
324	59.3	ET311	3	1	1	9	--
739≠	58.8	ET216*	3	1	1	9	--
1,176≠	59.9	ET111##	1	--	--	--	1,176 K cycles
1,362≠	59.4	ET112##	1	--	--	--	1,362 K cycles

*   SEM-EDX characterization.

≠   Statistical outlier (<21 or >674).

** Specimen nearest statistical mean is underlined.

\#\# Invalid test due to grip failure, data not included in average.

45

Table 12c

Smooth Axial Fatigue, R = 0.1, Forging Specimens (L)

Cycles to Failure (kilocycles)	Maximum Stress (ksi)	Specimen Number**	Failure Location 1=Grip 2=Shoulder 3=Gage	Type of Initiation 1=Single 2)=Multiple 3)	Initiation Site 1=Surface 2=Subsurface 3=Interior	Initiation Angle 4=±45° 9=±90°	Remarks
97	59.5	FLS31*	3	1	1	9	Secondary Cr II T.A.
109	59.5	FLC11	3	1	1	9	
111	59.9	FLS48	3	1	1	90	Secondary Cr II T.A.
159	59.5	FLC34	3	1	1	90	Secondary Cr II T.A.
168	59.1	FLS34	3	1	1	90	
177	59.9	FLS10	3	1	1	90	Secondary Cr II T.A.
544	59.5	FLC5*	3	1	1	90	Secondary Cr II T.A.
652	59.0	FLS23	3	1	1	90	Secondary Cr II T.A.
1,687≠	59.7	FLC42*	3	1	1	90	Secondary Cr II T.A.
5,025≠	59.3	FLS2#	Run out	--	--	--	

*   SEM-EDX characterization

≠   Statistical outlier (<55 or >1,092)

** Specimen nearest statistical mean is underlined.

Run out not included in averaging.

46

Table 12d

Smooth Axial Fatigue, R = 0.1, Forging Specimens (T-L)

Cycles to Failure (kilocycles)	Maximum Stress (ksi)	Specimen Number **	Failure Location 1=Grip 2=Shoulder 3=Gage	Type of Initiation 1=Single 2) Multiple 3)	Initiation Site 1=Surface 2=Subsurface 3=Interior	Initiation Angle 4=±45° 9=±90°	Remarks
34	59.3	FTC46*	3	1	3	9	Secondary Cr II T.A.
36	60.4	FTC10	3	1	1	9	Secondary Cr II T.A.
42	59.9	FTS38	2	1	1	9	Secondary Cr II T.A.
55	59.9	FTC16	3	1	1	9	--
58	59.9	FTC44	3	1	1	9	Secondary Cr II T.A.
68	60.1	FTC14*	3	1	1	90	Secondary Cr II T.A.
150	59.8	FTC3	2	1	1	90	Secondary Cr II T.A.
156	59.2	FTC4	3	1	1	90	Secondary Cr II T.A.
187	59.1	FTS1	3	1	1	90	--
208	59.7	FTC19*	3	1	1	90	--

*   SEM-EDX characterization.

Statistical outlier (<27 or >230)

** Specimen nearest statistical mean is underlined.

47

Table 13

OPTICAL FRACTOGRAPHY SUMMARY

Percentage of Specimens With	Bil-let	1.65% Strain Control				67 ksi (462 MPa) Load Control				60 ksi (413 MPa) Load Control			
		Extrusion		Forging		Extrusion		Forging		Extrusion		Forging	
		L	L-T	L	L-T	L	L-T	L	L-T	L	L-T	L	L-T
ONE INITIATION SITE	66	80	86	57	0	90	100	90	100	100	100	100	100
TENSILE AXIS PERPENDICULAR TO FRACTURE PLANE	66	0	0	43	86	100	100	100	100	100	100	100	100

Table 14

Characteristics of Short and Long Lived Strain Controlled Test Specimens

Spec. No.	N_f (Cycles)	Initiation Site: Size and Chemistry
Short-lived Specimens:		
FLC 39	1053	300 μm dia. Zn rich area.
FTC 2	1003	400 μm dia. Al-Si-S-Ca Oxide (3 sites), 7 μm dia. Si rich phase (one site)
Average	1028	
Long-lived Specimens:		
EL 110	1159	100 μm Fe rich ribbon.
ET 214*	1643*	Smeared fracture surface, no fractography.
ET 118	1166	25 μm dia. Al-Si-S-Ca Oxide (2 sites)
FLS 12*	1624*	30 to 150 μm dia. Al-Si-S-Ca Oxides (5 sites).
FTS 39*	1928*	10 μm dia. Si rich rod (one site), 7 μm dia. Ca rich phase (one site)
B 11	1137	10 μm dia. Al-Si-S-Ca Oxide.
Average	1443	
	1731*	

* Statistical outlier.

49

Table 15

Characteristics of Short and Long Lived Load Controlled Test Specimens
($S_{max} = 67$ ksi)

Spec. No.	N_f (Kilocycles)	Initiation Site: Size and Chemistry
Short-lived Specimens:		
EL 218*	18	40 x 100 μm Mg-Al-S inclusion.
ET 218	17	12 x 60 μm Mg-Zn inclusion.
FLC 35*	14	70 μm dia. Zn rich area
FTC 23*	19	70 μm dia. are Stage I cracking.
Average	17	
Long-lived Specimens:		
ET 215	131	10 x 30 μm Al-S-Ca Oxide
FLC 44*	140	10 μm dia. Al-K-Cl Oxide
FTS 44*	114	7 x 33 μm Al-Si-K-S Oxide
Average	128	

* Statistical outlier.

Table 16

Characteristics of Short and Long Lived Load Controlled Test Specimens
(S_{max} = 60 ksi)

Spec. No.	N_f (Kilocycles)	Initiation Site: Size and Chemistry
Short-lived Specimens:		
EL 315	59	70 μm dia. Mg rich inclusion.
ET 211	30	300 μm dia. Al Oxide (one site), 10 μm dia. Fe inclusion
FLS 31	97	50 μm dia. area Stage I cracking
FTC 46	34	20 μm long cavities in grain boundary
Average	55	
Long-lived Specimens:		
EL 310*	3,067	Smeared fracture surface, no fractography
EL 212*	5,981	7 x 30 μm Al-Si-S-Ca Oxide
ET 216*	739	10 x 30 μm Al-Si-Ti inclusion
FLC 42*	1,687	7 μm dia. Al-Si inclusions
FTC 19	208	50 μm dia. internal area defect.‡
Average	2,336	

* Statistical Outlier.

‡ Surface rather than internal initiation is the norm (see Tables 10-12).

Table 17

Verification Test Results for Extrusions in L Orientation

Spec. No.	N_f (Kilocycles)	$N_f - 37$ (Kilocycles)
EL 3E 5	38	1
14	54	17
315	59	22
EL 311	65	28
1E2	65	28
33	68	31
EL 2E3	68	31
2E4	72	35
2E2	91	54
EL 319	101	64
210	103	66
21	110	73
EL 1E6	145	108
213	148	111
3E4	171	134
EL 1E1	180	143
11	182	145
25	207	170
EL 22	223	186
32	242	205
3E3	267	230
EL 34	346	309
112	425	388
116	426	389
EL 35	520	483
2E1	1,044	1,007
310	3,067	3,050
EL 13	4,859	4,822
318	5,135	5,098
212	5,981	5,944

Table 18

Verification Test Results for Extrusions in L-T Orientation

Spec. No.		N_f (Kilocycles)	$N_f - 28$ (Kilocycles)
ET	3E6	30	2
	211	30	2
	24	31	3
ET	316	33	5
	3E4	46	18
	1E5	47	19
ET	32	55	27
	318	59	31
	34	66	38
ET	213	74	46
	3E5	90	62
	3E2	95	67
ET	1E3	106	78
	25	124	96
	12	134	106
ET	1E1	138	110
	13	145	117
	2E 2	153	125
ET	3E1	155	127
	114	160	132
	33	211	183
ET	22	236	208
	14	244	216
	220	257	229
ET	2E1	265	237
	311	324	296
	3E3	433	405
ET	21	716	688
	216	739	711
	2E3	1,101	1,073
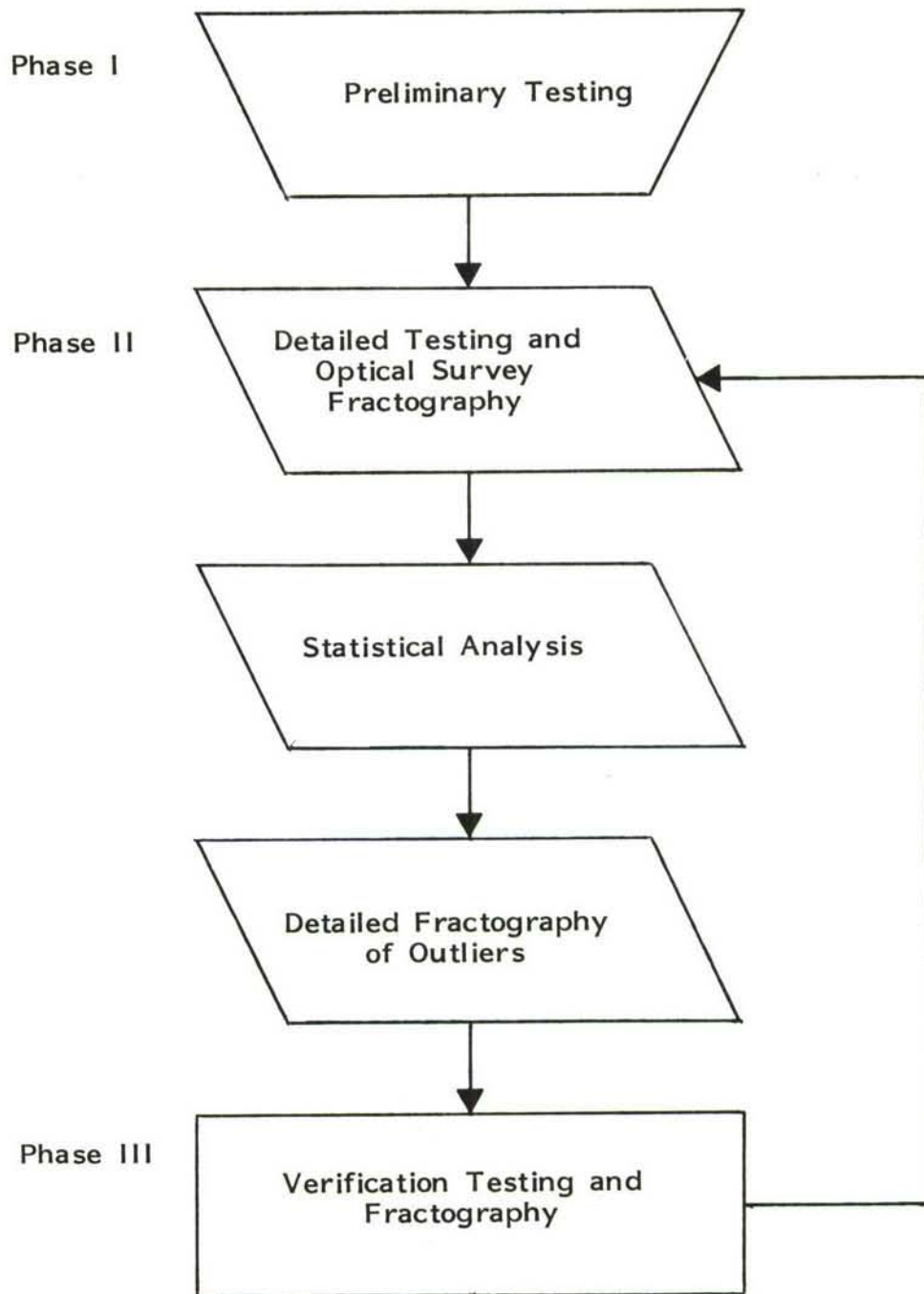
Fig. 1   Flow diagram for determining the sensitivity of CT91 to foreign contaminants and processing anomalies.

(a) Extrusion

1 2

Edge Middle Edge

(b) Forging

Surface
Center
Center
Surface

1 2
3 4

Edge Middle Edge
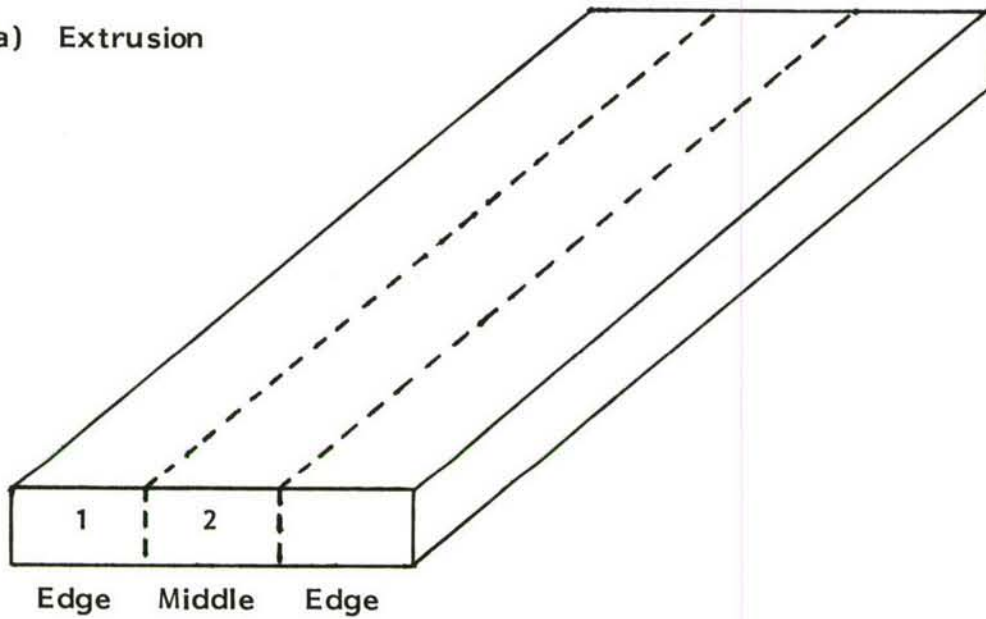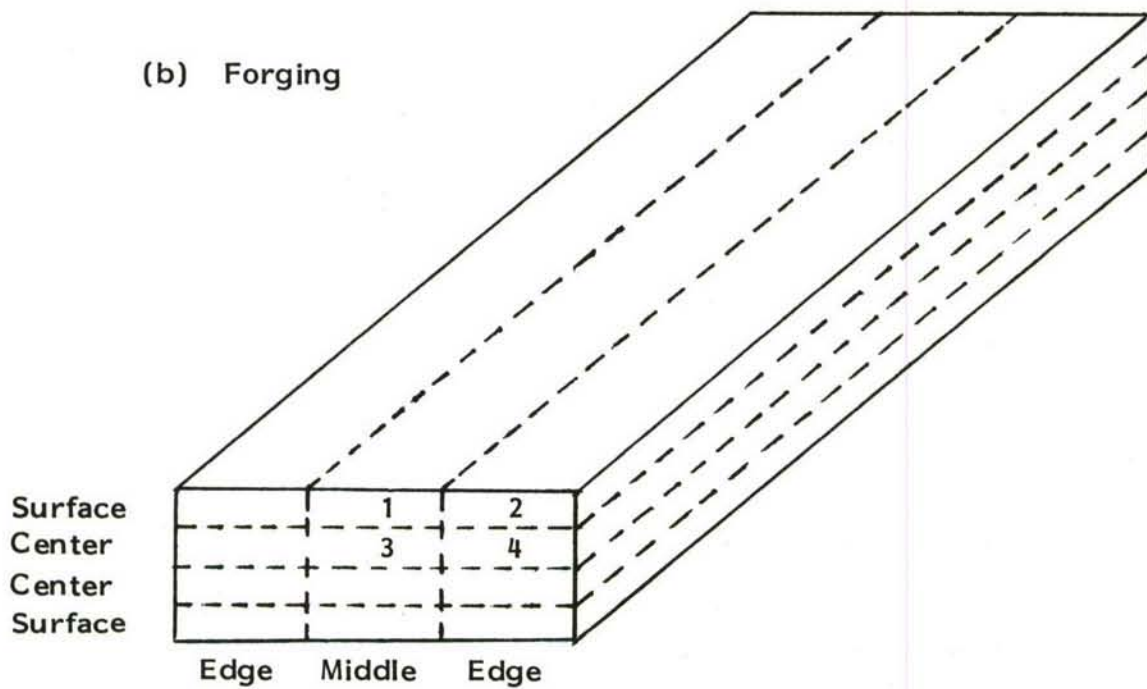
Fig. 2   Schematic diagram showing (a) two regions of different
amounts of local strain for the extrusion, and four differ-
ent regions for the forging.

Detail A

$K_t = 10$

$r = 0.001 \begin{smallmatrix} +0 \\ -0.0005 \end{smallmatrix}$

Note 2

0.090

$K_t = 3$

$r = 0.014 \begin{smallmatrix} +0 \\ -0.0005 \end{smallmatrix}$

0.090

45°C

0.500

$\frac{1}{8}$ D, Note 3

0.386

0.253

Detail A

1.000

0.500

0.500

2.000

1.000

1.000

0.500 x 20 NF BA
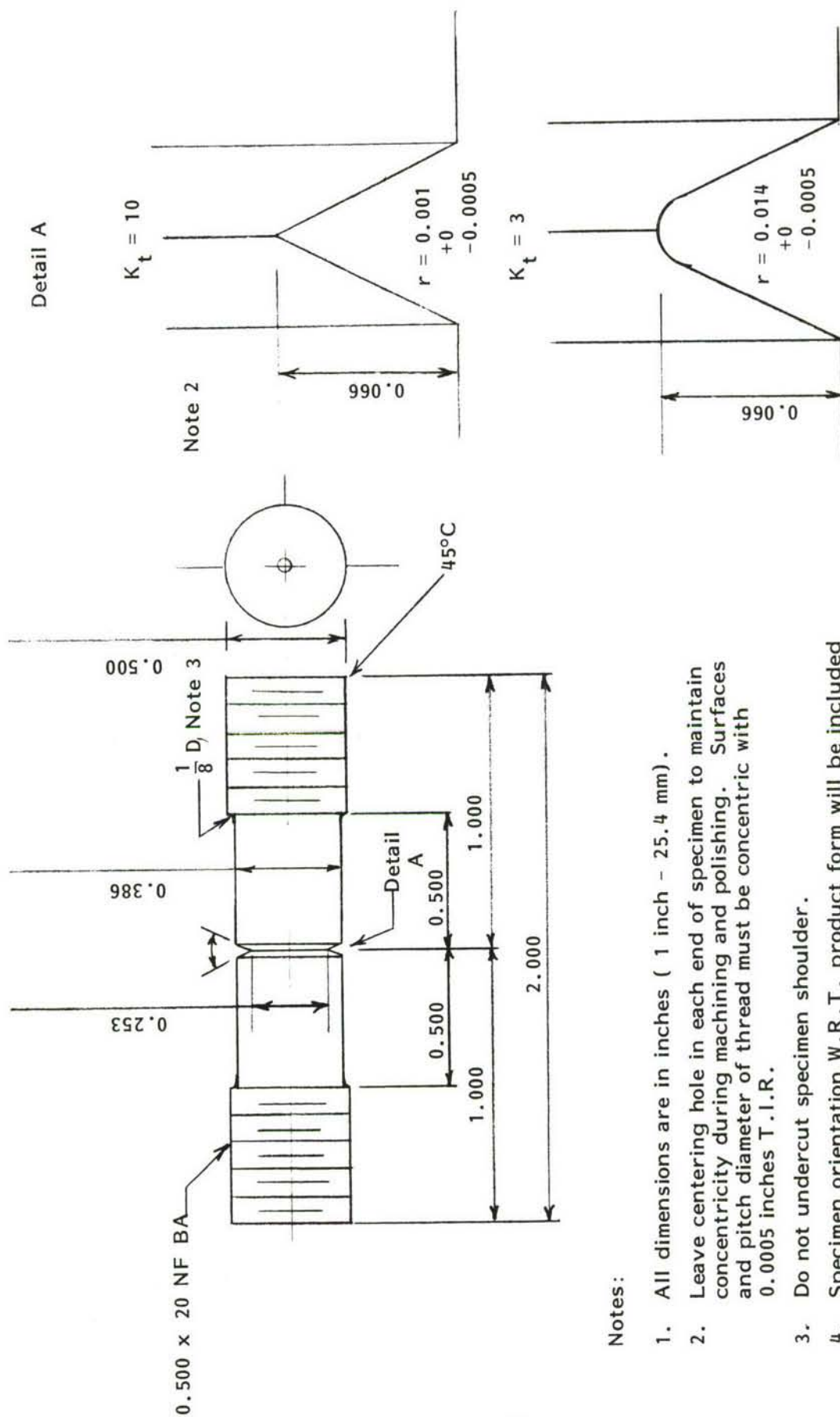
Notes:

1. All dimensions are in inches (1 inch – 25.4 mm).

2. Leave centering hole in each end of specimen to maintain concentricity during machining and polishing. Surfaces and pitch diameter of thread must be concentric with 0.0005 inches T.I.R.

3. Do not undercut specimen shoulder.

4. Specimen orientation W.R.T. product form will be included with the identification.

5. Use MRL procedure for round notched fatigue specimens to machine specimen.

Fig. 3   Notched Fatigue Specimen Design.

(a)
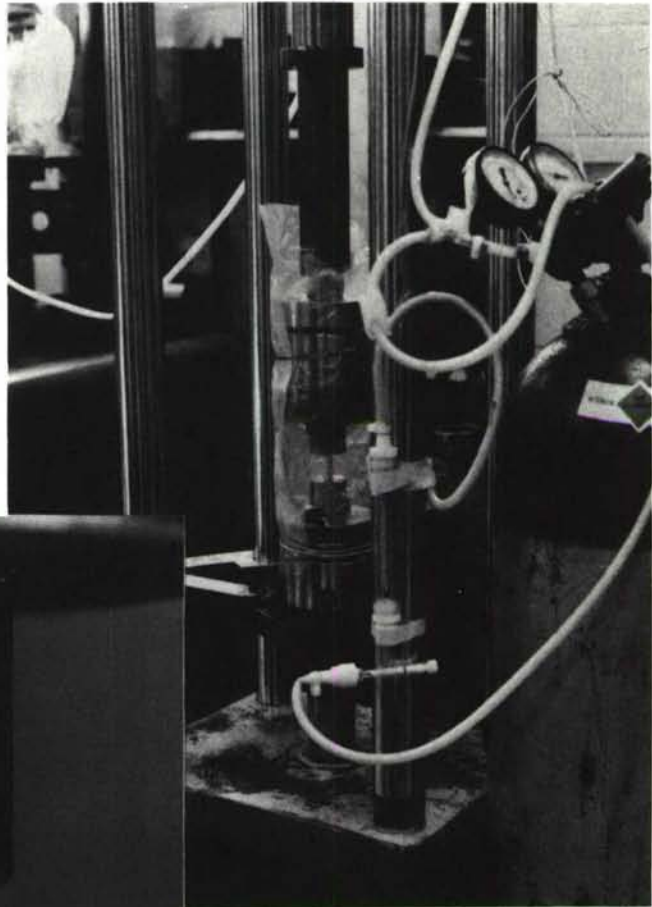
(b)
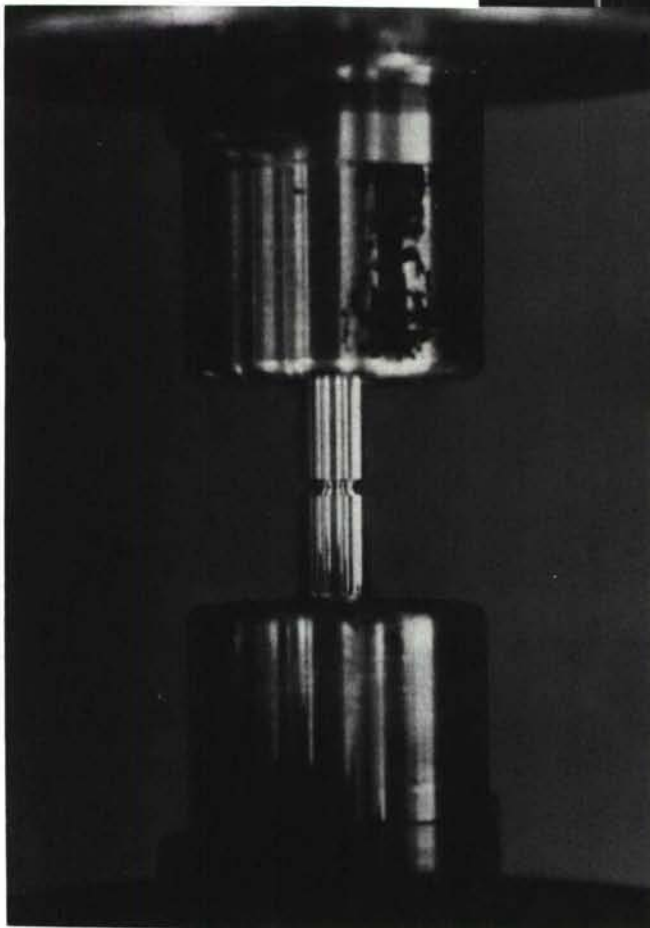
Fig. 4   Experimental arrangement for notched fatigue tests, (a),
and close-up of specimen in fixturing, (b).

(0.500 x 20 NF Thread)
Both sides

22.23 (0.875) D, Note 3

4.75 (0.188) D, Note 1

Note 2

Note 1

$\frac{1.60}{(0.063)}$ 45°C

12.70
(0.500)

12.70
(0.500)

25.40
(1.000)

12.70
(0.500)

(0.500)
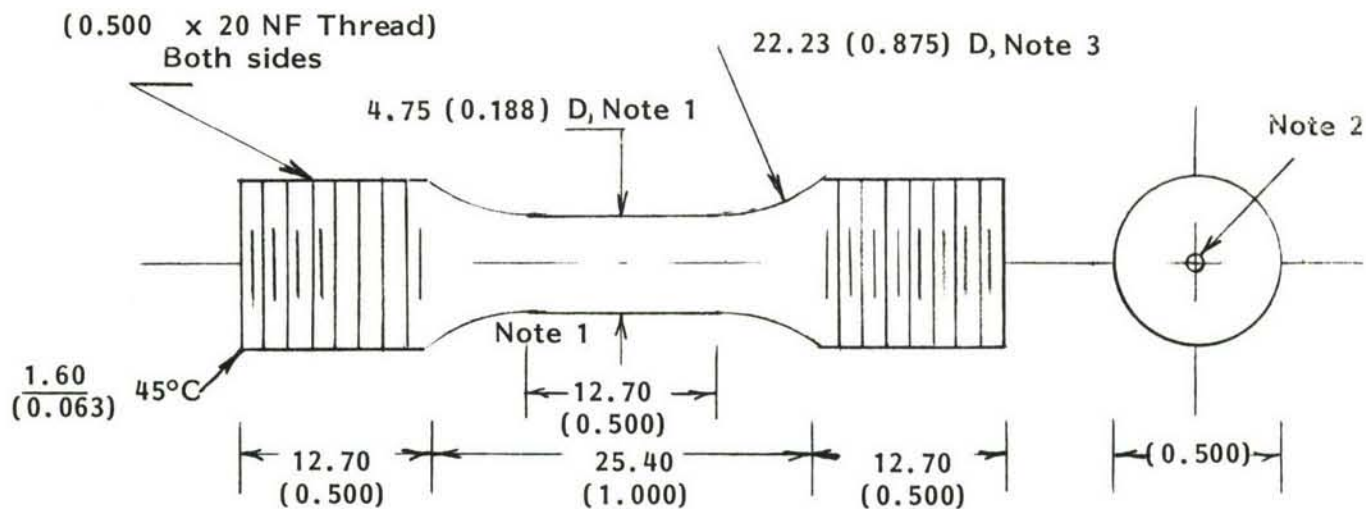
Notes:

1. Use MRL Procedure for Round smooth fatigue specimen to machine specimen and prepare surface for testing.

2. Leave center holes in each end of specimen to maintain concentricity during machining and polishing. Surfaces and pitch diameter of thread must be concentric within 0.0005 in. TIR.

3. Do not undercut specimen shoulder.

4. Specimen orientation W.R.T. product form will be included with the identification.

5. All dimensions are in mm (inches).

Fig. 5   Preliminary Smooth Fatigue Specimen.

Test Number	Product (Orient.)	Max. Stress (ksi)	Kilocycles-to-Failure
1	EXT (T)	39.5	440
2	FOR (L-T)	39.9	401
3 *	FOR (L-T)	41.3	4,652 (run-out)
4 *	FOR (L)	57.8	516
5 *	EXT (L-T)	57.5	37

* Gage diameter reduced from 0.250 inches to 0.1875 inches.

Fig. 6   Results of preliminary smooth fatigue tests.
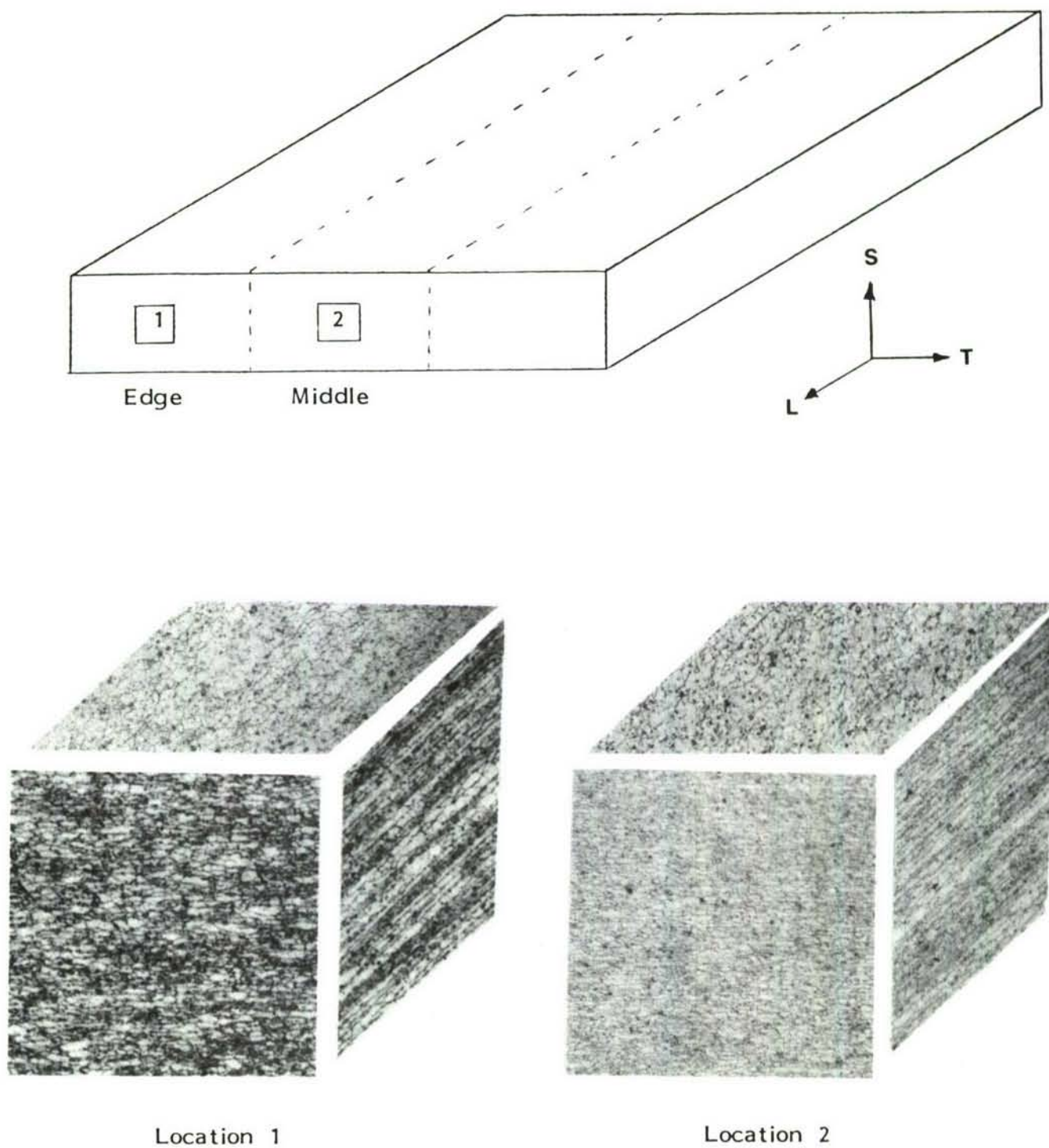
Fig. 7   CT91 extrusion microstructure (500X).

Surface		1		2	
Center					
Center					
Surface					

Edge   Middle   Edge

S
T
L
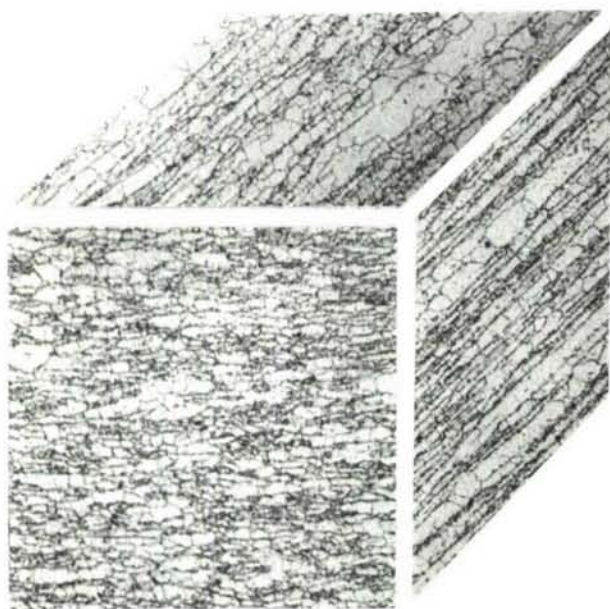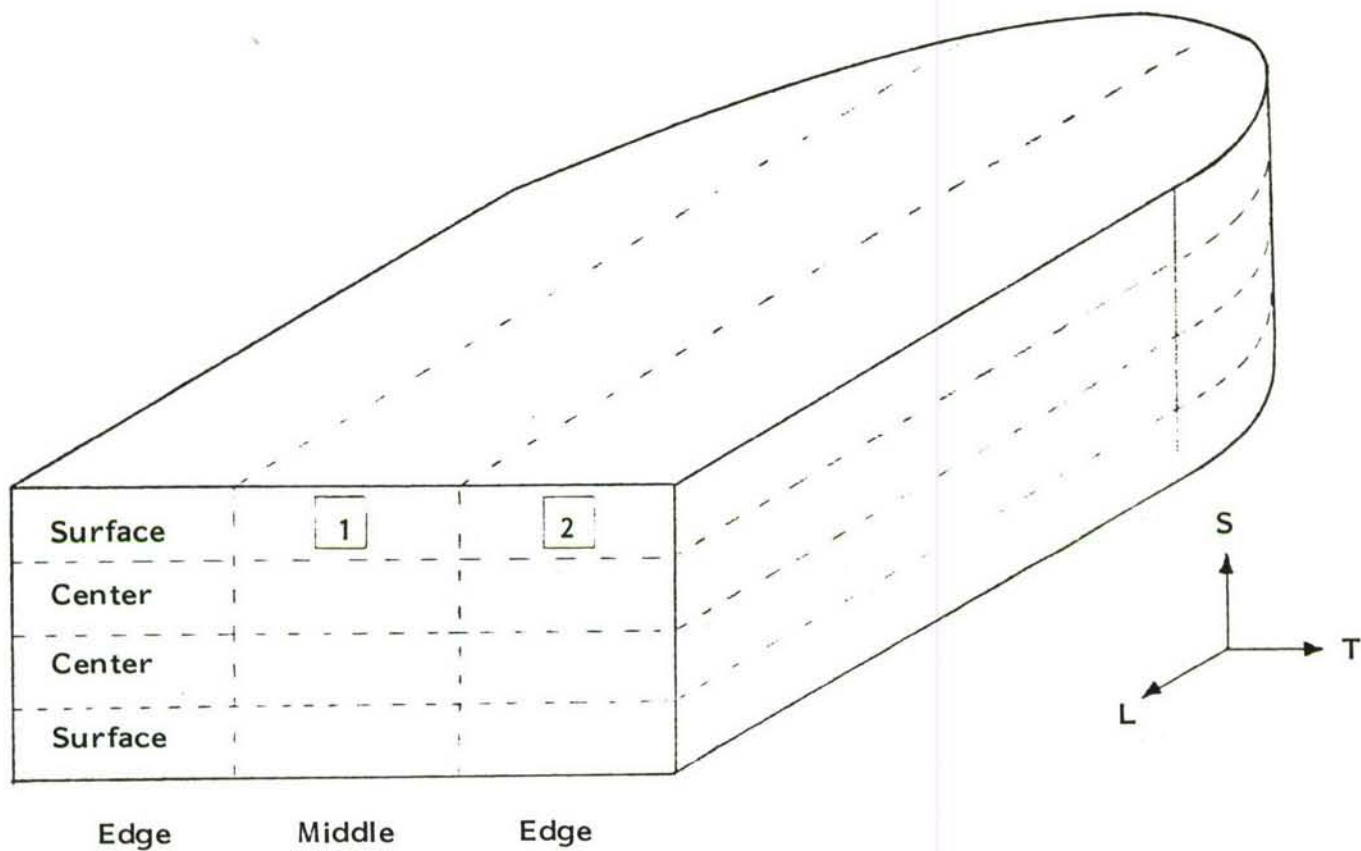
Location 1

Location 2

Fig. 8a   CT91 forging microstructure (500X) locations defined in Fig. 2.

61

Surface

Center   3   4

Center

Surface

Edge   Middle   Edge

S

T

L
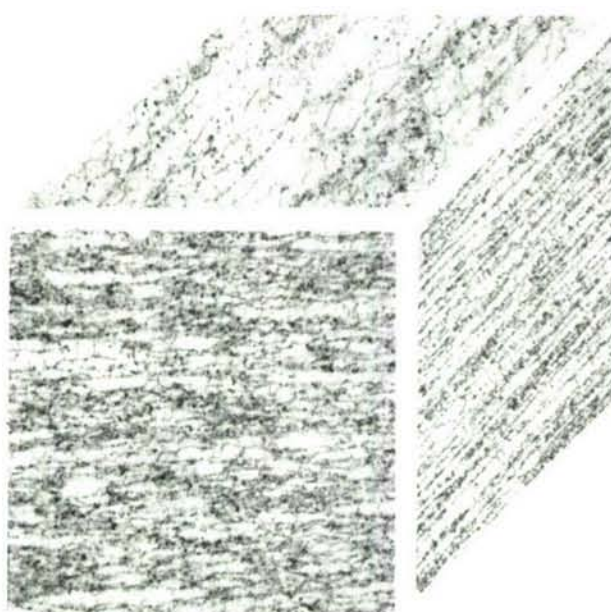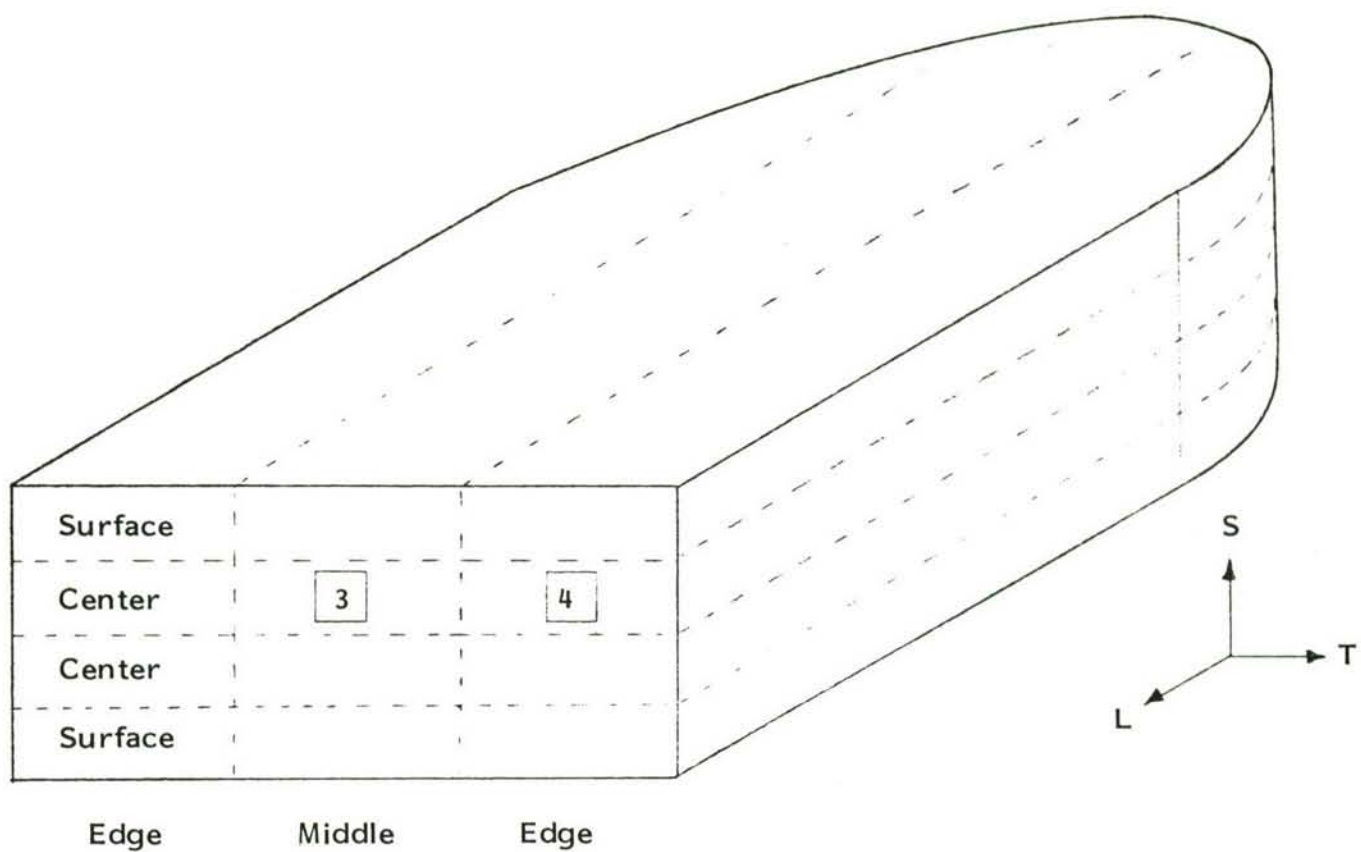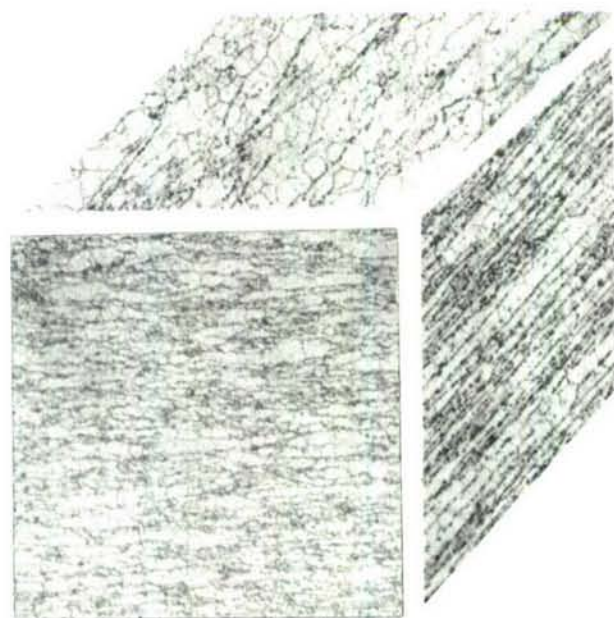
Location 3   Location 4

Fig. 8b   CT 91 Forging Microstructure (500X).
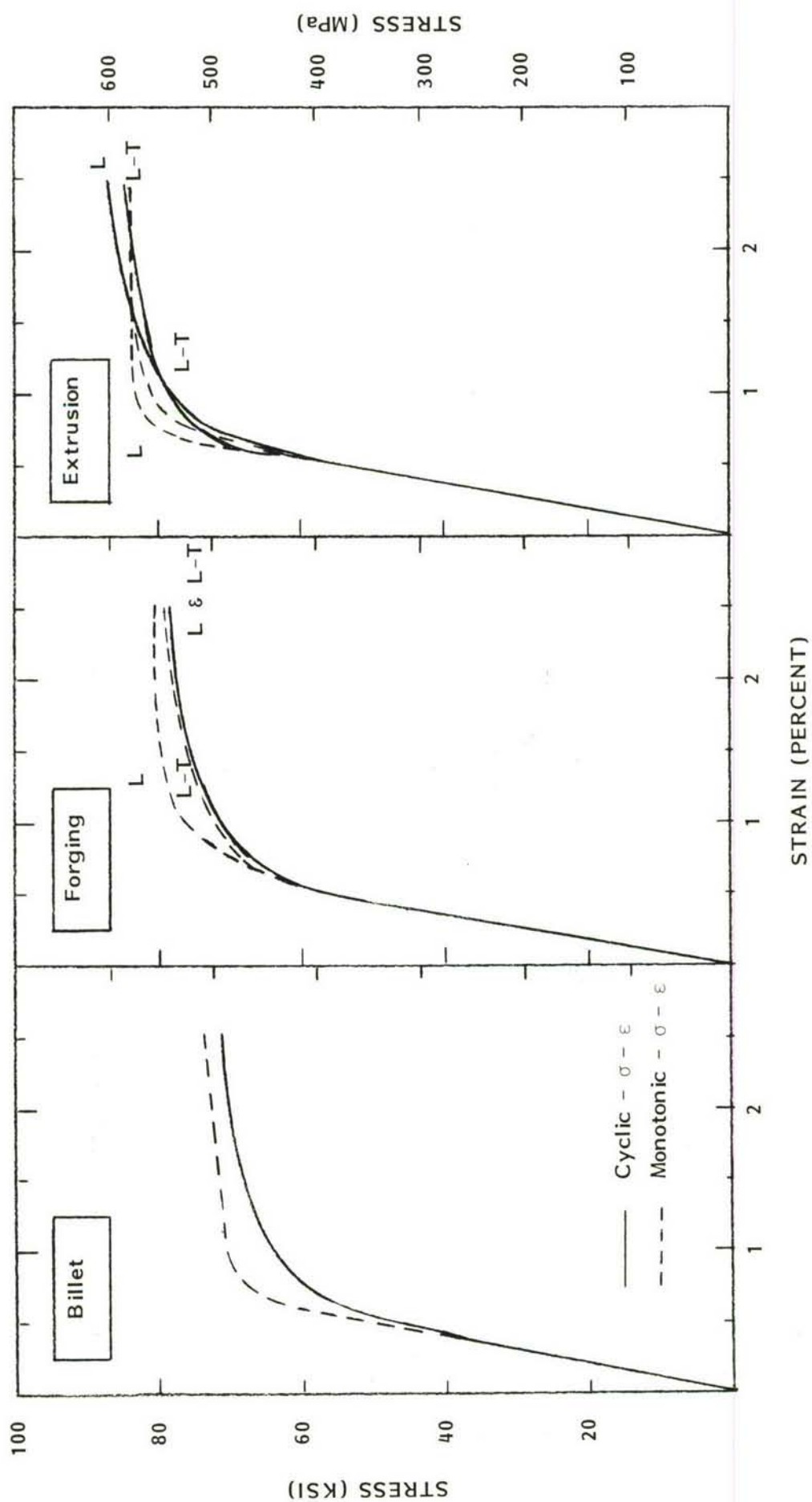
Fig. 9   Comparison of monotonic and cyclic stress-strain curves.

63
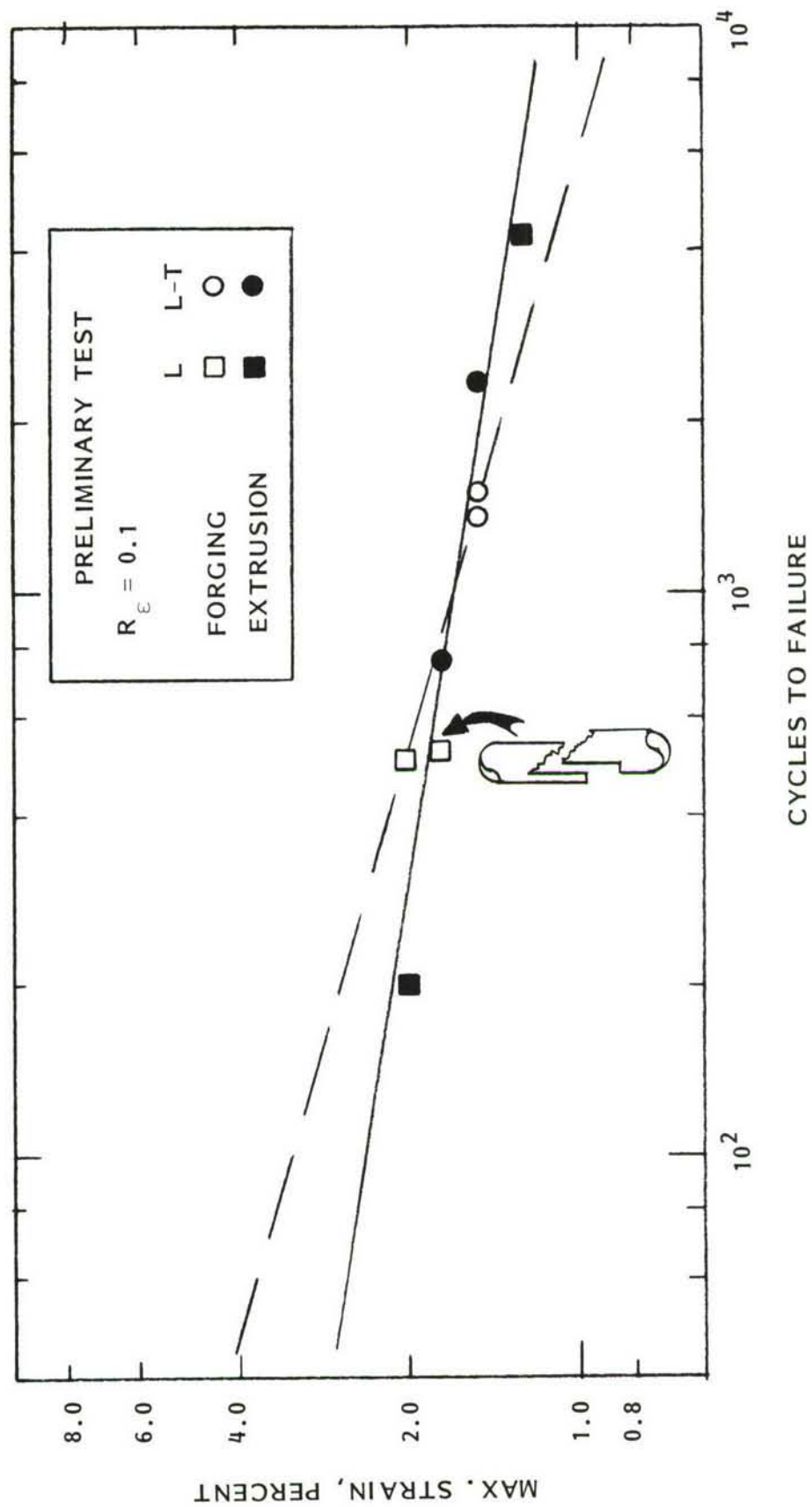
Fig. 10   Preliminary strain control   low cycle fatigue tests.
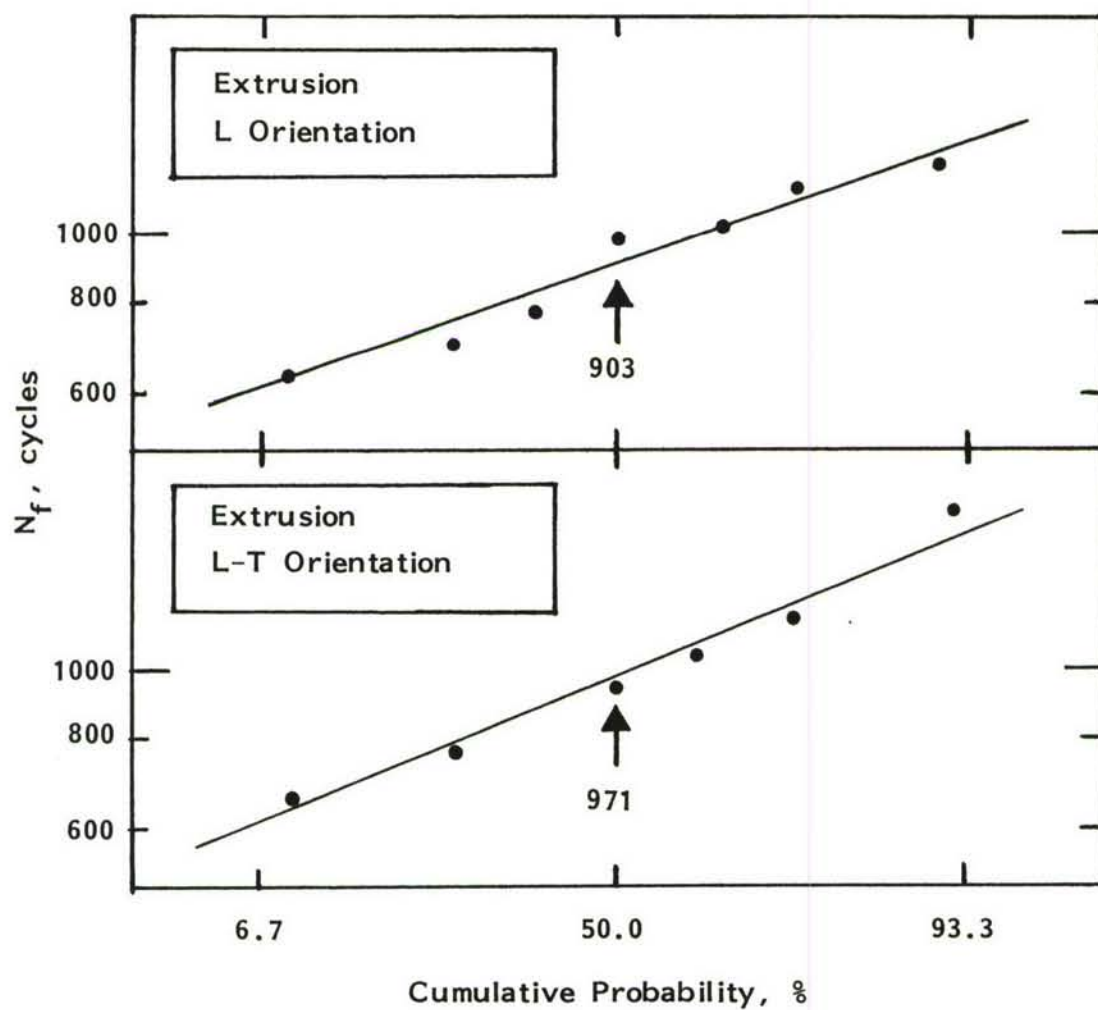
Fig. 11 Strain control (1.65 percent maximum strain) fatigue test
results for extrusions.
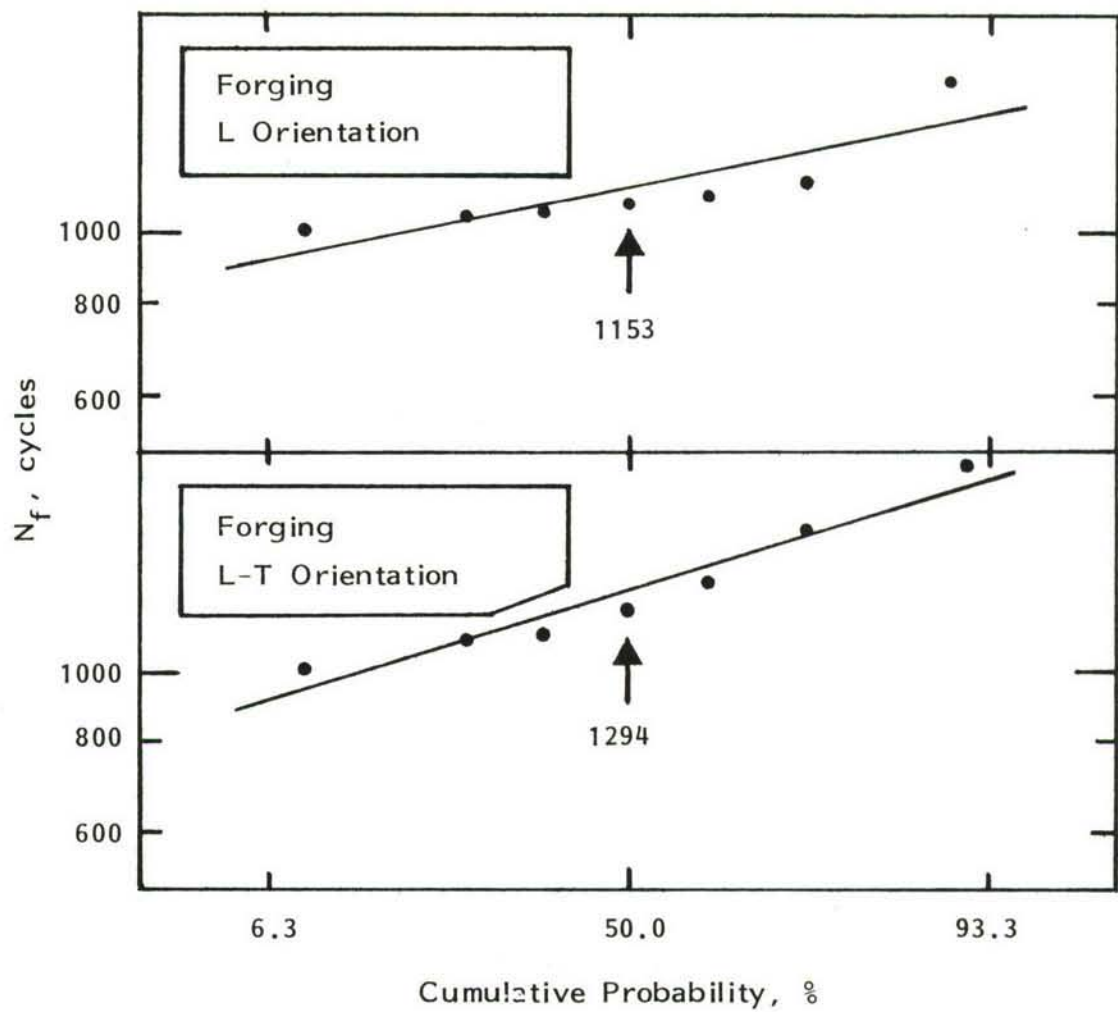
Fig. 12   Strain control (1.65 percent maximum strain) fatigue
test results for forgings.
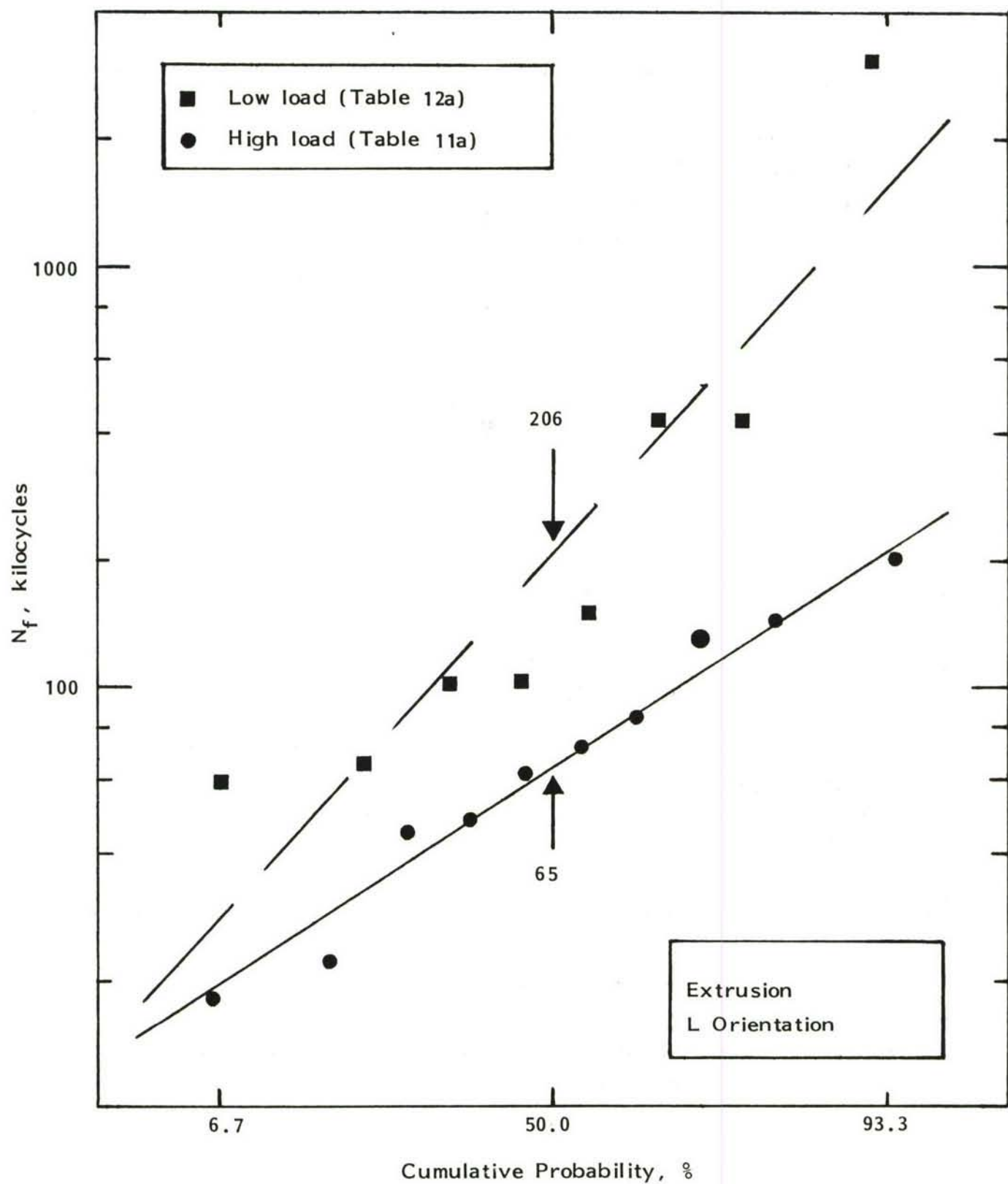
Fig. 13 Load control test results for the L orientation specimens from the extrusion.
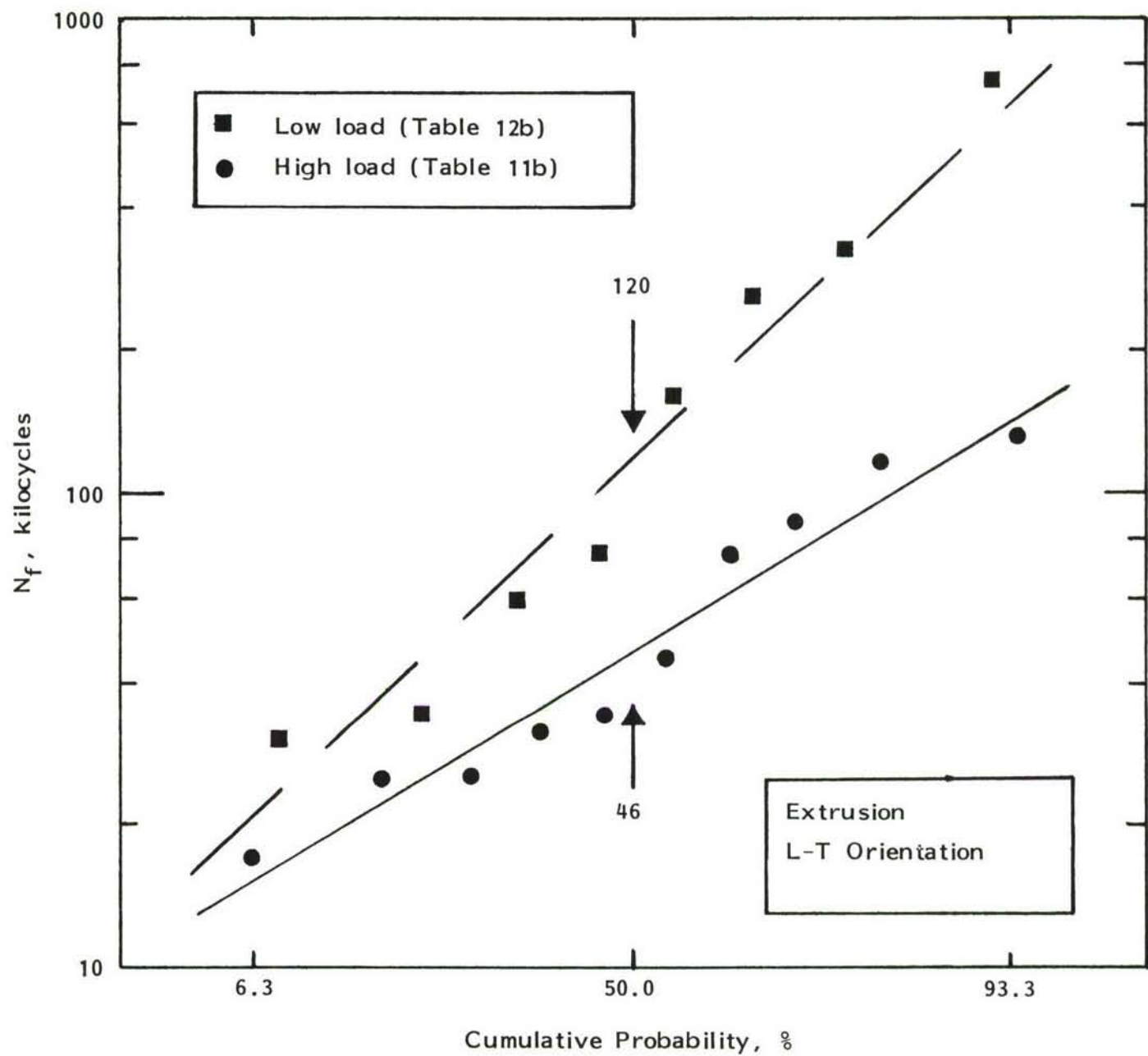
Fig. 14   Load control test results for the L-T orientation specimens
           from the extrusion.
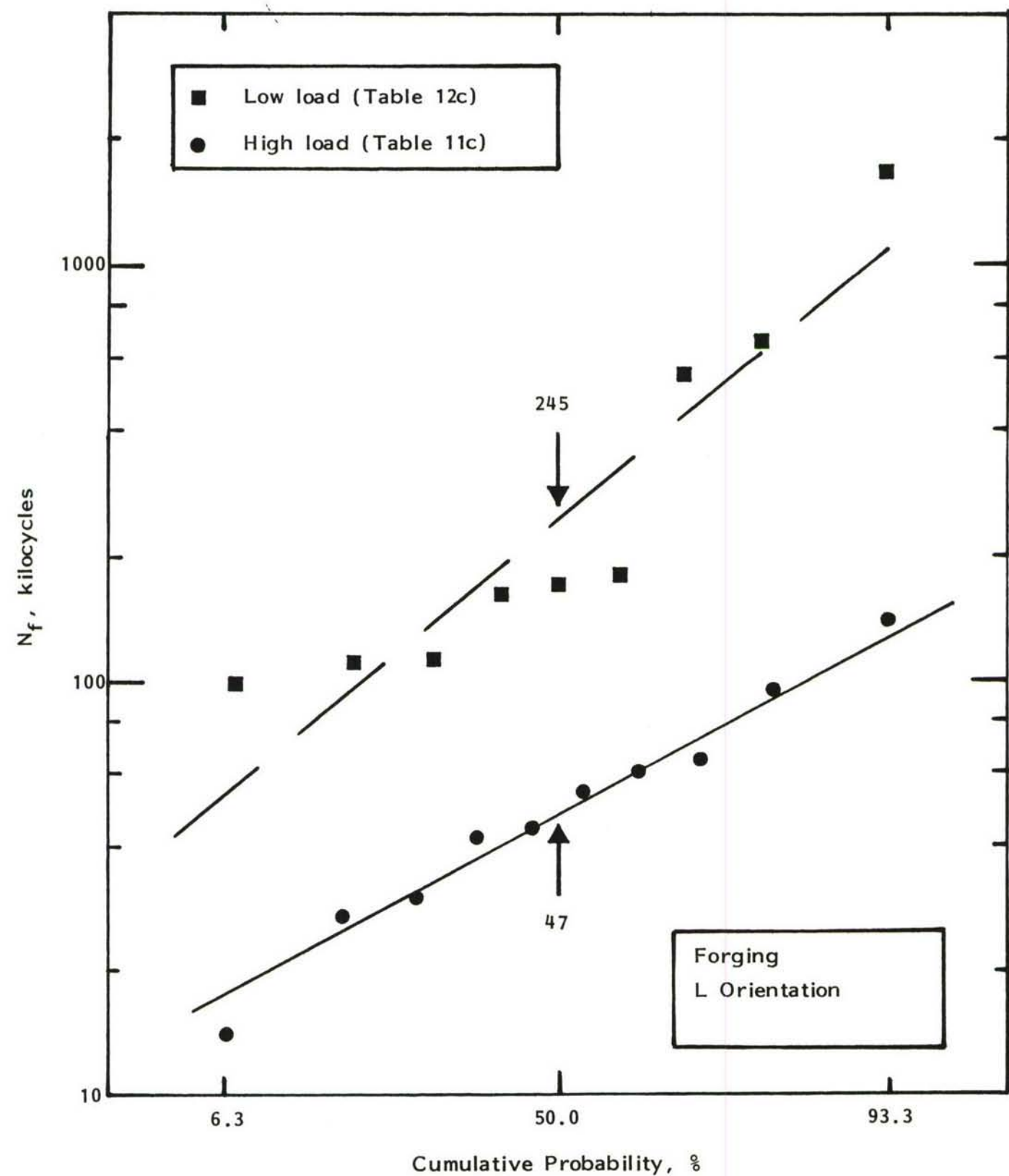
Fig. 15 Load control test results for the L orientation specimens from the forging.
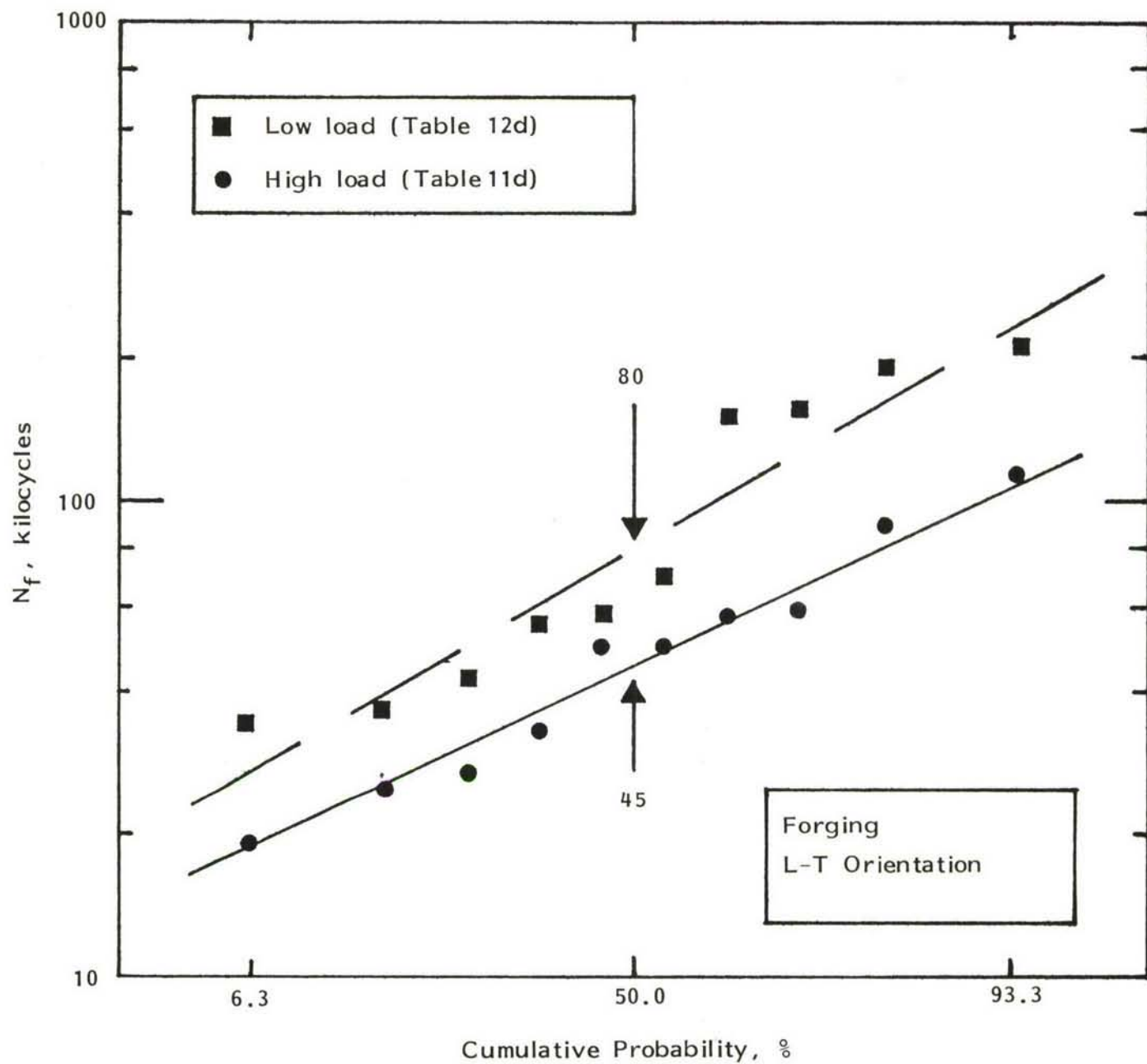
Fig. 16 Load control test results for the L-T orientation specimens
from the forging.
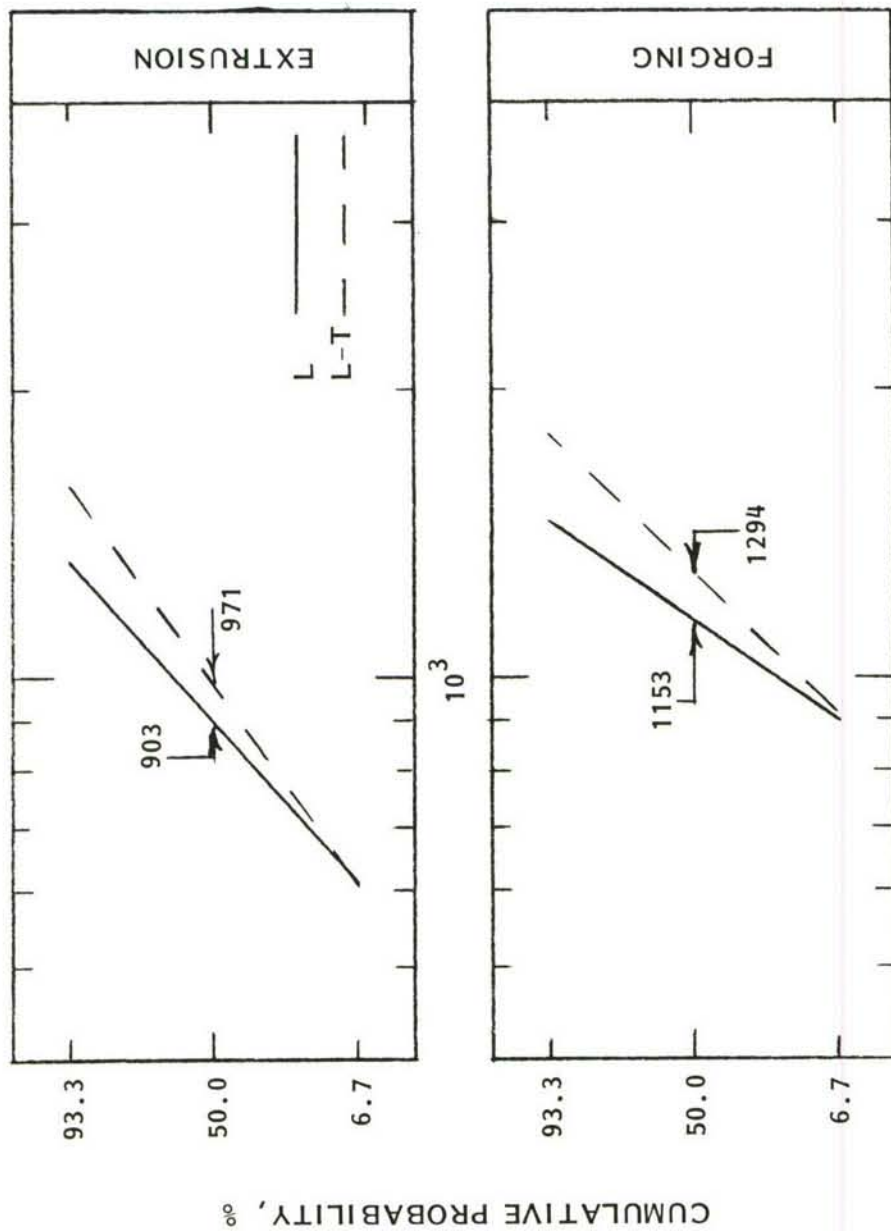
Fig. 17 Strain control (1.65 percent maximum strain) fatigue test results.
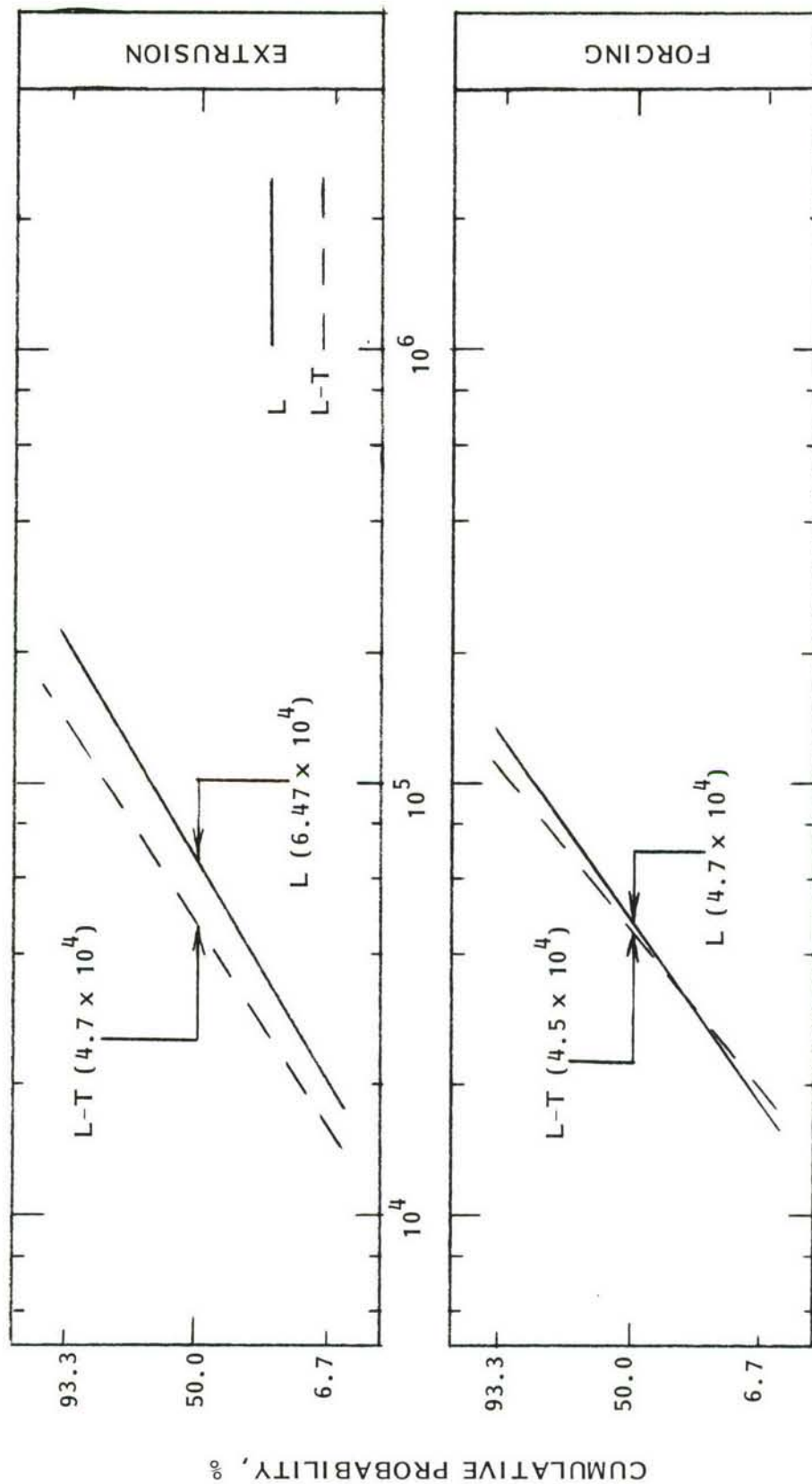
Fig. 18   HIGH LOAD (67 ksi, 462 MPa, MAXIMUM STRESS) FATIGUE TEST RESULTS
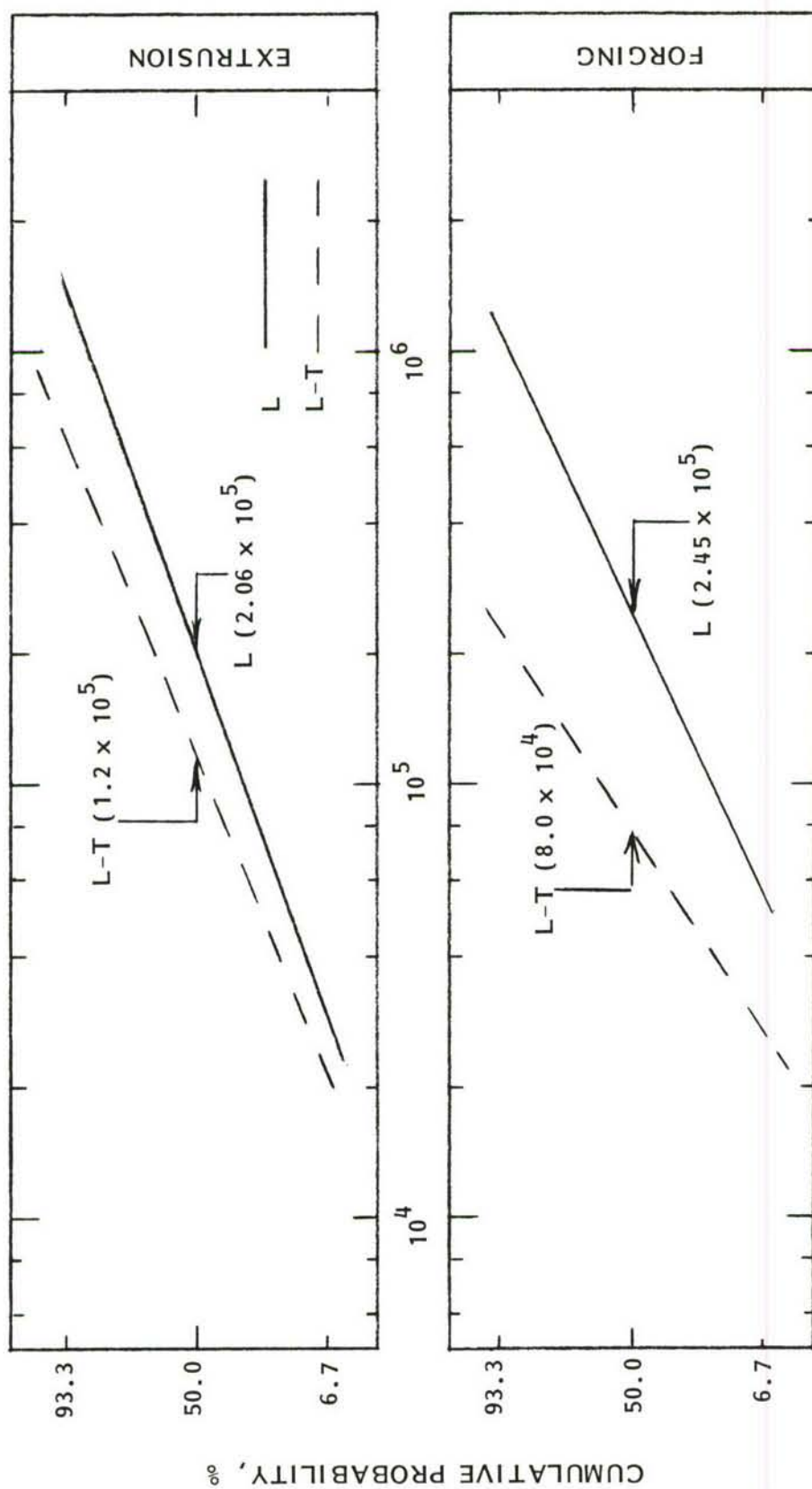
Fig. 19   LOW LOAD (60 ksi, 413 MPa, MAXIMUM STRESS) FATIGUE TEST RESULTS
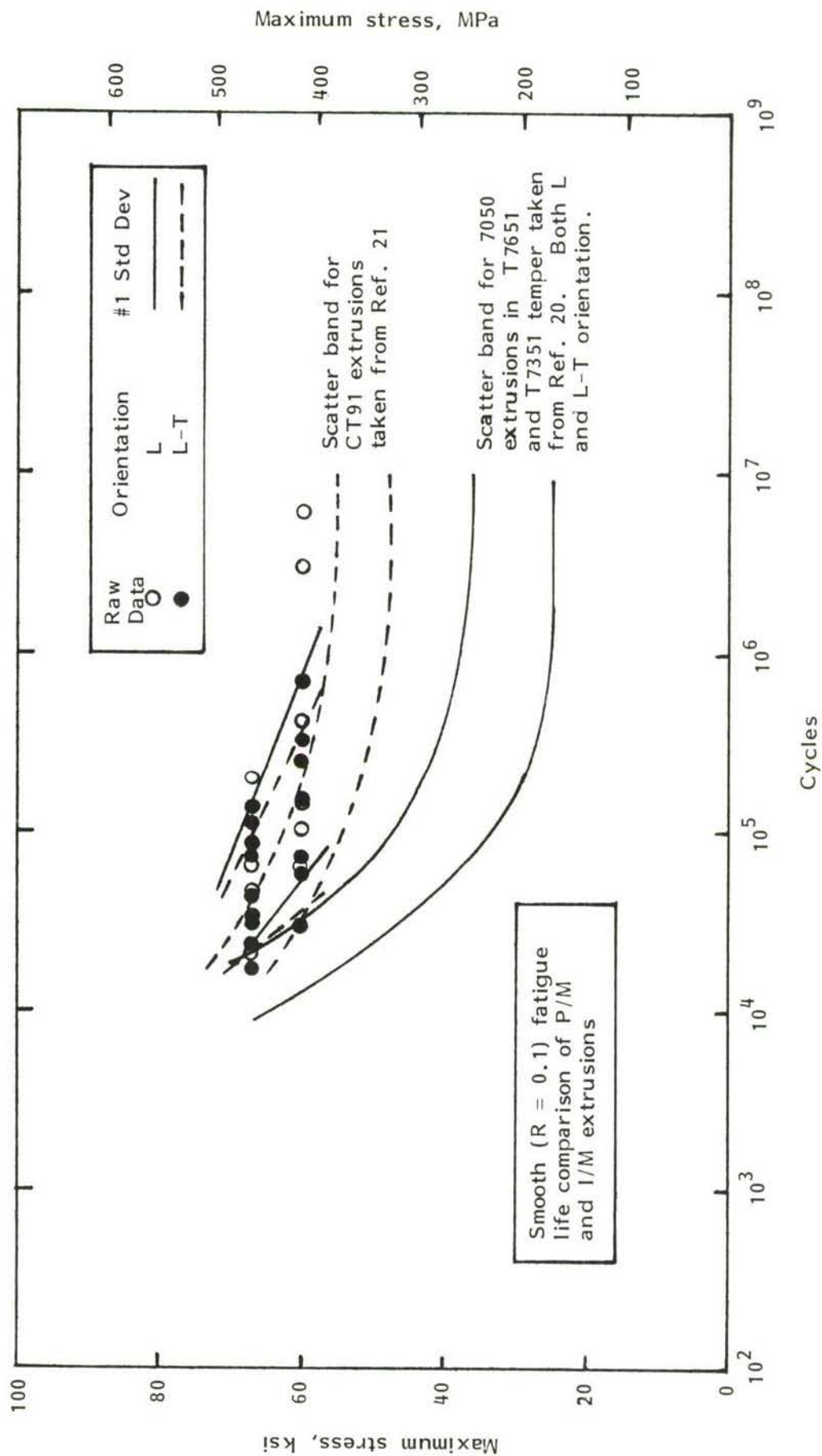
Fig. 20   Comparison of smooth fatigue life of P/M and I/M extrusions.
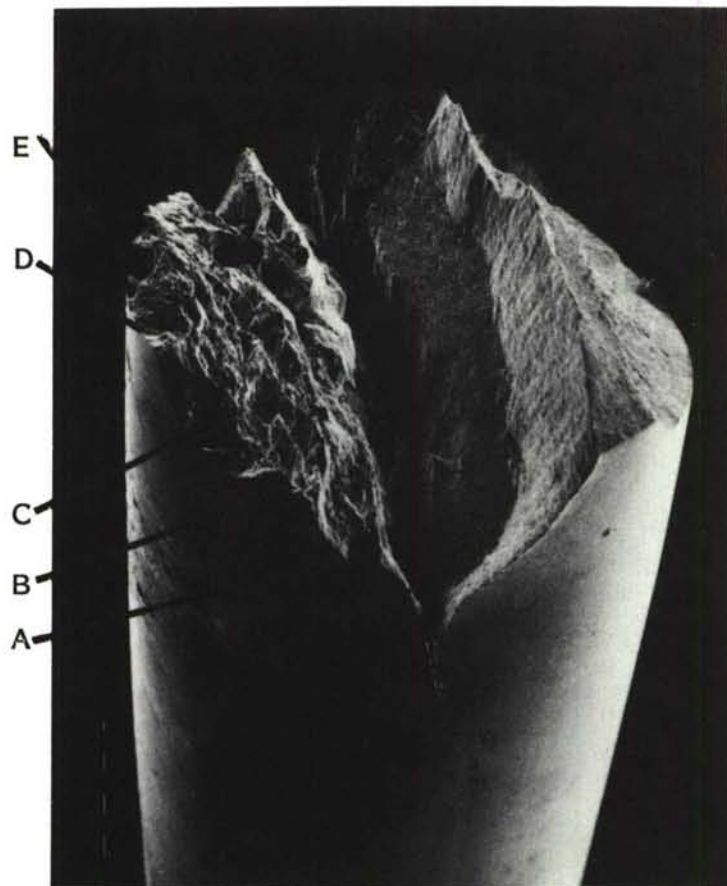
15X

Fig. 21   Multiple initiation and secondary cracking from a strain-
control specimen which is a statistical outlier.

100X

1000X

LINES   13%   10:52 19 MAY 81
SI S CL K CA FE
F1,F0   CUR 498EV   AL KA   CNTS 0   FS=201   XG=2
498EV   T=300   %DT=1   CRATE=0   WRATE=0   10514EV
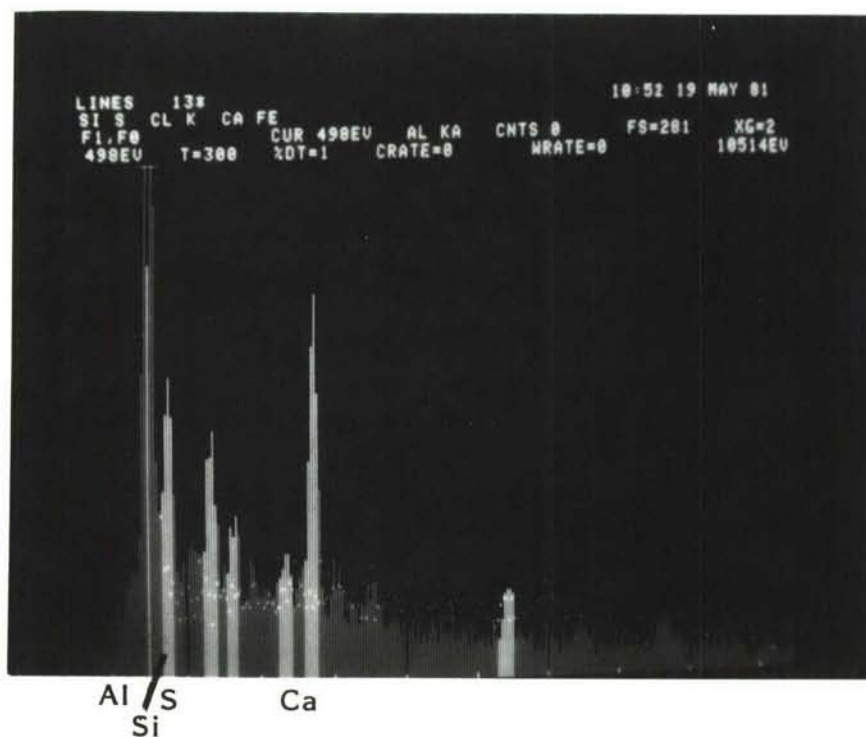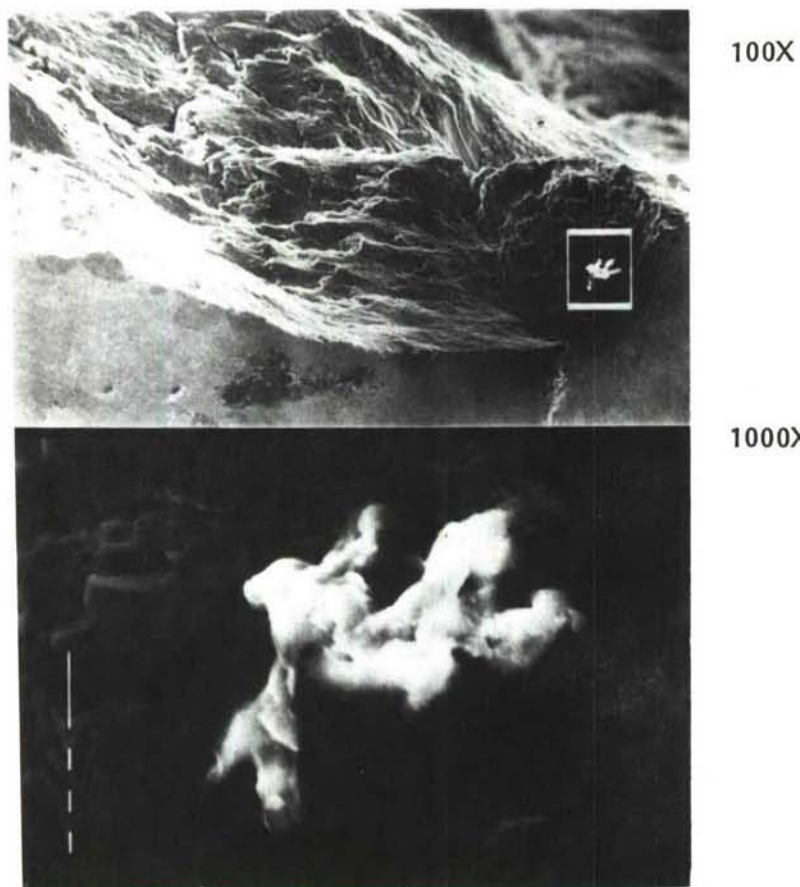
Al / S   Ca
  Si

Fig. 22a   CT91 forging (L), 1624 N_f initiation site A.
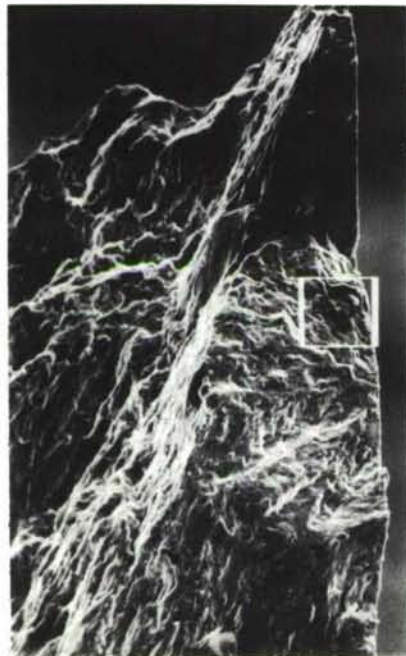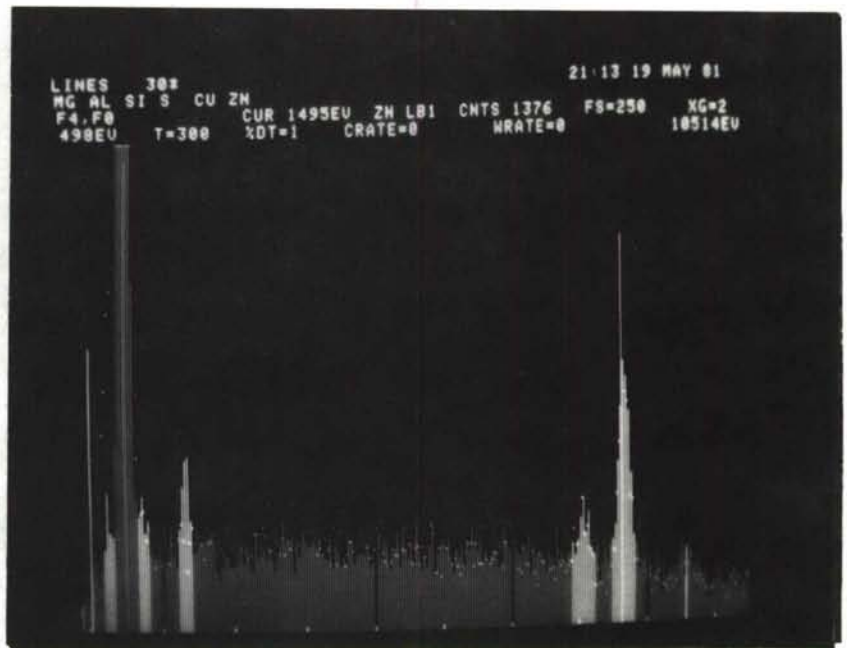
200X

Al S
Si
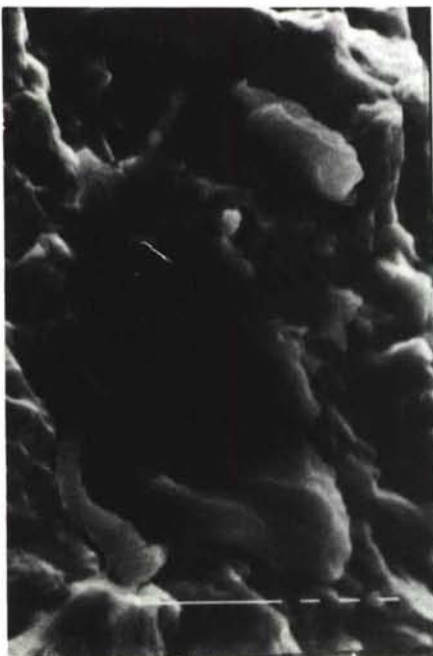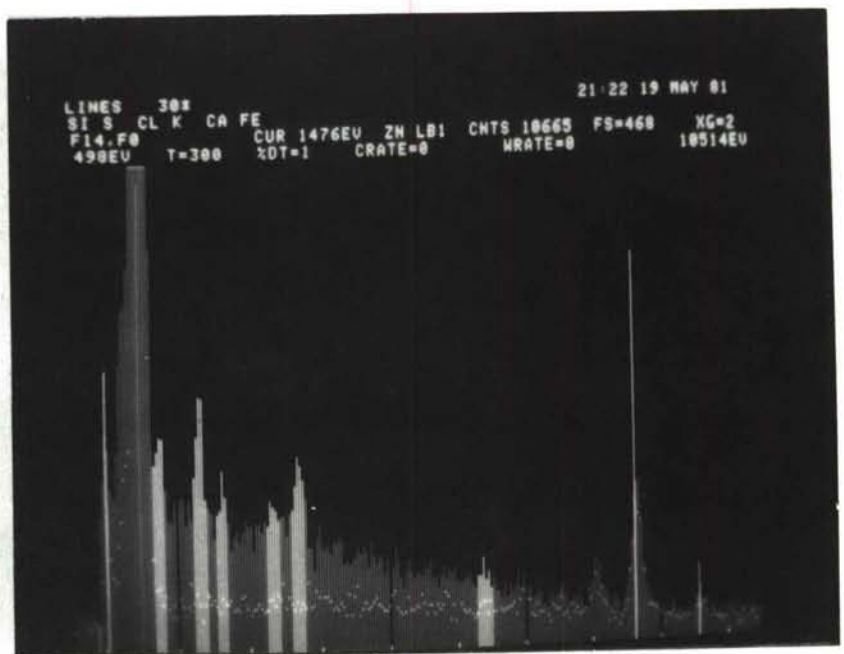
2000X

Al S   Ca
  Si

Fig. 22b   CT91 forging (L), 1624 N_f initiation site B.

77

100X

1000X

2000X

TRACE

Si
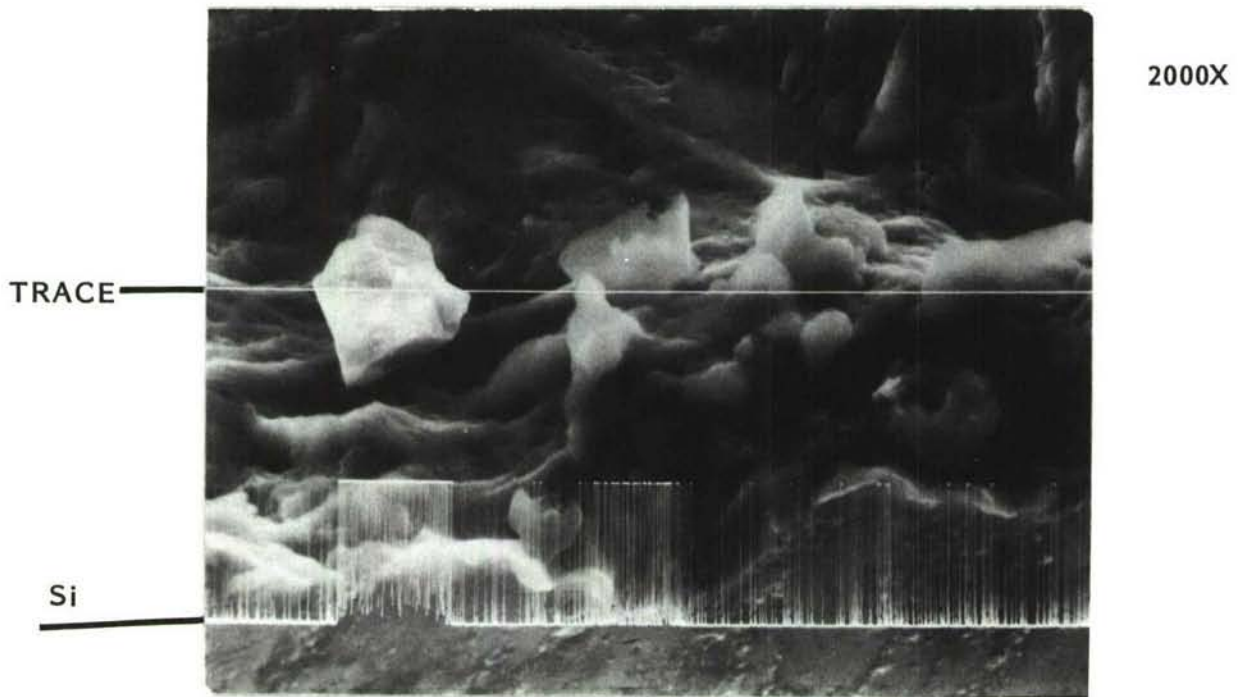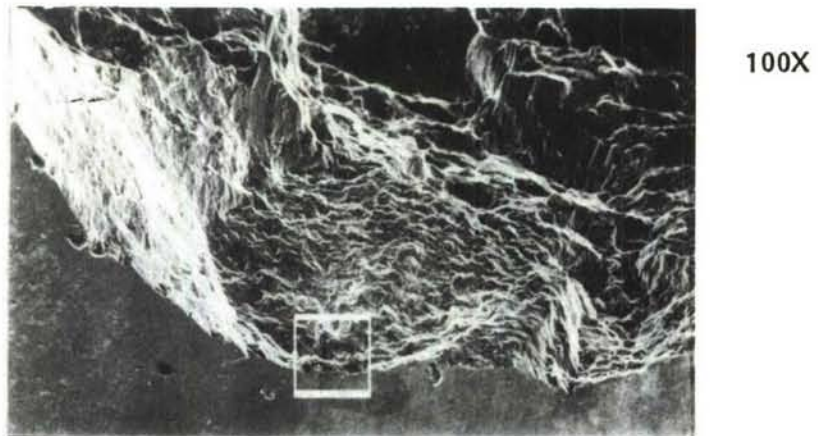
Fig. 22c   CT91 forging (L), 1624 N_f initiation site C.
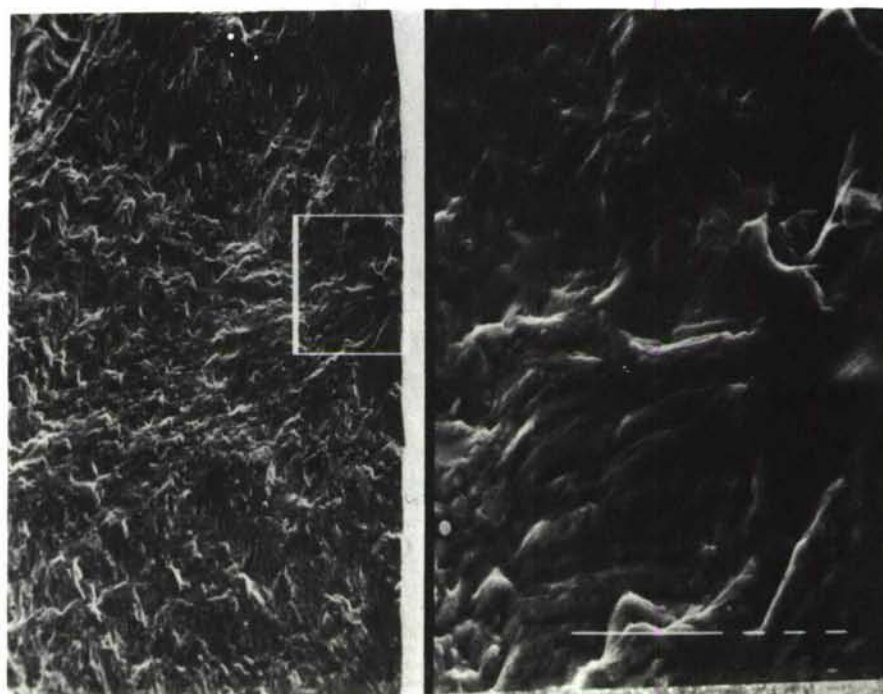
200X   1000X

TRACE

P

2000X

Fig. 22d   CT91 forging (L), 1624 N_f initiation site D.

500X

5000X

30X
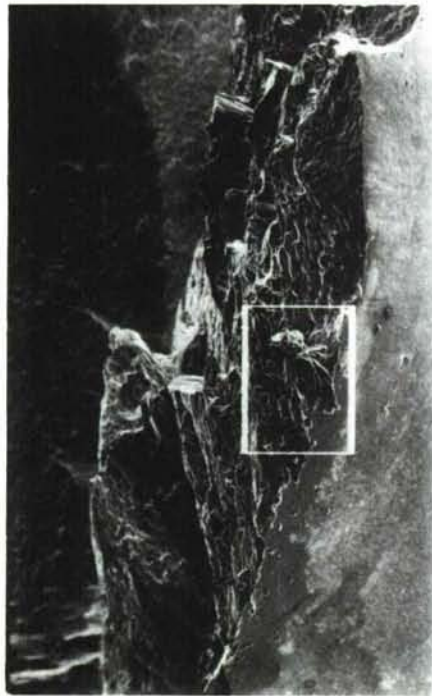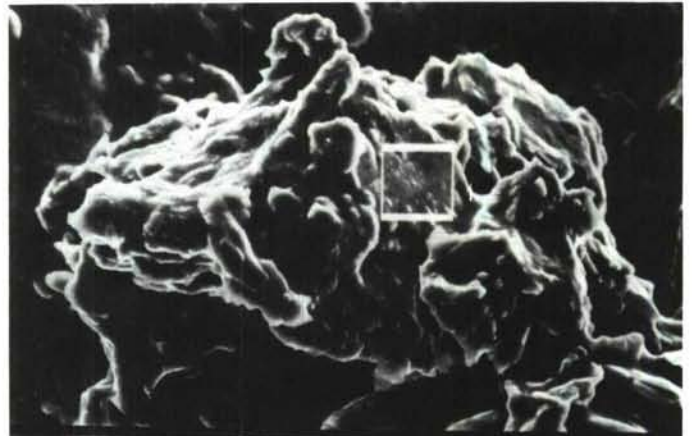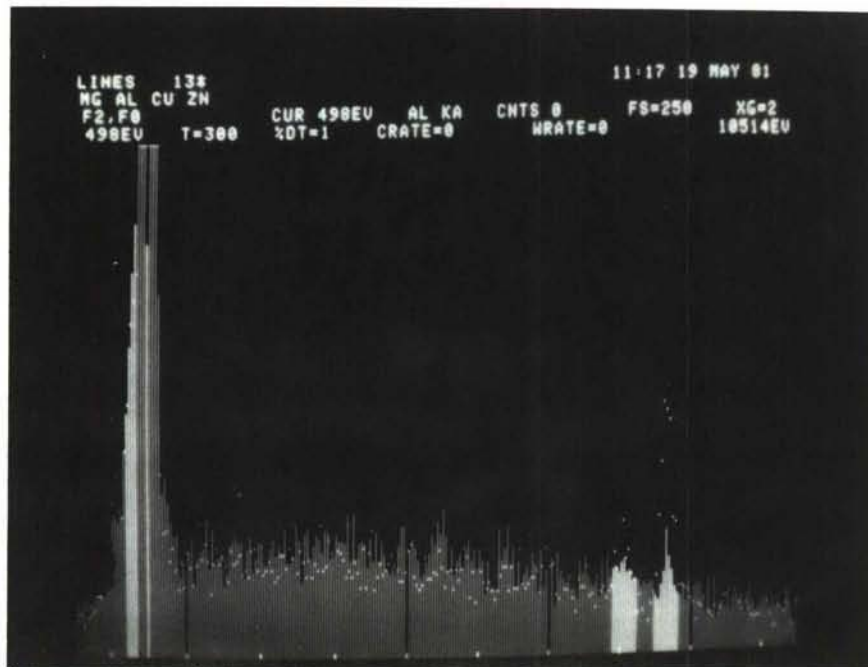
Bars = Inclusion
Dots = Adjacent Area

LINES   13#   11:17 19 MAY 81
MG AL CU ZN
F2,F0   CUR 490EV   AL KA   CNTS 0   FS=250   XG=2
490EV   T=300   %DT=1   CRATE=0   WRATE=0   10514EV

Al

Fig. 22e   CT91 forging (L), 1624 N_f initiation site E.
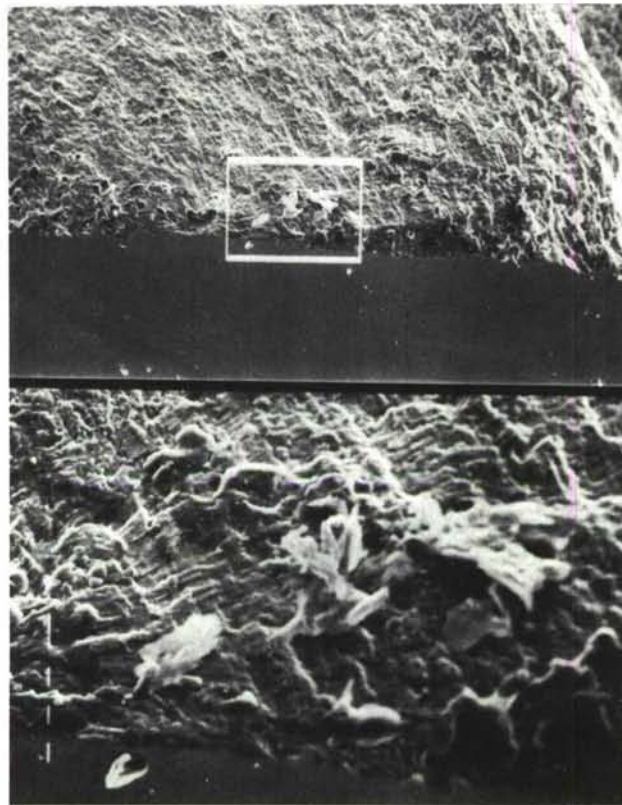
SE Image 50X

250X

BSE Image
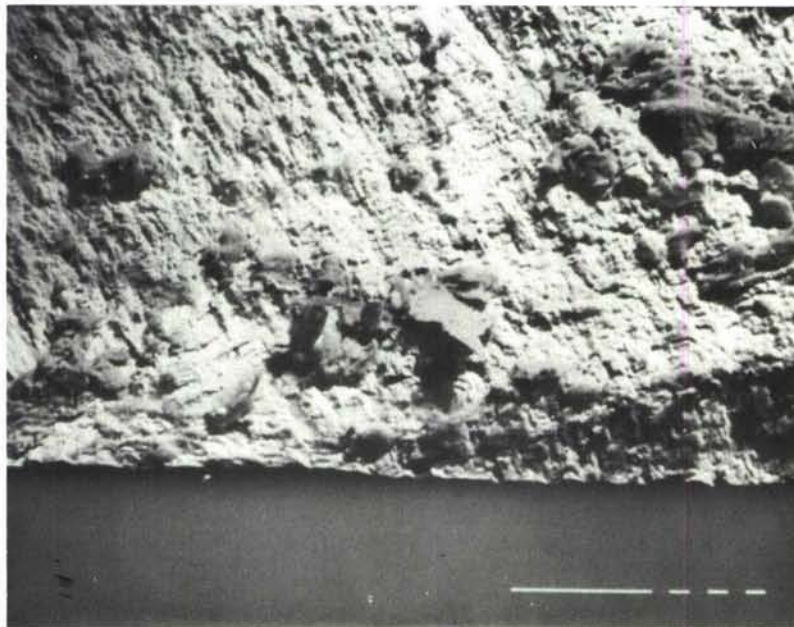
200X

Fig. 23 Comparison of BSE and SE images of aluminum rich inclusion at crack initiation sites for a forging (a), and an extrusion (b).

81
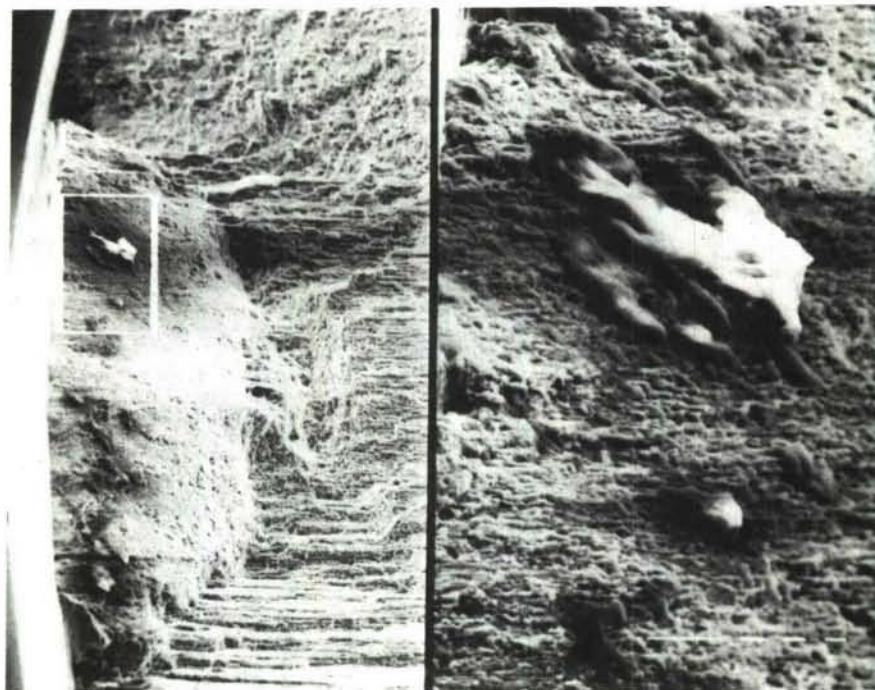
SE Image

100X   500X

BSE Image
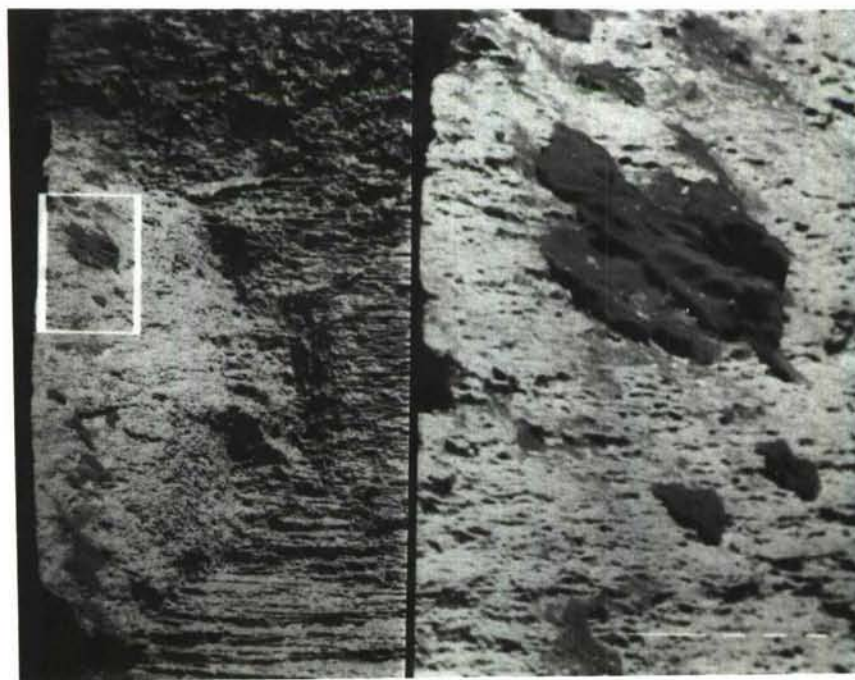
100X   500X

Fig. 23 (Continued) (b) extrusion.

Trace

Zn
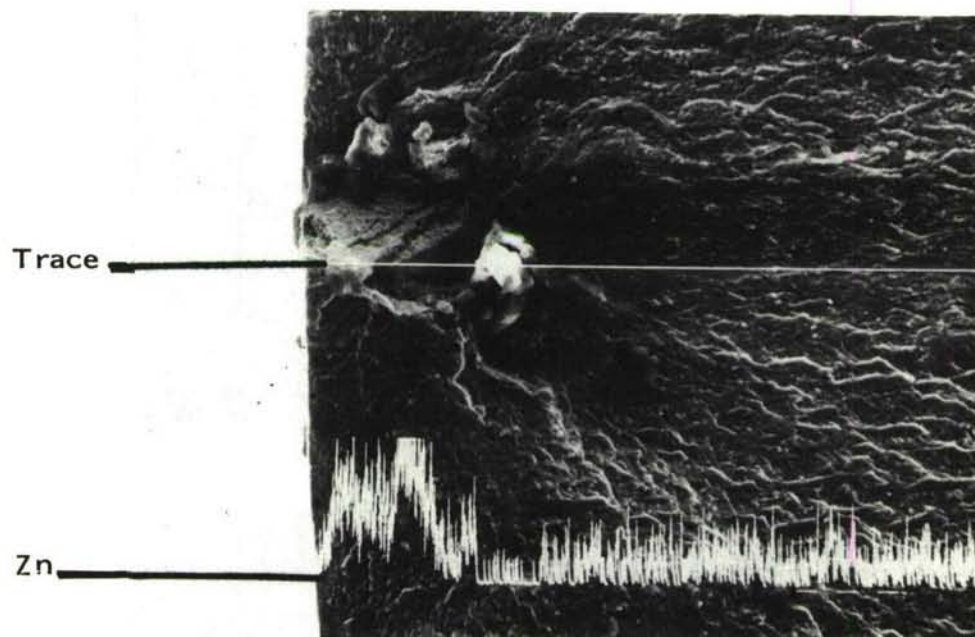
300X

Fig. 24   Surface initiation at a zinc rich inclusion.

Trace

Fe

2000X

300X
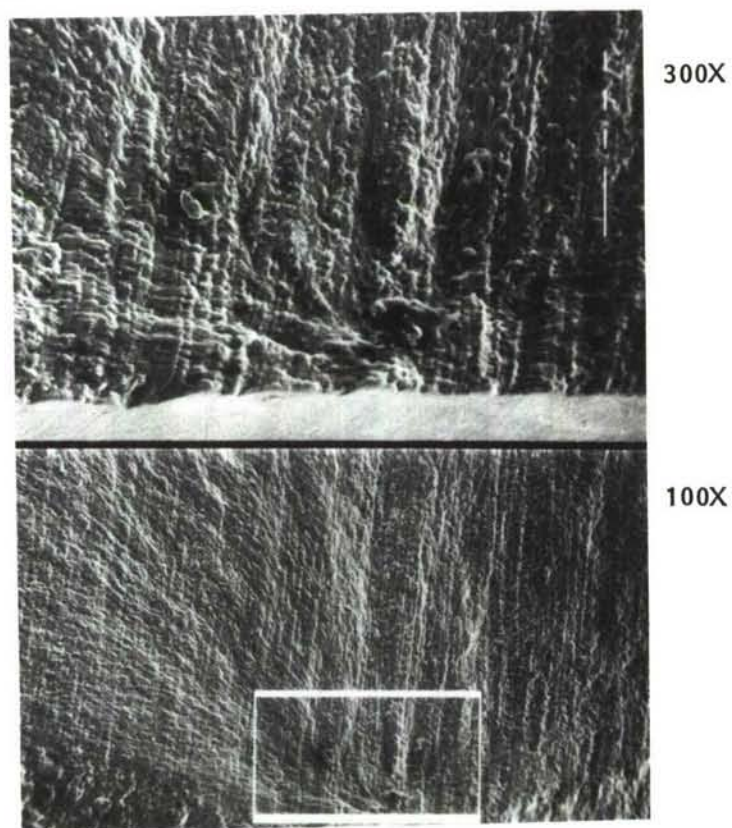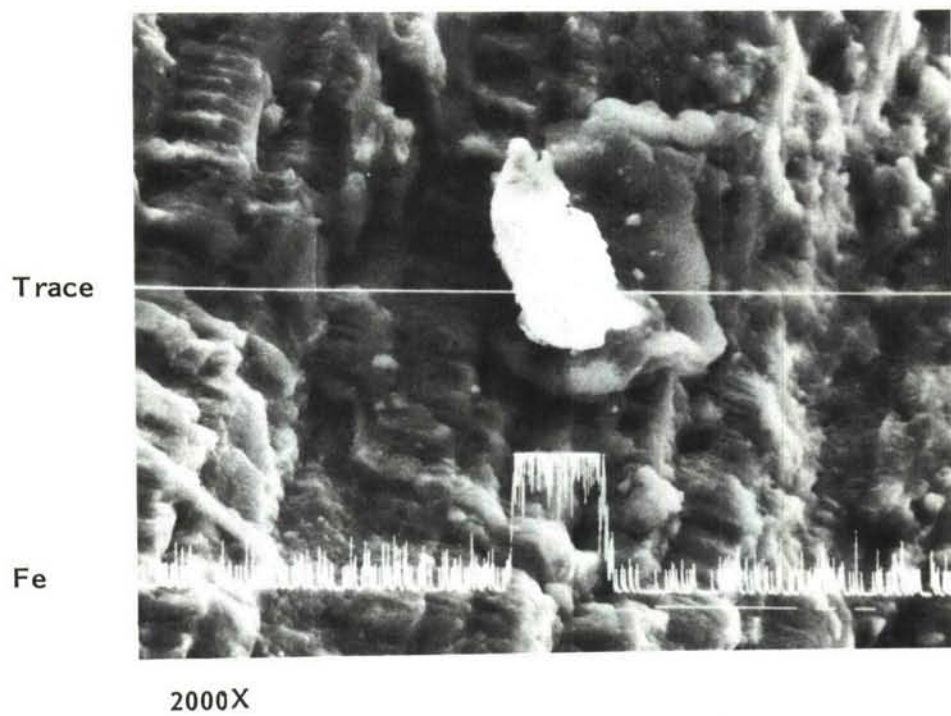
100X

Fig. 25 Surface initiation site at an iron rich inclusion.

15X

(a) Overview

Fig. 26   Fatigue initiation from a microstructural boundary.

(b)

50X   150X

(c)

200X   2000X
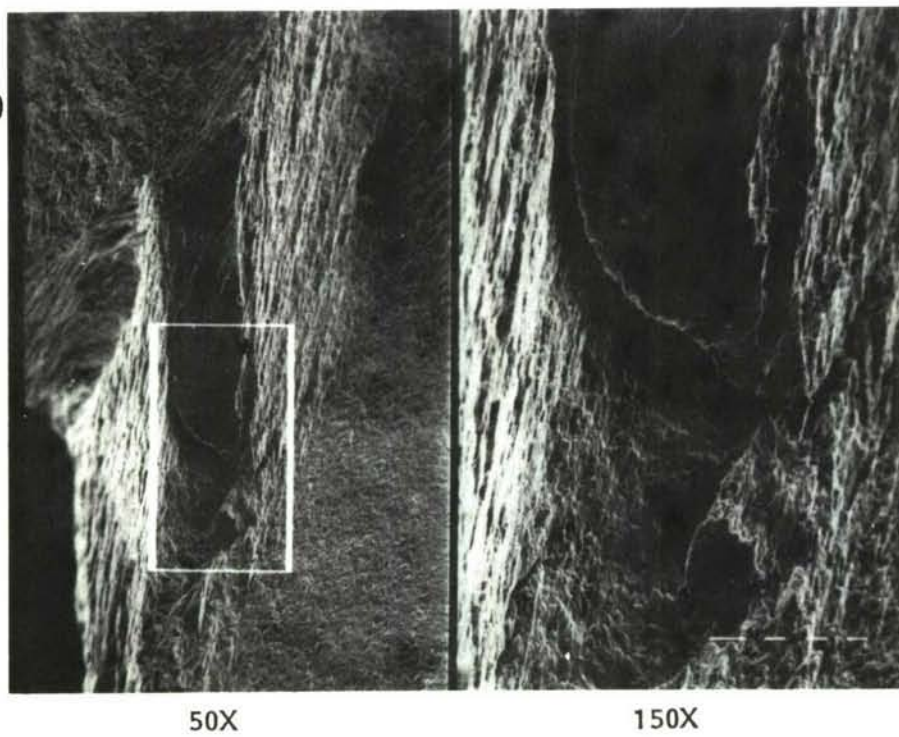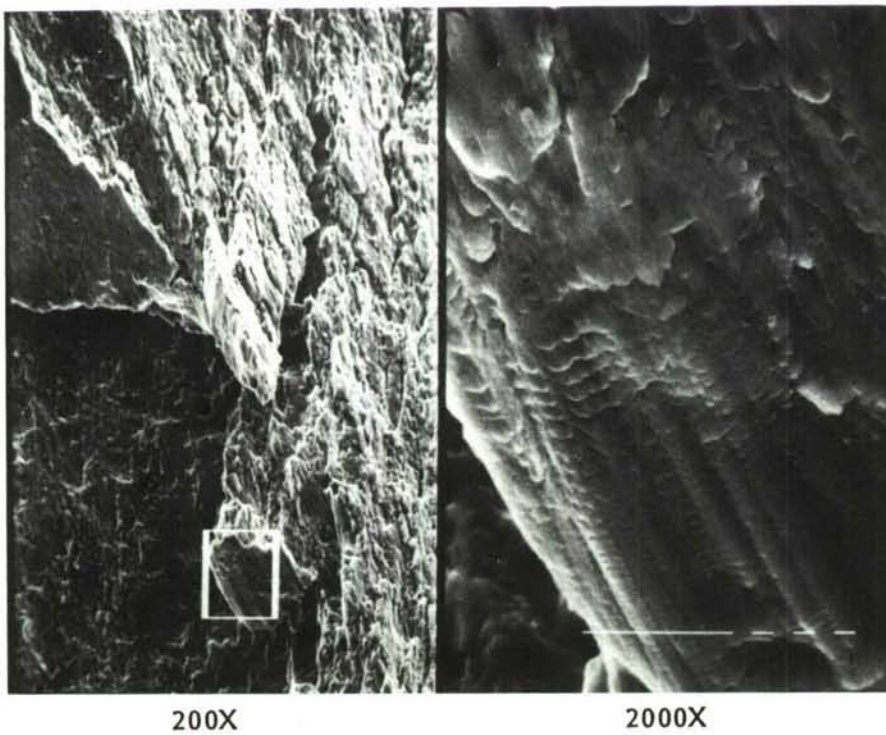
Fig. 26, continued.
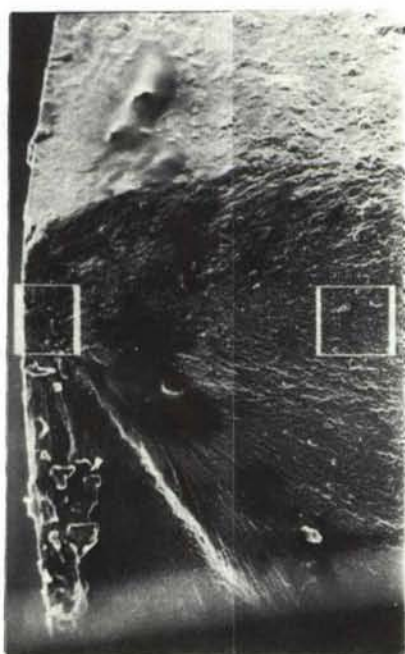
(a) 1000X   (b) 100X   (c) 1000X
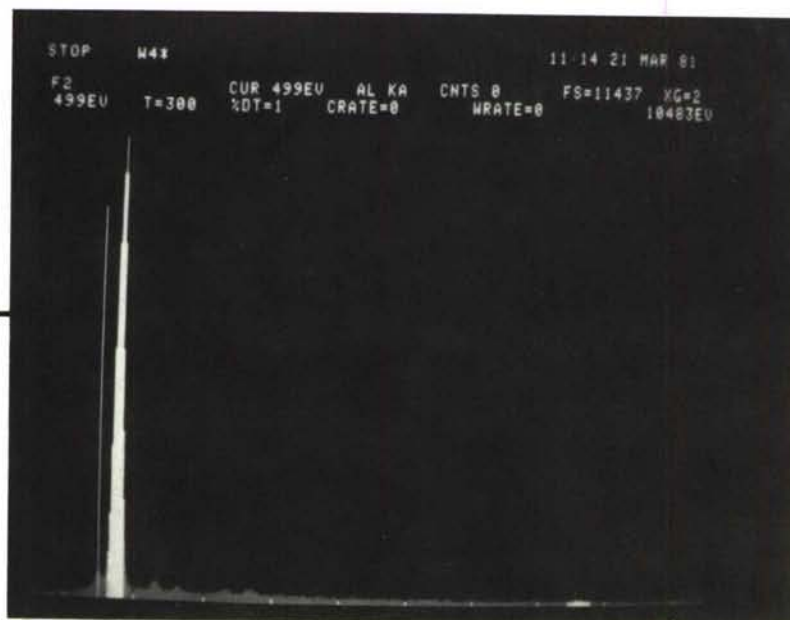
Fig. 27   Silicon segregation forming a microstructural boundary at the crack initiation site.

1000X

500X

Bars: Defect area
Dots: Matrix
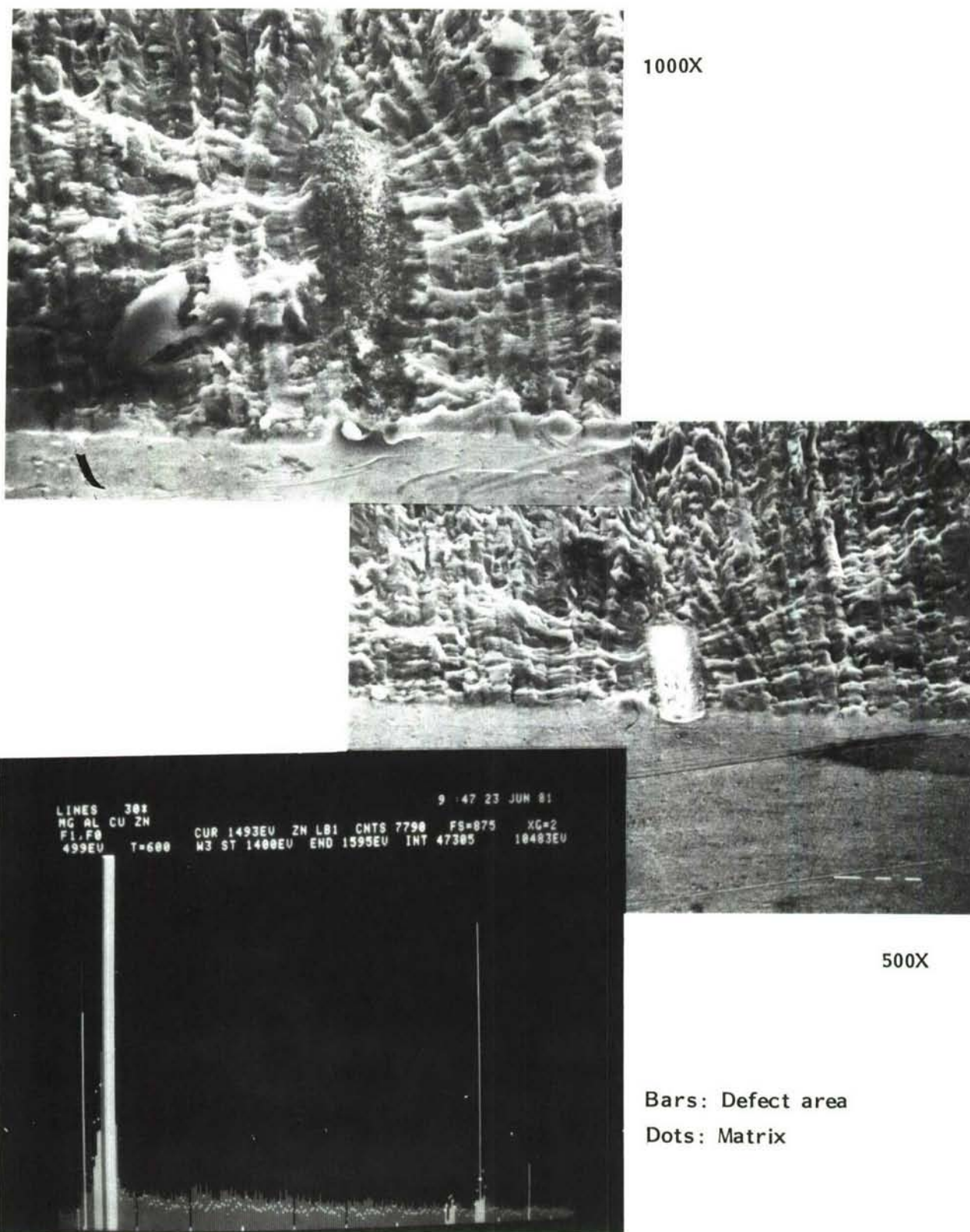
Fig. 28   Precision sectioning of a 60 μm long aluminum rich area in
a short lived extrusion specimen.

(a)

20X   200X

(b)   200X

                       20X
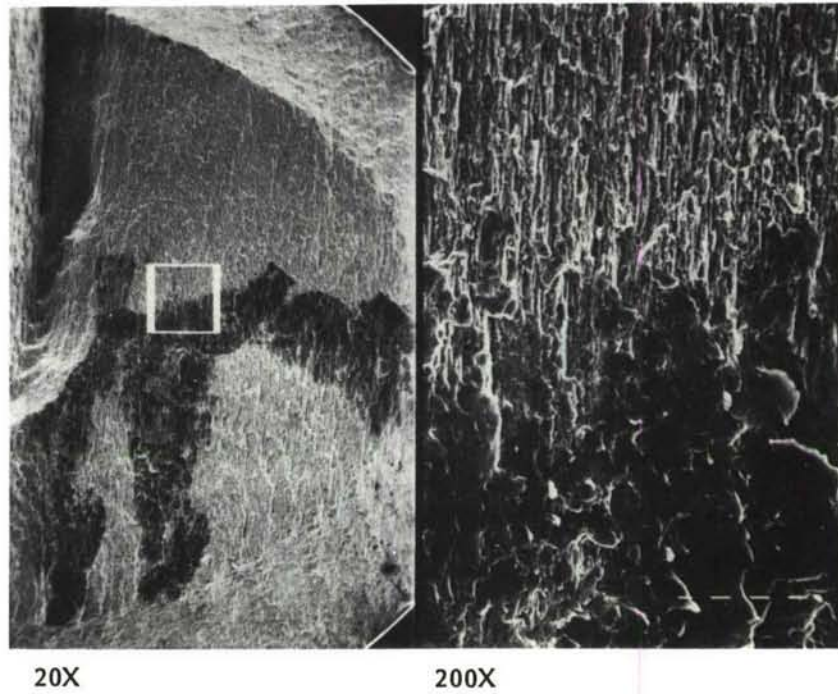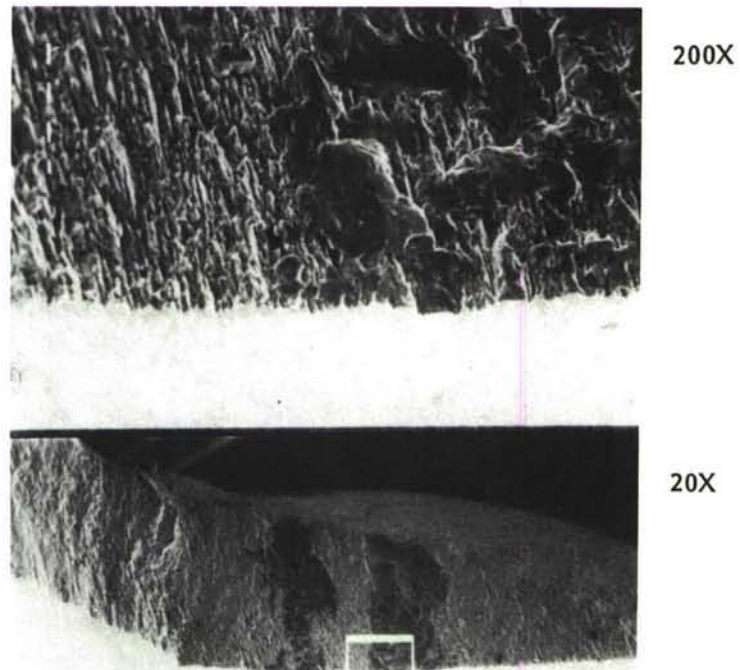
Fig. 29   Precision sectioning of a short lived forging specimen
           tested at 60 ksi (415 MPa maximum cyclic stress).

89

(c)

500X   2500X

(d)

500X   1500X

Fig. 29   Continued.

(a)

18X

(b)

500X

(c)

Bars: Defect

Dots: Defect
  minus
  background

Mg
  Al

Zn
  Cu
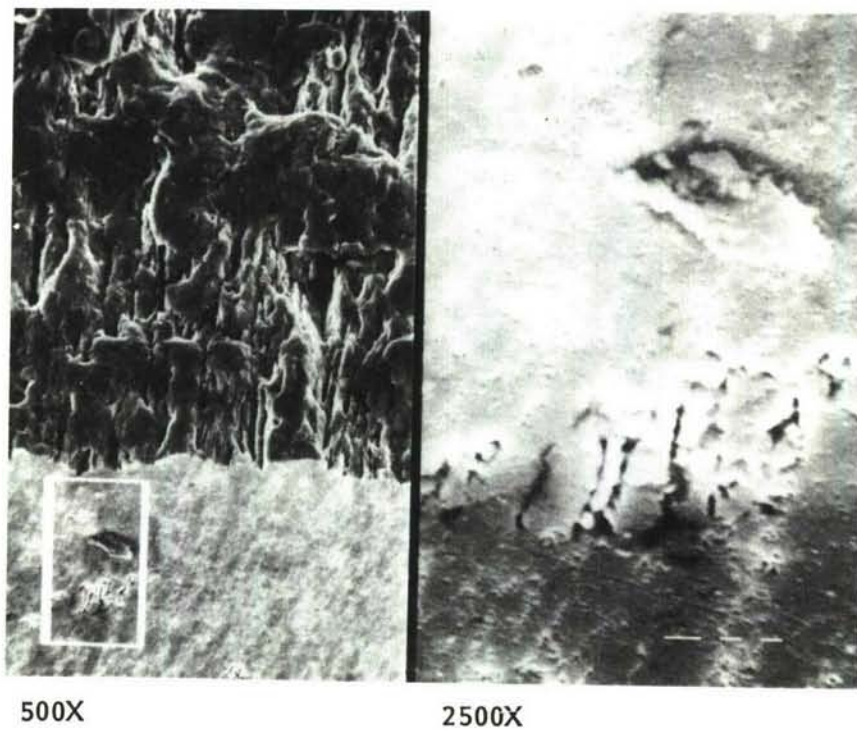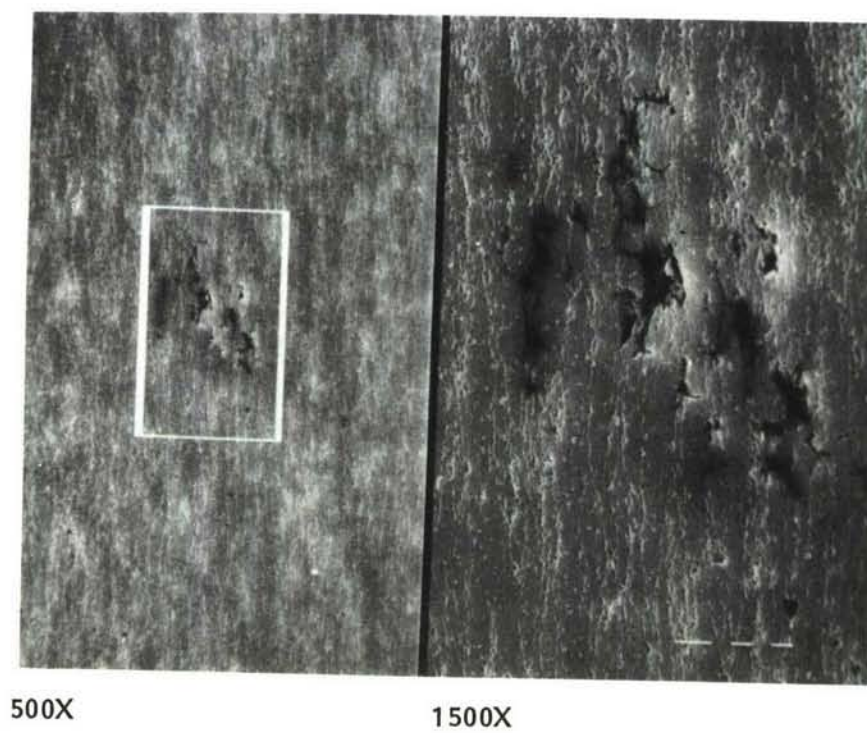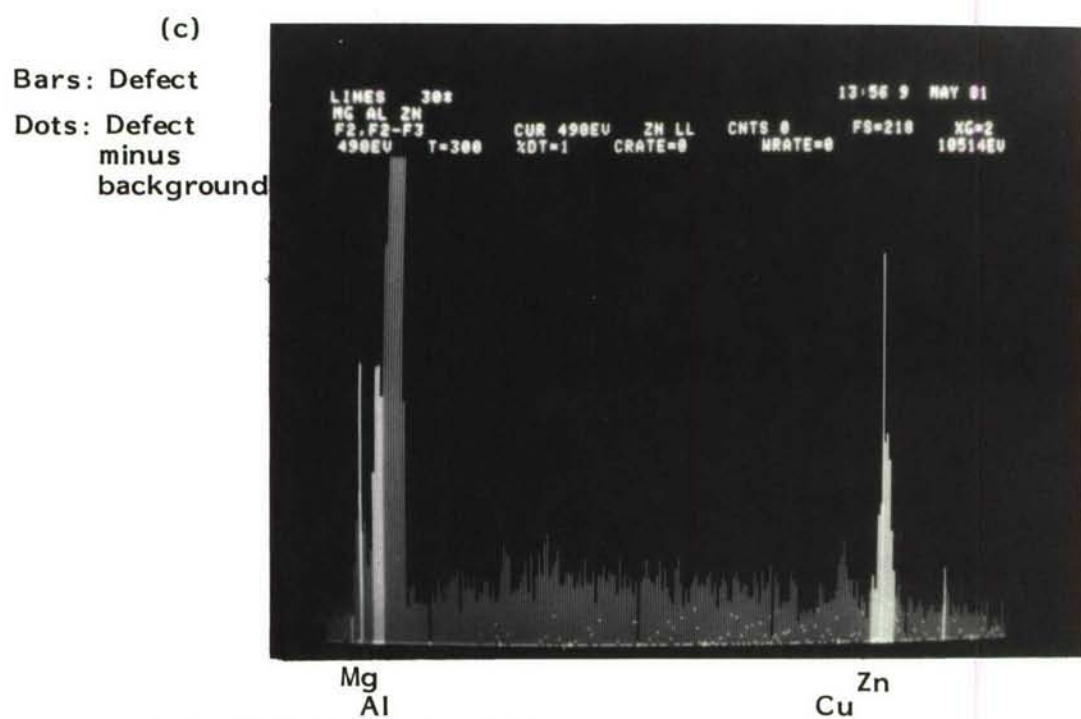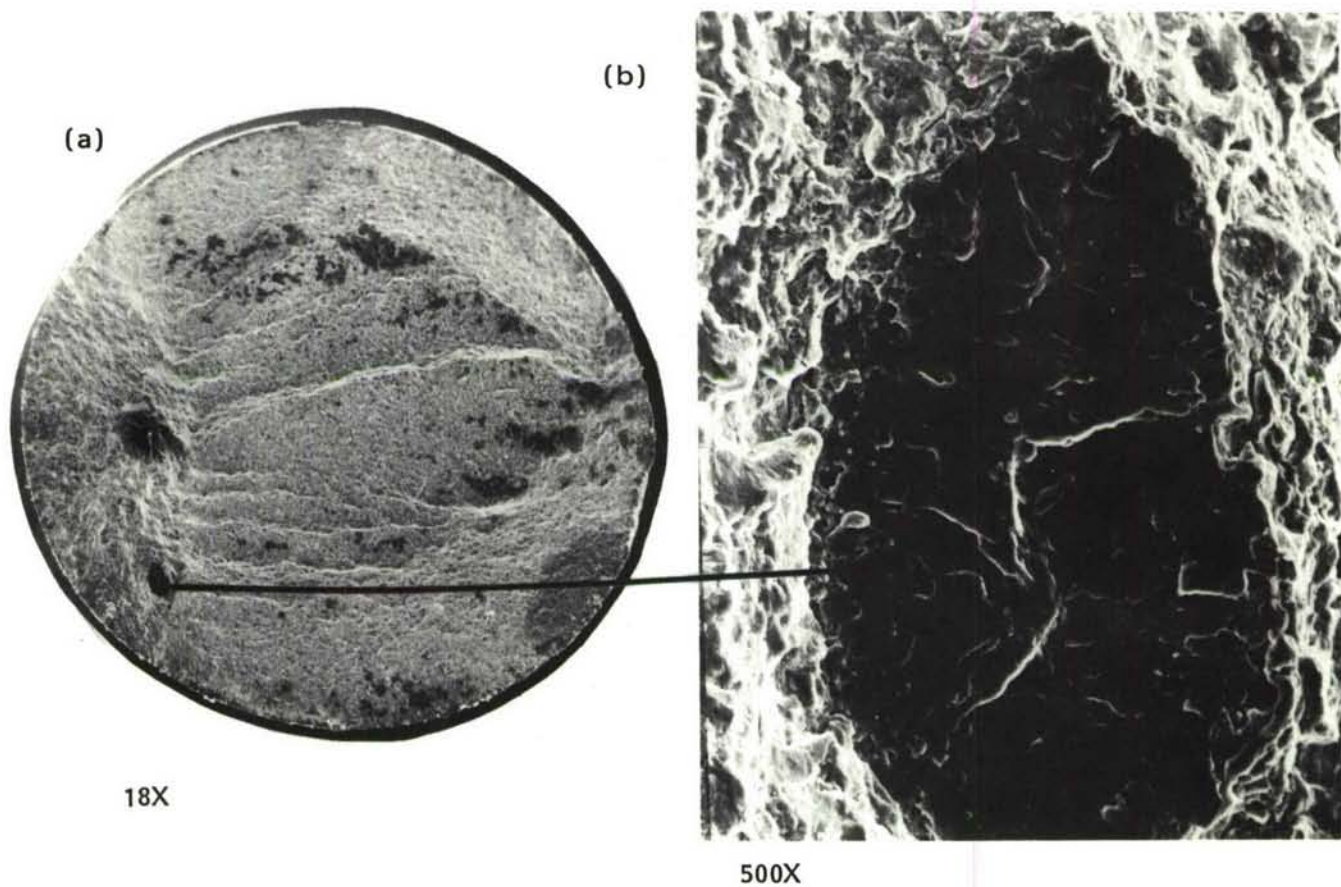
Fig. 30 Defect in CT91 billet.

91
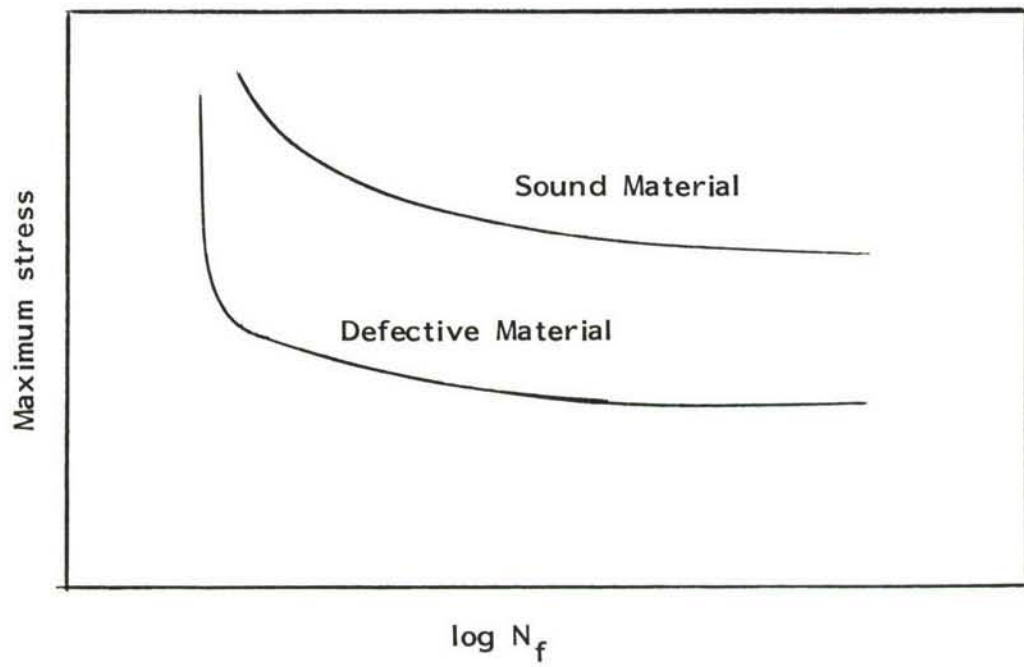
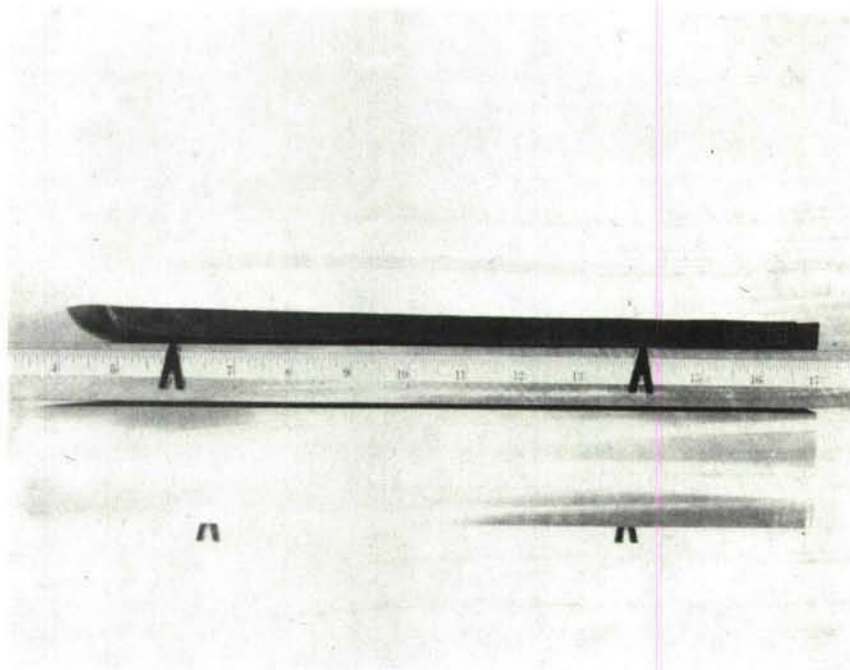Fig. 31   Schematic representation of high cycle fatigue in P/M
titanium.

Fig. 32   Distortion of a ½ inch (12.5 mm) surface slice through
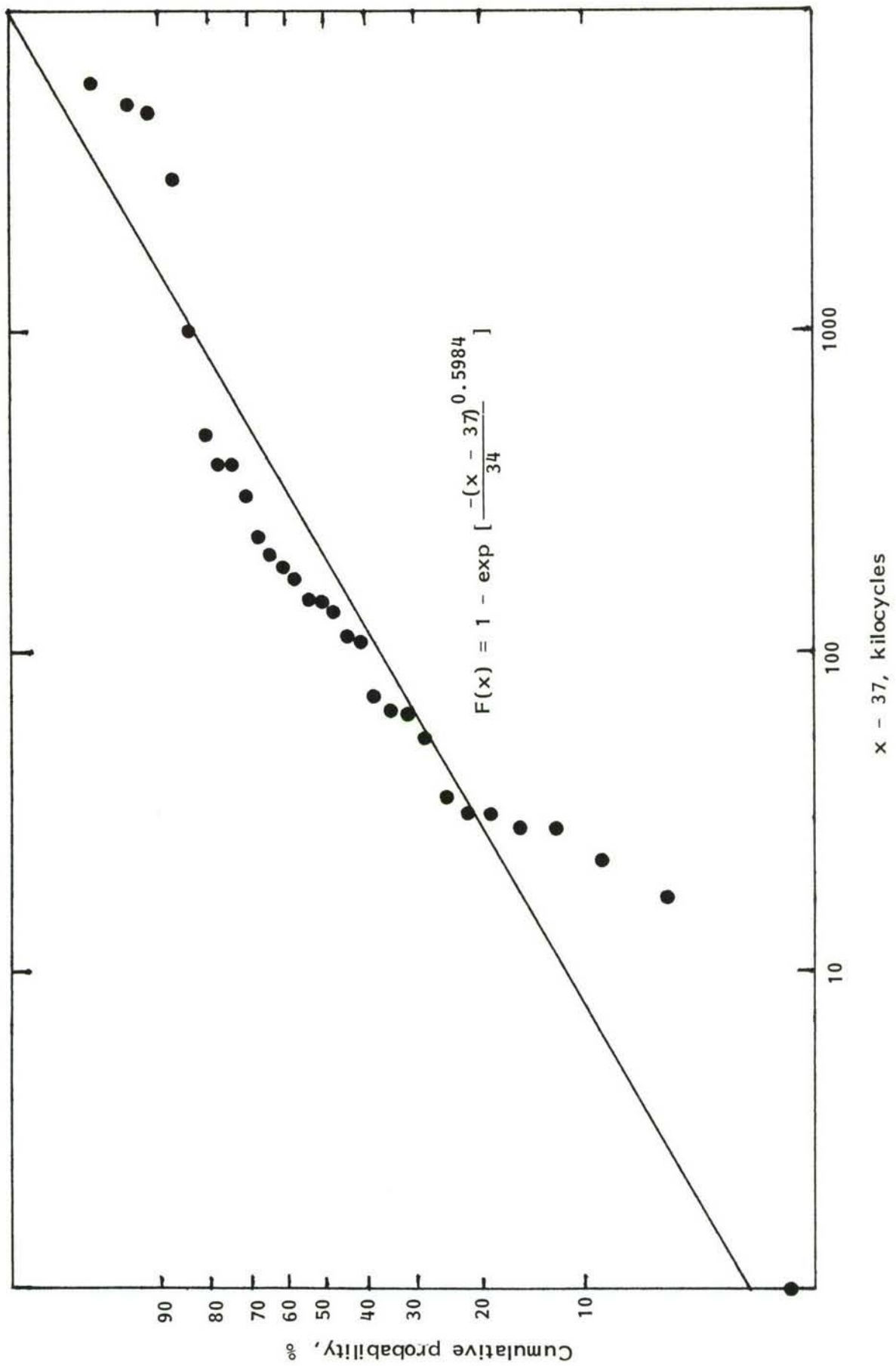the thickness of the 2 inch (50 mm) forging.

Fig. 33   Weibull plot for longitudinal extrusion specimens tested at a maximum cyclic stress of 60 ksi (415 MPa), R = 0.1.
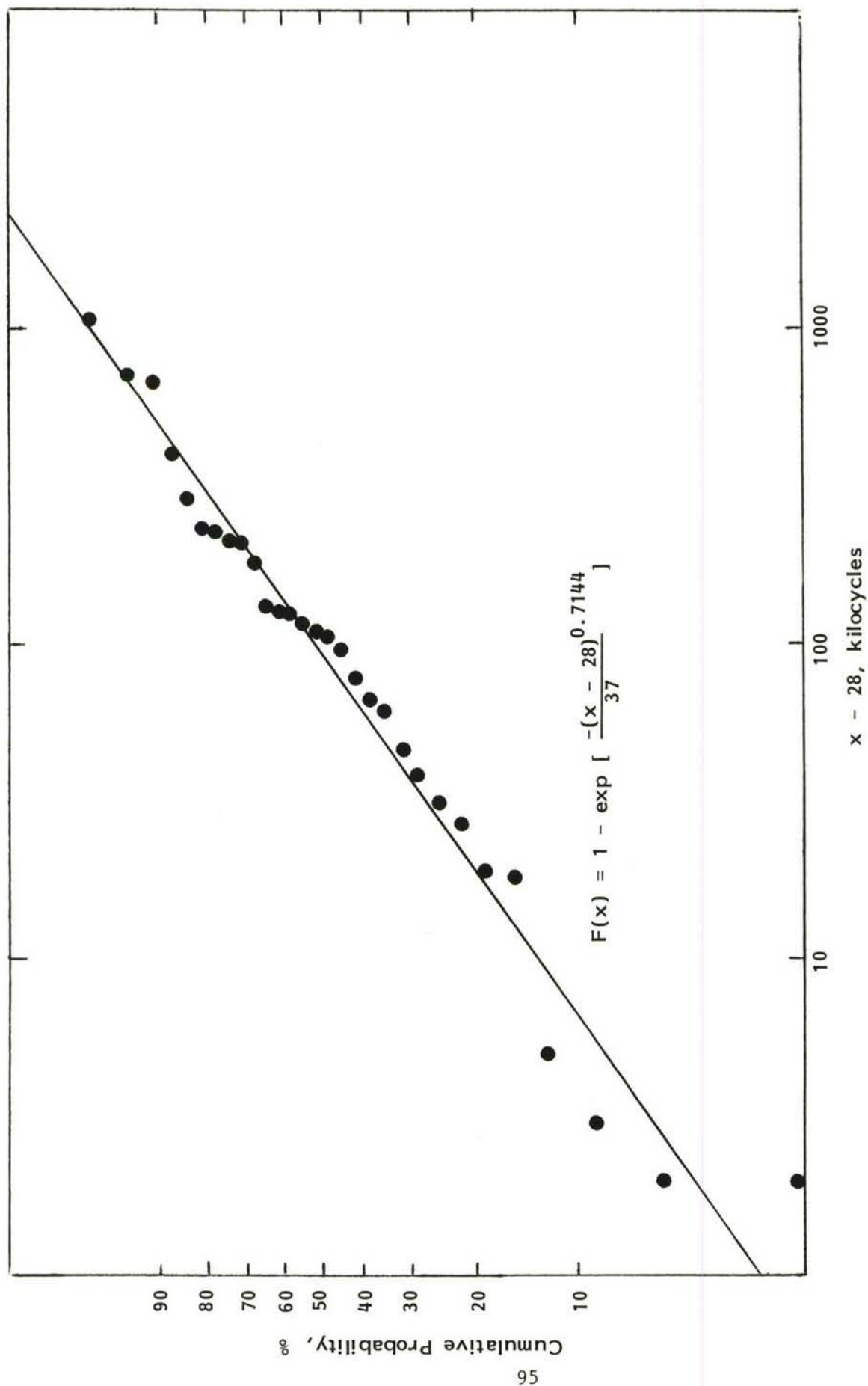
$$F(x) = 1 - exp \left[\frac{-(x - 37)}{34}^{0.5984} \right]$$

x - 37, kilocycles

Cumulative probability, %

Fig. 34   Weibull plot for long-transverse extrusion specimens tested at a maximum cyclic stress
of 60 ksi (415 MPa), R = 0.1.

$$F(x) = 1 - \exp \left[\frac{-(x - 28)}{37}^{0.7144} \right]$$

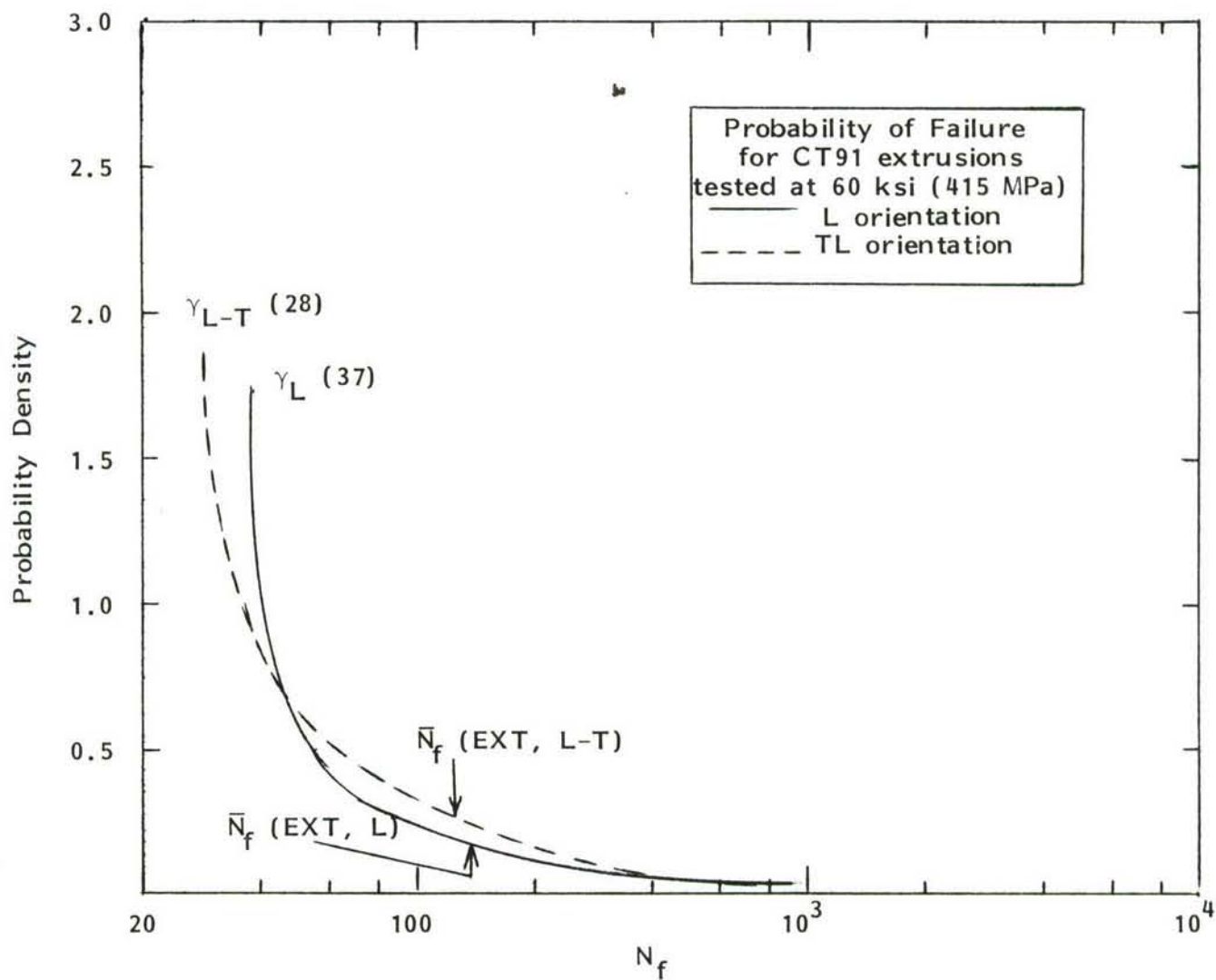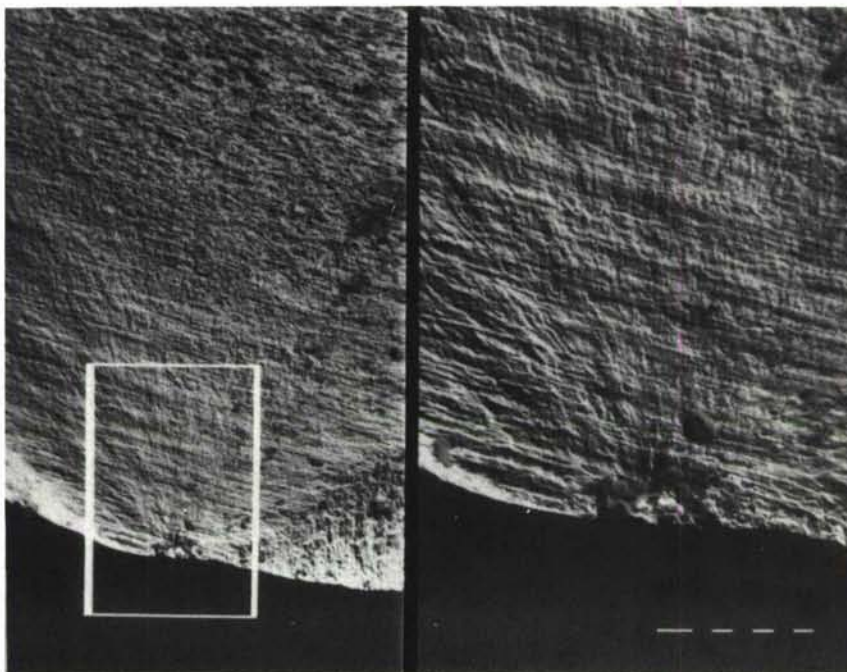x – 28, kilocycles

Cumulative Probability, %

Fig. 35   Weibull probability density function for P/M alloy CT91 extrusion
in the L and L-T orientation.

(a)

(b)

Fig. 36   Several oxide inclusions in a 100 μm diameter area at
the initiation site of a short lived specimen.